# Chapter 1: INTRODUCTION

## 1.1 Background

"Clean air is considered to be a basic requirement of human health and well-being. However, air pollution continues to pose a significant threat to health worldwide" [1].

Global warming has become perhaps the most intricate issue faced by world leaders. It is an undeniable impact to earth and humanity. On the one hand, admonitions from the scientific community are becoming louder. Scientists learned long ago that the earth's climate has powerfully shaped the history of the human species - biologically, culturally and geographically [2, 3]. But only in the last few decades research [4, 5] has revealed that human can be a powerful influence on the climate as well.

Apparently, carbon dioxide ($CO_2$) is a major anthropogenic greenhouse gas (GHG) that contributes to earth's global warming. The $CO_2$ molecule (O=C=O) contains two double bonds and has a linear shape. It has no electrical dipole, and as it is fully oxidized, it is moderately reactive and is non-flammable. $CO_2$ is toxic, and is an acidic oxide; becoming corrosive acid in the presence of water. It is the anhydride of carbonic acid, which is unstable in aqueous solution, from which it cannot be concentrated. At standard temperature and pressure, the density of $CO_2$ is around 1.98 kg/ $m^3$.

Serious atmospheric pollution began during the industrial revolution. For about 400,000 years the atmosphere's $CO_2$ level remained the same, but it is now rapidly rising. As reported by Mauna Loa Observatory, Hawaii [6], since 1958 the annual mean concentration of $CO_2$ has only increased from one year to the next. In 1959, the concentration for atmospheric $CO_2$ was about 315.98 parts per million (ppm). The upper safety limit for the atmosphere is 350 ppm, which has been attained in 1987. Appallingly, based on data for the first three quarters of 2010, 389 ppm concentration of atmospheric $CO_2$ has been recorded. Table 1.1 shows the annual rate of increase from 1960 to 2009.

Table 1.1. An annual rate of atmospheric $CO_2$ increment from 1960 to 2009 [6].

| Decade | Annual Rate of Increase (Atmospheric $CO_2$) |
|---|---|
| 2000 – 2009 | 1.92 ppm |
| 1990 – 1999 | 1.52 ppm |
| 1980 – 1989 | 1.61 ppm |
| 1970 – 1979 | 1.22 ppm |
| 1960 – 1969 | 0.86 ppm |

* Data source: Earth Systems Research Laboratory (ESRL) / National Oceanic and Atmospheric Administration (NOAA).

$CO_2$ levels rose with industrialization. Evidently, large-scale systems of industry are responsible for most of the environmental damage that stresses and destroys biodiversity worldwide [7-15]. In order to truly tackle the large-scale problem of biodiversity loss, people need to make big changes in industry and business practices at a speed and scale that are much faster and farther reaching than individual actions like using mineral based sunscreen or planting flowers for bees.

$CO_2$ capture has actually been in use for years. The oil and gas industries have used $CO_2$ capture for decades as a way to enhance oil and gas recovery. Only recently have people started thinking about capturing carbon for environmental reasons. There are three main steps to carbon capture and storage (CCS) [16-19]. It entails scrubbing the $CO_2$ from a variety of gas streams, such as natural gas, refinery gas, synthetic gas, *etc.* of power plant, transporting the purified captured $CO_2$ to a storage location, and storing the compressed $CO_2$ safely in geological formations, like aquifers and oil and gas reservoirs.

Carbon is taken from a power plant source in three basic ways: post-combustion, pre-combustion, and oxy-fuel combustion. Post combustion $CO_2$ capture is a process where the $CO_2$ is separated, or removed, from a flue gas containing $CO_2$ mixed with other gasses after the combustion of fossil fuel. The immense advantage of post-combustion $CO_2$ capture which is the technology is much more mature than the alternatives of pre-combustion capture and oxy-fuel combustion with $CO_2$ capture [20, 21].

There are five main technologies that exist for separating $CO_2$ from a gas stream which are, membranes, solvent absorption, adsorption, cryogenic and chemical looping [22, 23]. The solvent absorption process involves a cyclical process, in which $CO_2$ is absorbed from a gas stream directed into a liquid, typically an alkanolamine. The gas stream, with most of the $CO_2$ removed, is then emitted to the atmosphere. The liquid is processed to remove the $CO_2$, which is then compressed for storage. The resulting $CO_2$ - free liquid is used again for absorption and the process continues. This technique is widely used in a range of applications, but it needs a large amount of power to regenerate the solvent.

## 1.2 Problem statement

For more than 70 years, it has been common practice in $CO_2$ capturing is done in transport- and reaction-controlled absorption process, by employing aqueous solutions of alkanolamine mainly monoethanolamine (MEA), diethanolamine (DEA) and *N*-methyldiethanolamine (MDEA). Although it is technically feasible to remove $CO_2$ from flue gas, the use of alkanolamine presents several concerns: (1) corrosion of amines systems limits the concentration of amine in the solution and causes extra cost; (2) amines are prone to degrade under high temperature especially in the regeneration process; (3) oxidative degradation of amines occurs in the presence of oxygen; (4) amines are volatile and lost into the gas stream. The loss of absorbents not only produces extra waste streams but also leads to additional absorbent cost [24].

It should be noted that among the amines used, MDEA has lower volatility, thermal stability, less alkaline, higher $CO_2$ load (up to 1.0 mol $CO_2$/ mol amine) and less regeneration cost, though the absorption rate of $CO_2$ into MDEA is quite slow since MDEA just promotes $CO_2$ hydrolysis to form bicarbonate. On account of that, typically in industrial application, aqueous solution of MDEA is usually mixed with activators of fast reactivity, including MEA, piperazine (PZ), and DEA.

Nonetheless, recently ionic liquids (ILs) have grabbed the attention through their promising and unique features, particularly task specific ionic liquids (TSILs). Despite their importance and interest, properties of the blended ILs with organic molecular liquids that are paramount for the design of technological process particularly are still meager, which greatly restrict their applications and further development. Thus, there is a need for thermo-physical property data such as density and viscosity for the systems to be studied.

In addition, TSILs do have drawbacks to use in $CO_2$ separation such as having relatively high viscosities in pure state, yet upon contact with $CO_{2,}$ the viscosity increases dramatically, forming a gel-like substance. The viscosity of many ILs which affected the transport properties such as diffusion, is relatively different from one to three orders of magnitude higher, compared to the conventional solvents.  Liu *et al.* [25] used molecular simulations to explain for the high viscosity of the neat TSILs. They claimed that the anions prefer to interact strongly with the –$NH_2$ tails of the cations via hydrogen bonding which led to the high viscosity.

Therefore, in one embodiment of the ternary blended MDEA - TSIL or aqueous binary of TSIL, is to lower the viscosity whilst enhance the performance of the systems. Thus, being an aqueous binary or ternary system, the chemical reaction is allowed to occur at a faster rate and more feasible to the overall process. As a guideline, the successful ILs absorbent will have high $CO_2$ capacity (*i.e.*, a Henry's law constant lower than 10 bar) with a low energy requirement for regeneration (*i.e.*, an enthalpy of absorption less than 60 kJ/ mol).

### 1.3 Scope and research objectives

A review on ILs has brought a logical resurgence of interest to commit an effort in exploring new solvents and improve related processes. Amongst the criteria, which define the performance of alkanolamine-based solvents for the removal of $CO_2$, is the ultimate $CO_2$ uptake capacity ($CO_2$ equilibrium solubility). Therefore, the aim of this work was to investigate $CO_2$ solubility in the aqueous medium of MDEA - guanidinium trifluoromethanesulfonate, [gua][OTf] system. MDEA was chosen as the chemical solvent while [gua][OTf] is the physical solvent. The cation of this new TSIL consists of a guanidinium ion to which a tertiary amine moiety was covalently tethered. The effect on solubility of $CO_2$ in the presence of doubled amine function was also disclosed.

The absorption experiments were conducted at high pressures from 500 to 3000 kPa and also at low pressures (below 100 kPa) to have a better understanding on the performance of MDEA - [gua][OTf] systems in capturing the $CO_2$. The solubility correlations as a function of concentration, pressure and temperature were also obtained.

Thus, the objectives of this work are as follow:

i) To determine the densities at different compositions of aqueous binary and blended ternary of MDEA – [gua][OTf] systems at different temperatures. The data obtained were then correlated and compared. The thermal expansion coefficients for all systems under study were calculated based on the measured densities, using the empirical correlations.

ii) To obtain the viscosities of different concentrations of aqueous guanidinium trifluoromethanesulfonate, [gua][OTf] and to examine the effect of the addition of [gua][OTf] to MDEA as a function of temperature. Also, a correlation of viscosity as a function of concentration of MDEA and [gua][OTf] at temperatures from 303.2 to 333.2 K was also determined.

iii) To investigate the $CO_2$ absorption potential of the aqueous mixture of MDEA - [gua][OTf] system at high pressures (500 to 3000 kPa) with temperature range between 303.2 and 333.2 K. The correlation of $CO_2$ solubility as function of temperature and pressure was also obtained.

iv) To study the performance of aqueous mixtures of MDEA – [gua][OTf] systems in capturing $CO_2$ at relatively low pressures of 10, 50 and 100 kPa and temperature 303.2 K. A simple correlation was developed to predict the $CO_2$ loading for these systems.

v) To compare the performance of aqueous [gua][OTf] with other type of ionic liquids or MDEA at high and low pressures and different temperatures.

## 1.4 Outline of the thesis

In order to accomplish the objectives, a number of detailed studies were conducted, which are presented in the following eight chapters.

Chapter 1 provides a general idea of the related research, which briefly describes the rationality and the importance of $CO_2$ capture study and its existing technologies. This overview was followed by several problem statements, which justified this research. The scope, aims and objectives of this thesis were also defined in this section.

Chapter 2 discusses the theoretical background of $CO_2$ absorption process including treating plant, related parameters, solvent selection and reaction mechanisms. A broad literature review on alkanolamines and ILs were also summarized in this chapter. In addition, the physicochemical properties such as density, viscosity and their thermodynamic characters were also reviewed. The experimental data for the $CO_2$ solubility and physical properties published in the open literatures were also detailed.

The chemicals used, samples preparation and experimental procedures were described in Chapter 3. This chapter discusses the methodology used for the physicochemical experiments *i.e.,* density and viscosity. The experimental set-up for high and low pressures at different temperatures for the absorption of $CO_2$ in the aqueous MDEA - [gua][OTf] blended systems were detailed. For the low pressure study, acid-base titration method was used to obtain the $CO_2$ loading, meanwhile, for high-pressure work, a different approach *i.e,* pressure change measurement was used.

Chapter 4 presents the density of the binary and ternary MDEA – [gua][OTf] blended systems at temperature range of 293 to 333 K and constant atmospheric pressure. Extended data on thermal expansion and correlation of density as a function of temperature, concentrations of MDEA and [gua][OTf] were also presented.

Chapter 5 reports the viscosity of aqueous [gua][OTf] and the effect of the addition of [gua][OTf] to 4 M MDEA. A correlation of viscosity as a function of concentration of MDEA and [gua][OTf] at temperature of 303.2 K to 333.2 K was also obtained.

The effect of 1 M [gua][OTf] addition to 4 M MDEA and the aqueous [gua][OTf] itself to the capturing of $CO_2$ at high pressures was discussed in Chapter 6. The experiments were done at pressure range of 500 to 3000 kPa and temperature range of 303 to 333 K. The experimental data were then correlated in a single equation that takes into account the effect of temperature, pressure, and concentration of ionic liquids and amine.

Chapter 7 presents the $CO_2$ solubility analysis at different composition of aqueous MDEA – [gua][OTf] blended systems at low pressures. Tests were conducted at $CO_2$ partial pressures of 10, 50 and 100 kPa and temperature of 303.2 K. The simplified overall equilibrium constant was developed for the systems and the modeled results were compared with experimental results. The comparison to the other amines and other ionic liquids were also made and discussed in this chapter.

Finally, chapter 8 summarizes the conclusion of the research and recommendations for future work in this area.

# Chapter 2: LITERATURE REVIEW

## 2.1 Carbon capture technology

There are three technological pathways that can be used for $CO_2$ capture: post-combustion capture, pre-combustion capture and oxy-combustion [26-30]. In post-combustion capture, the $CO_2$ is separated from other flue gas constituents either originally present in the air or produced by combustion. In pre-combustion capture, carbon is removed from the fuel before combustion, and in oxy-combustion, the fuel is burned in an oxygen stream that contains little or no nitrogen. Generally, post-combustion capture applies primarily to coal-fueled power generators that are air fired. Pre-combustion capture applies to gasification plants. Oxy-combustion can be applied to new plants or retrofitted to existing plants [31].

In an industrial gas absorption process, it is desirable to achieve fast absorption rates and high solute capacities into a solvent that is easily regenerated and which volume make-up is minimized [32, 33]. The judging criteria for acid gas removal (AGR) process are generally the capture effectiveness, process economy, energy consumption, and other technical and operational issues [34]. Table 2.1 discusses the advantages and disadvantages of post-combustion, pre-combustion and oxy-combustion [26].

Table 2.1. The advantages and disadvantages of post-combustion, pre-combustion and oxy-combustion [26].

| | Advantages | Barriers to implementation |
|---|---|---|
| Post-combustion | • Applicable to the majority of existing coal-fired power plants<br>• Retrofit technology option | Flue gas is:<br>• Dilute in $CO_2$<br>• At ambient pressure<br>This results in:<br>• Low $CO_2$ partial pressure<br>– Significantly higher performance or circulation volume required for high capture levels<br>– $CO_2$ produced at low pressure compared to sequestration requirements |
| Pre-combustion | • Synthesis gas is:<br>Concentrated in $CO_2$<br>• High pressure<br>This results in:<br>• High $CO_2$ partial pressure<br>– increased driving force for separation<br>– more technologies available for separation<br>• Potential for reduction in compression costs/ loads | • Applicable mainly to new plants, a few gasification plants are currently in operation<br>• Barriers to commercial application of gasification are common to pre-combustion capture<br>– availability<br>– cost of equipment<br>– extensive supporting systems requirements |
| Oxy-combustion | • Very high $CO_2$ concentration in flue gas<br>• Retrofit and repowering technology option | • Large cryogenic $O_2$ production requirement may be cost prohibitive<br>• Cooled $CO_2$ recycle required to maintain temperatures within limits of combustor materials<br>– decreased process efficiency<br>– added auxiliary load |

Absorption is undoubtedly the single most important operation of a gas purification process, which, in term, refers to the transfer of a component in a gas phase to a liquid phase in which it is soluble. It occurs physically and/ or chemically. The physical gas absorption can be enhanced chemically through reactions between the gas and the solvent. The absorption process depends on the operating temperature and pressure, as well as on the nature of the gases and the absorption liquid. Typically, the gas absorption takes place at low temperatures (around or somewhat above room temperature) and elevated pressures (up to ~ 4 MPa or more), whereas the gas desorption (*i.e.* the solvent regeneration in the stripper) occurs at elevated temperatures (~390 K or more) and low pressures (in particular at low partial pressures of the gas) [35]. Since absorption increases with pressure, operating pressures are determined by $CO_2$ removal specifications and economics. In acid gas absorption processes, a solvent is used to dissolve preferentially more $CO_2$, and/ or $H_2S$ than the other stream gas constituents such as oxygen, nitrogen, carbonyl sulfide (COS) and other minor and volatile impurities present in the gas.

A favorable characteristic of the acid gas absorption is that, with the choice of the proper solvent, the absorption and stripper steps can be coordinated in order to create an efficient continuous process, and as well it is possible to carry selective removal of $H_2S$ from $CO_2$ containing gas streams. The absorption is competitive for large-scale applications, especially at high $CO_2$ partial pressures, and when contaminants and other solvent-reactive gases are present in a minimum proportion in the gas stream.

The most commonly used technology today for low concentration $CO_2$ capture is absorption with chemical solvents. Chemical absorption [36] is typically used for the removal of remaining acid impurities such as $CO_2$ and when the gas purity is a downstream constraint. It uses the different reactivities of various gases with sorbents to separate them. The separation of $CO_2$ by chemical means involves one or more reversible chemical reactions between $CO_2$ and another material to produce a liquid or solid species, afterwards the reacted species in the loaded solvent are decomposed by heating to liberate $CO_2$ and regenerate the material that reacted with $CO_2$.

For separating $CO_2$ from flue gas, chemical absorption appears appropriate since $CO_2$ is acidic and the majority composition of the rest of the flue gas is nitrogen. It has been used successfully for low-pressure gas streams containing between 3 % and 25 % of $CO_2$, but the large solvent regeneration costs associated with the process hamper its application to higher $CO_2$ contents. The degree of absorption is limited by the fixed stoichiometry of the chemical reaction. Consequently, the use of this process for $CO_2$ - rich gas streams will lead to high solvent circulation flow rates and high energy requirements [37]. In addition, other concern is the control of impurities and minor components in the flue gas including $SO_2$, $O_2$, *etc.* that may degrade the sorbents. These components have to be removed before the gas enters the absorber, or treated with appropriate measures. Lastly, because many sorbents are corrosive, only diluted solutions are used.

In fact, one of the most commercially applied technologies for capturing $CO_2$ is chemical absorption by using aqueous alkanolamine. The $CO_2$ will be partly converted to non-volatile ionic species by the basic alkanolamine and partly dissolved physically in this reactive absorption solvent [38]. However, problems of scale, efficiency, and stability become barriers when chemical solvents are used for high volume gas flows with a relatively smaller fraction of valuable product. The processes require large amounts of material undergoing significant changes in conditions, leading to high investment costs and energy consumption. In addition, degradation and oxidation of the solvents over time produces products that are corrosive and may require hazardous material handling procedures [39]. Figure 2.1 [40] illustrates a process flow diagram (PFD) of an alkanolamine treating unit that is being commonly practiced in the industry.

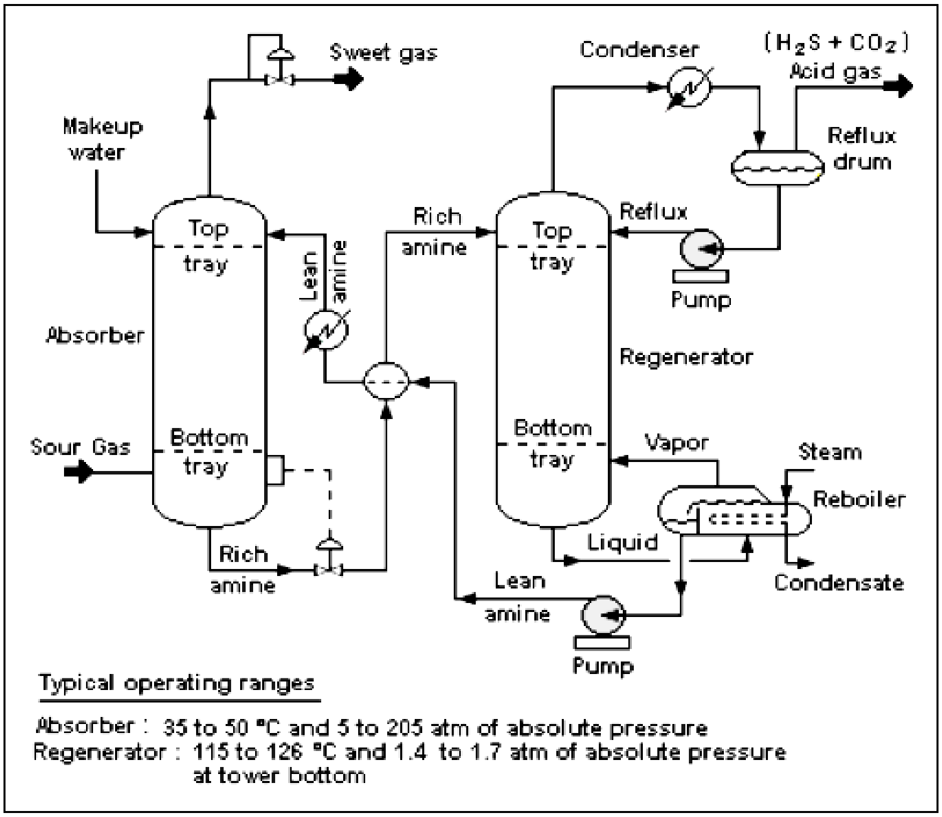

Figure 2.1. Process flow diagram (PFD) of an alkanolamine treating unit [40].

As illustrated in Figure 2.1, the lean alkanolamine solution is pumped to the top of an absorber where the $CO_2$ are removed from the gas by absorption into the solution. Here is where the physical property and the mass transfer efficiency are needed. The rich alkanolamine solution is then preheated and flows to a regenerator or still, where the acid gases are stripped from the solution by steam generated in a reboiler to produce concentrated $CO_2$ waste streams. The $CO_2$ are taken from the top of the still through a condenser, where most of the steam is condensed. This condensate is separated from the $CO_2$ and returned to the top of the still as reflux. The $CO_2$ would be vented, co-fed to the gas turbine, or even sequestered, if warranted. The lean alkanolamine solution is cooled and returned to the top of the absorber. It is generally considered advisable to have high solution rates to minimize corrosion [40]. However, high solution rates result in increased investment and utility costs, and therefore a compromise is made in the design and operating conditions.

On the other hand, there is a physical absorption, which can also be used just as successfully [41]. The main advantage of such process is that (unlike chemical absorption) physical solvents have no absorption limitation. In physical absorption, the gas $CO_2$ molecules are dissolved in a liquid solvent, and no chemical reaction takes place. This absorbent allows a gas to permeate a solid or liquid under one set of conditions, and desorb under others. The binding between the $CO_2$ molecules and solvent molecules, being either Van der Waals type or electrostatic, is weaker than that of chemical bonds in chemical absorption. The amount of $CO_2$ absorbed by the solvent is determined by the vapour-liquid equilibrium of the mixture, which is governed by the pressure and temperature. The rate of absorption or desorption is temperature and pressure dependent. Typically, it is linearly proportional to its partial pressure (Henry's law). Smaller differences in conditions require less energy, but require more absorbent to capture $CO_2$ at an equivalent rate.

Figure 2.2 gave the $CO_2$ gas loading in several solvents as a function of $CO_2$ partial pressure. The curves show linear relations between the partial pressure and $CO_2$ loading for physical solvents, and non-linear relations for chemical solvents. At high $CO_2$ partial pressure, the $CO_2$ loading capacity of the solvent is higher for a physical solvent than that of chemical solvent. Physical solvent processes are thus particularly appropriate for the treatment of $CO_2$ - rich gas streams and more effective when the partial pressure of the gas to be absorbed is high. The amount of gas absorbed also depends on the temperature. The lower the temperature, the more gas is absorbed.

Physical adsorption relies on the affinity of $CO_2$ to the surface of a material under certain conditions without forming a chemical bond. Adsorbents can separate $CO_2$ from a stream by preferentially attracting it to the material surface at high pressures through weak interactions such as van der Waals forces. During capture, the chemical potential of the adsorbed $CO_2$ is lower than the chemical potential of $CO_2$ in the gas mixture.

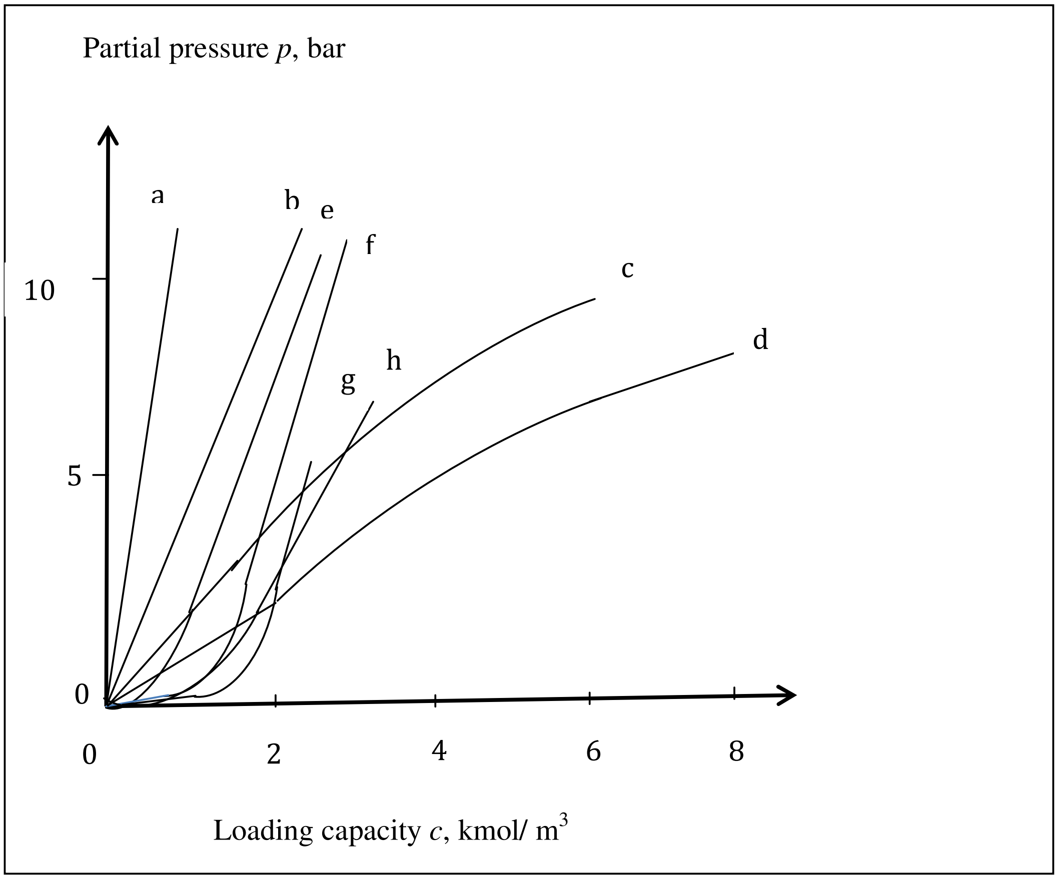

Figure 2.2. Equilibrium curves of $CO_2$ in various solvents. Physical absorption: a) $H_2O$ (30 °C); b) *N*-methyl-2-pyrrolidone (110 °C); c) Methanol (-15 °C); d) Methanol (-30 °C); Chemical absorption: e) Hot potassium carbonate solution (110 °C); f) Sulfinol solution (50 °C); g) 2.5 M Diethanolamine solution (50 °C); h) 3 M Amisol DETA solution [41].

The typical characteristics of chemisorption and physisorption processes tabulated in Table 2.2 [42].

Table 2.2. Typical characteristics of absorption processes [42].

| Characteristics | Chemisorption | Physisorption |
|---|---|---|
| Bonding | A chemical bond, involving substantial rearrangement of electron density, is formed between the absorbate and substrate. The nature of this bond may lie anywhere between the extremes of virtually complete ionic or complete covalent character | The only bonding is by weak Van der Waals-type forces. There is no significant redistribution of electron density in either the molecule or at the substrate surface |
| Material specificity (variation between substrates of different chemical composition) | Substantial variation between materials | Slight dependence upon substrate composition |
| Crystallographic specificity (variation between different surface planes of the same crystal) | Marked variation between crystal planes | Virtually independent of surface atomic geometry |
| Temperature Range (over which absorption occurs) | Virtually unlimited<br>(but a given molecule may effectively absorb only over a small range) | Near or below the condensation point of the gas<br>(*e.g.* Xe < 100 K, $CO_2$ < 200 K) |
| Absorption Enthalpy | Wide range<br>(related to the chemical bond strength)<br>- typically 40 - 800 kJ $mol^{-1}$ | Related to factors like molecular mass and polarity<br>- typically 5 – 40 kJ $mol^{-1}$ (similar to heat of liquefaction) |
| Nature of Adsorption | Often dissociative<br>Maybe irreversible | Non-dissociative<br>Reversible |
| Saturation Uptake | Limited to one monolayer | Multilayer uptake possible |
| Kinetics of Absorption | Varied – often an activated process | Fast – since it is a non-activated process |

## 2.2 The solvent capture for acid gas removal

Varieties of solvents have been used for AGR process either chemical and/ or physical. The advantages with chemical absorbents are strong bonding, due to chemical reactions, and low equilibrium partial pressure. However, after the solvent has reached chemical saturation only weak physical absorption takes place. Figure 2.3 exhibits the general trends of loading capacity for chemical and physical solvents at a range of partial pressure of $CO_2$.

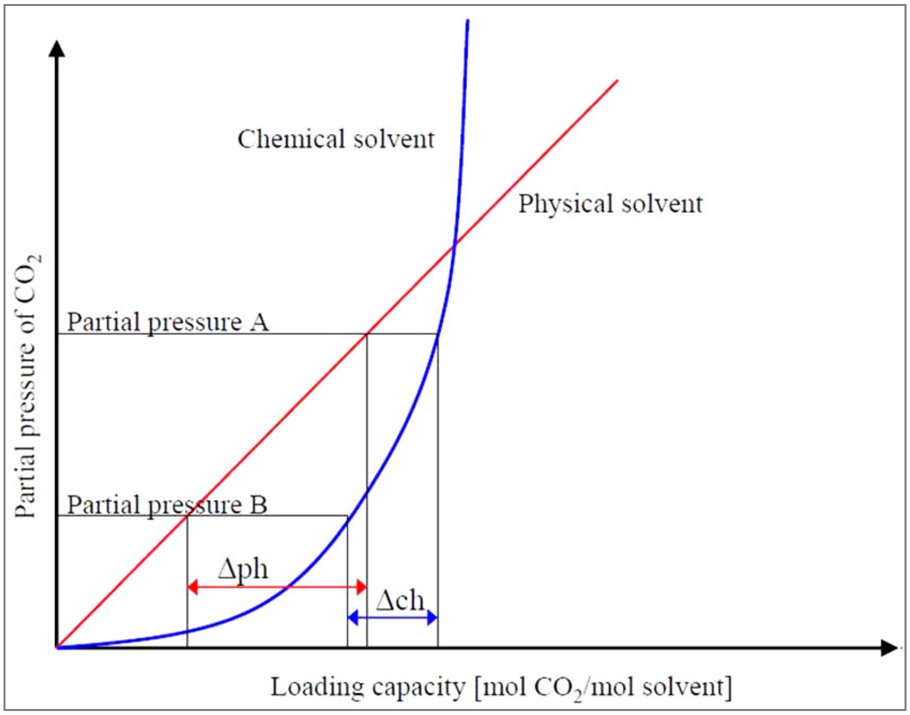

Figure 2.3. General trends for loading capacity of chemical and physical solvents at a range of partial pressure of $CO_2$.

The loading capacity for physical solvents increase as the partial pressure of $CO_2$ increases. Thus, chemical solvents have higher loading capacity at low partial pressures and physical solvents have higher loading capacity at high partial pressures. The solvent with the highest loading capacity is preferred, since less solvent is used to absorb the same amount of $CO_2$. Therefore chemical solvents are most common in post-combustion (low partial pressure of $CO_2$) and physical solvents most common in pre-combustion (high partial pressure of $CO_2$). Meanwhile, Table 2.3 summarized some of the advantages and disadvantages of chemical and physical solvents [43].

Table 2.3. Comparison of chemical and physical solvents [43].

| Solvent | Advantage | Disadvantage |
|---|---|---|
| Chemical | • Relatively favorable to $CO_2$ partial pressure<br>• Can reduce $CO_2$ to ppm levels | • High energy requirements for regeneration of solvent<br>• Generally not selective between $CO_2$ and $H_2S$<br>• Amines are in water solution, and thus the treated gas leaves saturated with water |
| Physical | • Low energy<br>• Requirements for regeneration<br>• Can be selective between $CO_2$ and $H_2S$ | • Maybe difficult to meet $H_2S$ specifications<br>• Very sensitive to acid gas partial pressure |

In regards, the factors defining a promising absorption solvent for acid gas removal are:

i) A solvent should have an increased $CO_2$ absorption capacity resulting in lower circulation rates. An estimated target for fuel plants absorption capacity would be about 1 kg of $CO_2$ per kg solvent.

ii) Solvent with higher gas selectivity and less co-absorption of the other gaseous components.
iii) Solvents with low vapor pressure for reducing make-up volume and contamination of the gas stream with a volatile solvent.
iv) Easier to regenerate and therefore less energy demanding.
v) Solvent with high degradation resistance, and wider range of operation temperatures.
vi) Solvent that does not promote corrosion of the equipment.
vii) Foaming of the solvent is minimized.
viii) Environmentally benign.

### 2.2.1 Chemical solvents

Chemical solvents are defined as solvents in which acid gases react to form a complex. They are typically used for the removal of the remaining acid impurities and when gas purity is a downstream constraint. The currently preferred chemical solvent technology for carbon capture is amine-based chemical solvent. $CO_2$ in the gas phase dissolves into a solution of water and amine compounds. The amines react with $CO_2$ in solution to form protonated amine ($AH^+$), bicarbonate ($HCO_3^-$), and carbamate ($ACO_2^-$). Reaction rates with specific acid gases differ among the various amines. In addition, amines vary in their equilibrium absorption characteristics and have different sensitivities with respect to solvent stability and corrosion.

In fact, the most commonly used chemical solvents are monoethanolamine (MEA), diethanolamine (DEA), methyldiethanolamine (MDEA), 2-amino-2-methyl-

1-propanol (AMP), diisopropanolamine (DIPA), diglycolamine (DGA) [44-46] and diamine 2-[(2-aminoethyl) amino]-ethanol (AEEA) [47]. There is also another type of chemical solvent such as hot potassium carbonate and $CO_2$-binding organic liquids ($CO_2$BOLs) [48], which has also been studied. Figure 2.4 showed the structural formulas for the common alkanolamines used in the gas treating [42].

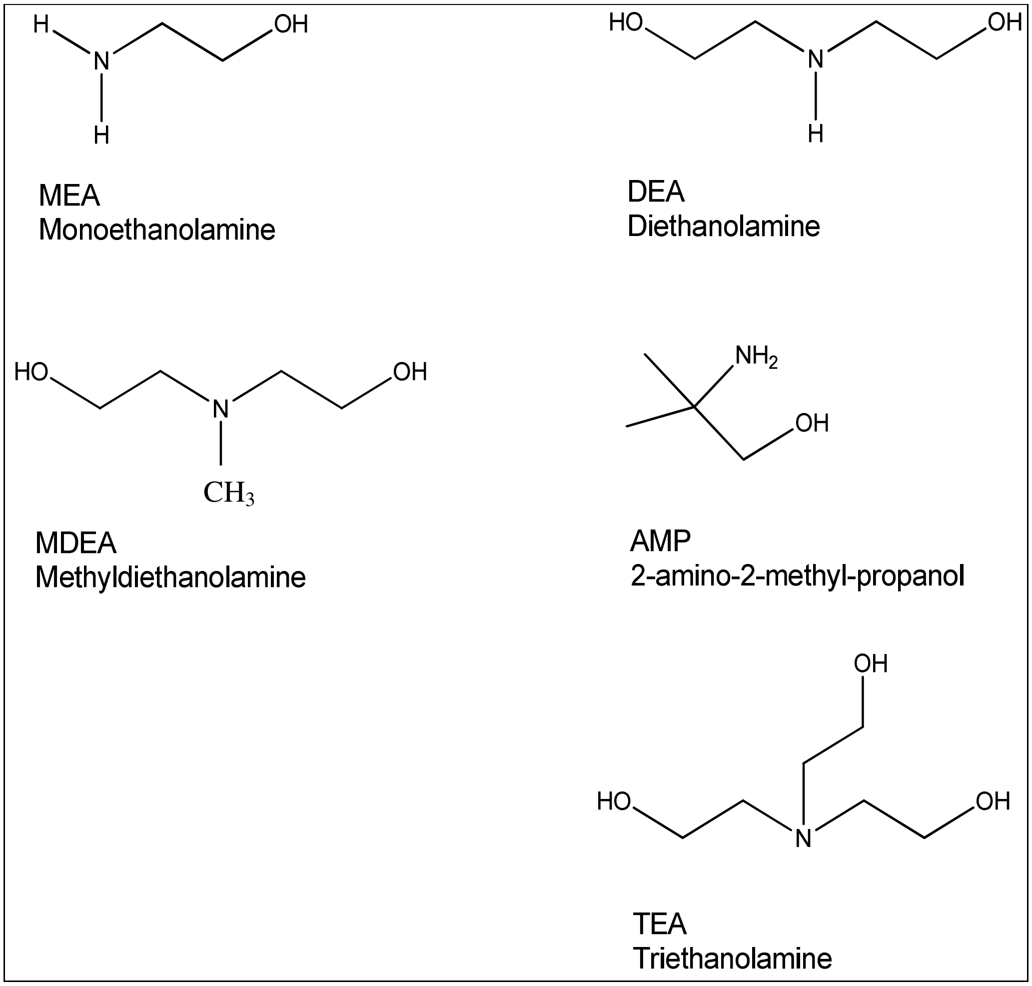

Figure 2.4. Several structural formulas for alkanolamines used in gas treating [42].

Visibly, each alkanolamine has at least one hydroxyl group (-OH) and one amino group ($NH_2$, -NHR, or $–NR_2$). In general, it can be considered that the hydroxyl group serves to reduce the vapour pressure and increase the water solubility, while the amino group provides the necessary alkalinity in water solutions to cause the absorption of acidic gases [49-51]. Alkanolamines which have two hydrogen atoms directly attached to a nitrogen atom, such as monoethanolamine (MEA), is called primary amines are generally the most alkaline. On the other hand, methyldiethanolamine (MDEA) represents completely substituted ammonia molecules with no hydrogen atoms attached to the nitrogen, and are called tertiary amines.

The effectiveness of any alkanolamine for $CO_2$ absorption is due primarily to its alkalinity. These types of solvents have the ability to remove the acid gases to ppm levels, even at low pressure. Although alkanolamines have been used for many years, especially in the removal of acid gases from natural gas, there are still several drawbacks, which need to be improved. Generally, the chemical solvents are not selective between $CO_2$ and $H_2S$, favor high energy for regeneration, amine solvent loss, degradation, release of volatile organic compounds, equipment corrosion and briefly limited to lower amine concentration [52].

From the absorption point of view, primary alkanolamine *i.e.* MEA is the most commonly used. About 75 – 90 % of the $CO_2$ is captured using a MEA-based technology, producing a gas stream of high $CO_2$ content (> 99 %) [53]. By taking into consideration of the costs of regeneration, tertiary alkanolamines which is *N*-metyldiethanolamine (MDEA) = 2, 2'-methyliminodiethanol is much more attractive [54]. MEA reacts rapidly with $CO_2$ to form carbamate with a stoichiometric loading of 0.5 mol of $CO_2$ per mole of amine [55]. Because of relatively higher enthalpy of absorption associated with the formation of carbamates ions, the cost of regenerating MEA is very high. MDEA shows high absorption capacity towards $CO_2$ and does not perform reaction which produces the carbamates, reducing the foaming, corrosion and fouling problems in equipment used in the industrial process for the purification of hydrocarbon rich gas streams [56-58].

On the other hand, MDEA has a low rate of reaction with (and therefore absorption of) $CO_2$ [59-61]. This cannot form the carbamate because MDEA does not posses a hydrogen atom attached to the nitrogen, thus cannot react directly with $CO_2$ to form carbamate. This leads to a much slower acid-base reaction. Thus, they are able to carry out a high total $CO_2$ removal, but at much lower rates.

### 2.2.2 Blended alkanolamines

Because of the need to exploit poorer quality crude and natural gas coupled with increasingly strict environmental regulations, highly economical and selective acid gas treating is becoming more important. As a result, there has been a resurgence of interest in improving alkanolamine solvents and particularly in aqueous blends of alkanolamines [62-65]. By utilizing the advantages of each amine, the blended amines have been suggested to be used in the absorption of acid gases.

This brings about a significant improvement in absorption capacity and absorption rate and a great saving in solvent regeneration energy requirement. Besides, it also offers the advantage of setting the selectivity of the solvent toward $CO_2$ by judiciously mixing the amines in varying proportions which results in an additional degree of freedom for achieving the desired separation to meet the required specification of the treated gas [66-70].

At present, mixture of primary (*i.e.* MEA) or secondary (*i.e.* DEA) alkanolamine with a tertiary alkanolamine (*i.e.* MDEA) is suggested to capitalize on the advantages of each amine. Some $CO_2$ capture applications benefit from a mixture of physical and chemical solvents. The most commonly used examples are Sulfinol, a mixture of the physical solvent sulfolane and the amines DIPA or MDEA, and Amisol, a mixture of methanol and secondary amines. Chakravarty *et al.* [71] suggested the use of blends. These hybrid solvents attempt to exploit the positive qualities of each constituent under special conditions.

However, the established alkanolamine system, are continuously facing several disadvantages [72];

i) solvent regeneration at high temperatures (up to 413 K) causes around 10 % decrease in power generation efficiency if the absorption process is integrated in the power plant
ii) solvent loses due to infinite vapor pressure of the solvent
iii) deactivation of the solvent by formation of heat-stable salts with oxygen (energy-intensive reclaiming is necessary)
iv) corrosion in the plant

Therefore, there are uprising attempts nowadays to diverge the focus for finding new solvents (absorbents) in capturing the $CO_2$.

### 2.2.3 Physical solvents

Typical physical solvents are methanol, N-methyl-pyrrolidone, polyethylene glycol, dimethylether, propylene carbonate and sulfolane. Unlike chemical solvents, physical solvents are non-corrosive, requiring only carbon steel construction.

Absorption in most current physical solvent systems occurs at high partial pressure of $CO_2$ and low temperatures. In general, the economics of $CO_2$ recovery is strongly influenced by the partial pressure of $CO_2$ in the feed gas. At low partial pressures, physical solvents are impractical because the compression of the gas for physical absorption is expensive. However, if the gas is available at high pressure, physical solvents might be a better choice than chemical solvents [73].

The concentration of heavy hydrocarbons in the feed gas also affects the choice of gas treating solvent. If the concentration of heavy hydrocarbons is high, a physical solvent may not be the best option due to higher co-absorption of hydrocarbons, particularly pentanes. Unlike natural gases where hydrocarbon co-absorption can be a problem for physical solvents, synthesis gases do not contain appreciable quantities of hydrocarbons. This makes physical solvents particularly applicable to synthesis gas treating. The interaction between $CO_2$ and the absorbent is weak relative to chemical solvents, decreasing the energy requirement for regeneration. Capacity can be higher than chemical solvents, since it is not limited by the stoichiometry of the chemical system [74].

Selexol, a liquid glycol-based solvent, has been used for decades to process natural gas, both for bulk $CO_2$ removal and $H_2S$ removal [75]. Glycol is effective for capturing both $CO_2$ and $H_2S$ at higher concentration. However, the $CO_2$ is released at near atmospheric pressure, requiring recompression for transportation and geologic storage. The Rectisol process, based on low temperature methanol, is another physical solvent process that has been used for removing $CO_2$. Glycerol carbonate is interesting because of its high selectivity for $CO_2$, but it has a relatively low capacity [76].

## 2.3 Process chemistry

Two molecules of an alkanolamine, in the presence of $CO_2$, react to form a carbamic salt, presumably by way of the corresponding carbamic acid. Carbamic anions can be further converted to isocyanates or may react with alkyl halides to yield urethanes, thus providing an alternative synthetic equivalent to highly toxic phosgene. Furthermore, carbamates are thermally unstable and release $CO_2$ upon heating [77]. This can be very useful under several circumstances.

The principal reactions occurring in the $CO_2$/ alkanolamine/ $H_2O$ system used to absorb $CO_2$ may be represented as follows;

Ionization of water:

$$H_2O \rightleftharpoons H^+ + OH^- \qquad (2.1)$$

Hydrolysis and ionization of dissolved $CO_2$:

$$CO_2 + H_2O \rightleftharpoons HCO_3^- + H^+ \qquad (2.2)$$

Protonation of alkanolamine:

$$RNH_2 + H^+ \rightleftharpoons RNH_3^+ \qquad (2.3)$$

Carbamate formation:

$$RNH_2 + CO_2 \rightleftharpoons RNHCOO^- + H^+ \qquad (2.4)$$

Reactions (2.1), (2.2), (2.3) and (2.4) account for the principal species present in aqueous alkanolamine treating solutions. These species are the unionized molecules $H_2O$, $CO_2$ and $RNH_2$ and the ions $H^+$, $OH^-$, $HCO_3^-$, $RNH_3^+$, and $RNHCOO^-$. Tertiary amine solutions undergo reactions (2.1) to (2.3), but cannot react directly with $CO_2$ to form carbamates by reaction (2.4). If reaction of equation (2.4) is dominant, as it is with primary alkanolamines, the carbamate ions ties up an alkanolammonium via equation (2.3) and the capacity of the solution for $CO_2$ is limited to approximately 0.5 mole of $CO_2$/ mole of amine, even at relatively high partial pressures of $CO_2$ in the gas.

The reason for this limitation is the high stability of the carbamate and its low rate of hydrolysis to bicarbonate. With tertiary alkanolamines, which are unable to form carbamates, a ratio of one mole of $CO_2$ per mole of amine can be achieved theoretically. However, the $CO_2$ reaction (2.2), which does not produce carbamate is very slow. In order to overcome the slow rate of reaction, an activator, typically another amine is added to increase the rate of hydration of dissolved $CO_2$ [78-82].

## 2.4 Ionic liquids

The first ionic liquid was synthesized in 1914 [83]. It was $[EtNH_3][NO_3]$ which has a melting point of 12 ºC [84, 85]. The most common ionic liquids, $[emim][PF_6]$ and $[emim][BF_4]$, where $[emim]^+$ is the 1-ethyl-3-methyl-imidazolium cation, were first discovered in 1994 and 1992, respectively [86]. The analogous [bmim][$PF_6$] and [bmim][$BF_4$] ionic liquids followed shortly after [87].

Ionic liquids have invoked a rising interest in the last decades with a diversified range of applications (refer to Figure 2.5) [88]. The types of ionic liquid available have also been extended to include new families and generations of ionic liquids with more specific and targeted properties. This expanding interest has led to a number of reviews on their physico-chemical properties, the design of new families, the chemical engineering and the wide range of arrangements in which ionic liquids have been utilized (liquid phase, multiphase, immobilized on supports and *etc.*) [89].

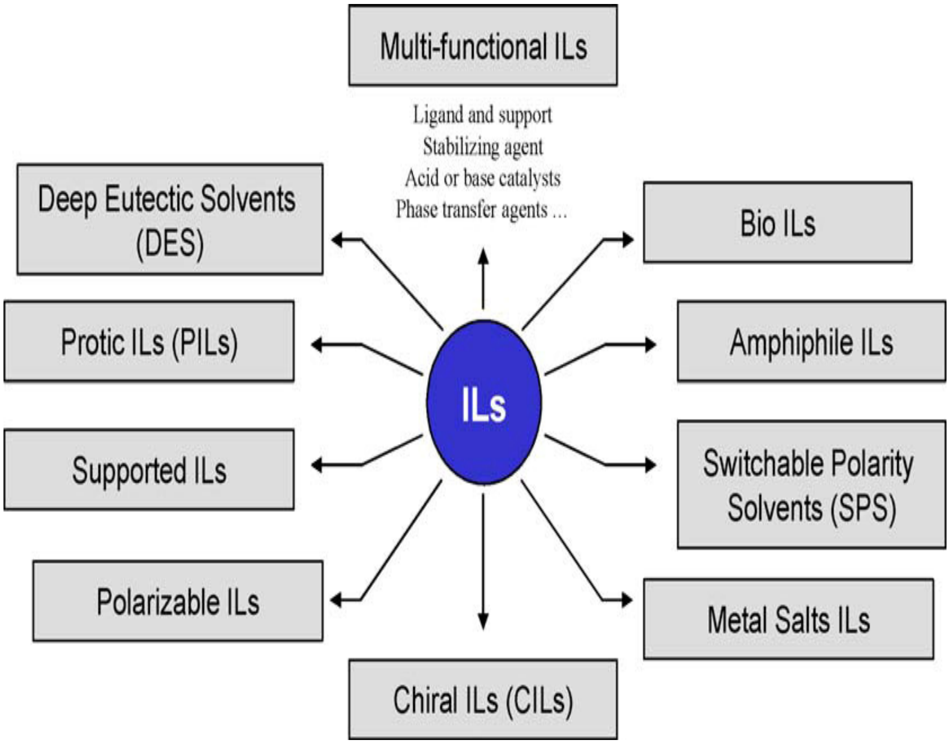

Figure 2.5. Evolution of ionic liquid generations [88].

Ionic liquids are a broad category of salts, typically containing a bulky asymmetric organic cation and either an inorganic or organic anion. The cations are generally bulky organic with low symmetry [90]. Those described are commonly based on ammonium, sulfonium, phosphonium, lithium, imidazolium, pyridinium, pyrroidium, thiazolium, triazolium, oxazolium and pyrazolium differently substituted as shown in Figure 2.6 [91].

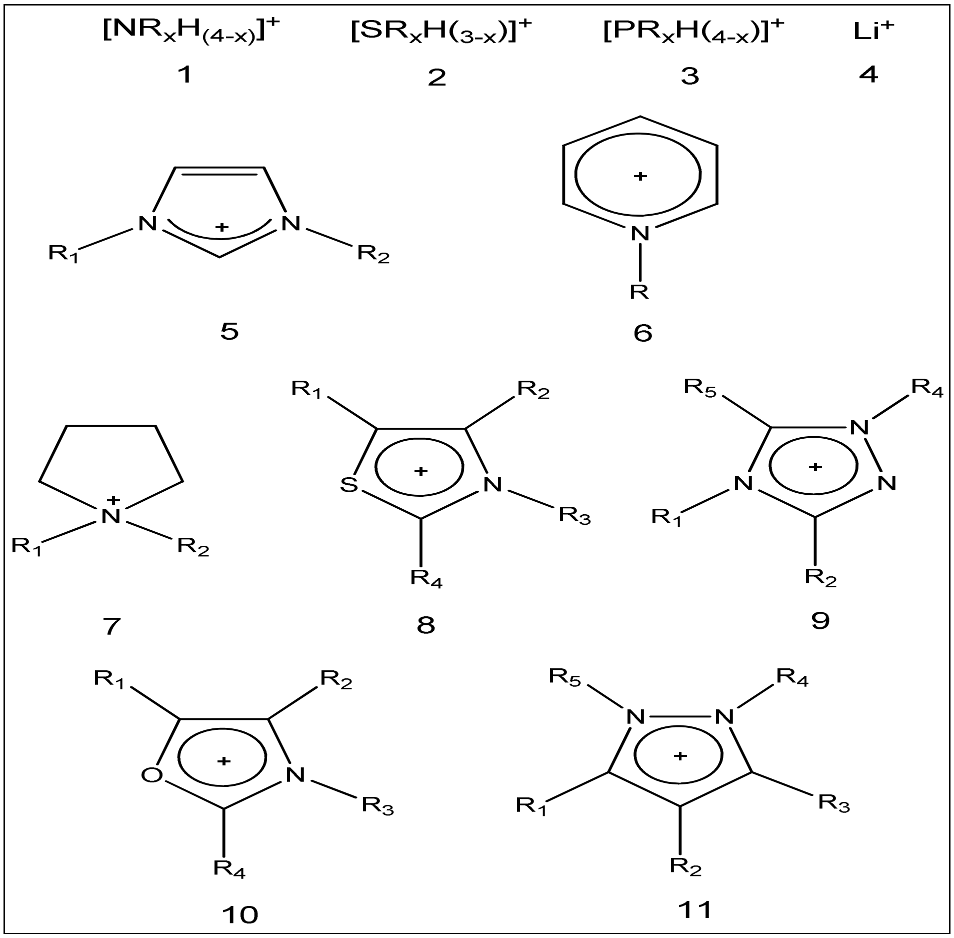

Figure 2.6. Some examples of cations described in ionic liquids based on 1-ammonium, 2-sulfonium, 3-phosphonium, 4-lithium, 5-imidazolium, 6-pyridinium, 7-pyrrolidium, 8-thiazolium, 9-triazolium, 10-oxazolium and 11-pyrazolium [91].

The anions of ionic liquids can be classified into two parts: those, which give polynuclear anions, *e.g.* $Al_2Cl_7^-$, $Al_3Cl_{10}^-$, $Au_2Cl_7^-$, $Fe_2Cl_7^-$, $Sb_2F_{11}^-$. These anions are formed by the reaction of the corresponding Lewis acid, *e.g.* $AlCl_3$ with the mononuclear anion, *e.g.* $AlCl_4^-$. They are particularly air and water sensitive. The second class of anions corresponds to mononuclear anions which lead to neutral, stoichiometric ionic liquids, *e.g.* $BF_4^-$, $PF_6^-$, $SbF_6^-$, $ZnCl_3^-$, $CuCl_2^-$, $SnCl_3^-$, $N(CF_3SO_2)_2^-$, $N(C_2F_5SO_2)_2^-$ $N(FSO_2)_2^-$, $C(CF_3SO_2)_3^-$, $CF_3CO_2^-$, $CF_3SO_3^-$, $CH_3SO_3^-$, *etc.* [92].

It has been shown that there are $10^{14}$ possible combinations for ionic liquids. The melting points of these ionic liquids are frequently found to be below 150 ºC [93] and occasionally as low as -96 ºC [94]. Some ionic liquids are stable up to 773 ºC [95-96]. The nature of the cation and anion determines the physical and chemical properties of the ionic liquids [97-98]. Ionic liquids have good thermal stability and do not decompose over a large temperature range, thereby making it feasible to carry out reactions that require high temperatures. They can be stored without decomposition for a long period of time.

Aside from these, ionic liquids have more general appealing properties such as non-flammability, high solvation capacity, slow degradation rates and lower heats of reaction. Ionic liquids are also termed as “green” and designer solvents because of their less degrading effects on the environment and they can be custom-made for specific applications [99-103]. This is due to the existing dependence between the properties and the structure of the constituent ions of the ionic liquids [104]. More interesting is that $CO_2$ can significantly dissolve in the ionic liquids as compared to conventional organic solvents even in the case of physical absorption. Such higher solubility shows great potential of ionic liquids to act as a good absorbent for $CO_2$ capture.

### 2.4.1 Ionic liquids for $CO_2$ absorption

Ionic liquids are experiencing an intense focus due to their diverse chemistry and potential applications. This material can be used as an absorbent for gas absorption operations in order to improve the process economy and general efficiency of gas separation. Figure 2.7 shows the computed electron density for a $CO_2$ molecule interacting with the ionic liquid [hmim][$NTf_2$]. The cation [hmim], charge +1, is shown at the top. The anion [$NTf_2$], charge -1, is at the bottom. A single $CO_2$ molecule is shown in between the two. The blue regions on the surface show areas of relatively large positive charge, while red areas show large negative charge. Green areas are more or less neutral [105].

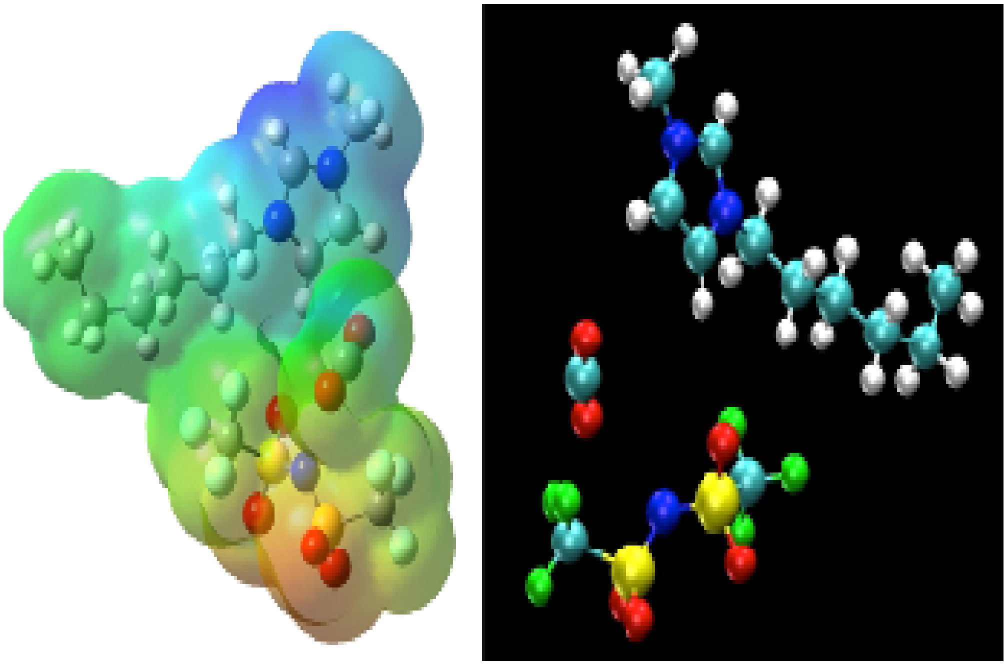

Figure 2.7. Schematic of an ionic liquid interaction with carbon dioxide [105].

Since the past decades, ionic liquids have been investigated by several groups of researches due to their appealing properties. These ionic liquids are regarded as a possible replacement to the conventional solvents (such as alkanolamines) in gas absorption process.

In term of physical solubility, it has been shown that $CO_2$ has the highest gas solubility in ionic liquids combined with a good selectivity of all measured gases including ethylene, ethane, methane, argon, oxygen, carbon monoxide, hydrogen, and nitrogen in ionic liquids as studied by several researchers [106-114]. The solubility of those gases in 1-butyl-3-methylimidazolium hexafluorophosphate, [bmim][$PF_6$] at the temperature range between 10 and 50 °C and pressure up to 13 bar proves the superiority of ionic liquids over various other organic solvents like heptane, cyclohexane, benzene, ethanol and acetone as shown in Figure 2.8 [115].

Of the ionic liquids studied, the anion played the biggest role in $CO_2$ solubility [116, 117], a fact that was supported by an X-ray diffraction study by Kanakubo *et al.* [118]. Anions that contain fluoroalkyl groups were found to have some of the highest $CO_2$ solubilities, and as the quantity of fluoralkyl group increased, the $CO_2$ solubility also increased. Previous study showed $CO_2$ solubility for 1-butyl-3-methylimidazolium ([bmim]$^+$) based ionic liquids at 363 K increased in the order of nitrate ([$NO_3$]$^-$) < tetrafluoroborate ([$BF_4$]$^-$) < dicyanamide ([DCA]$^-$) ~ hexafluorophosphate ([$PF_6$]$^-$) ~ trifluoromethanesulfonate ([OTf]$^-$) < bis(trifluoromethyl)sulfonylimide ([$Tf_2N$]$^-$) < tris(trifluoromethylsulfonyl)methide ([methide]$^-$).

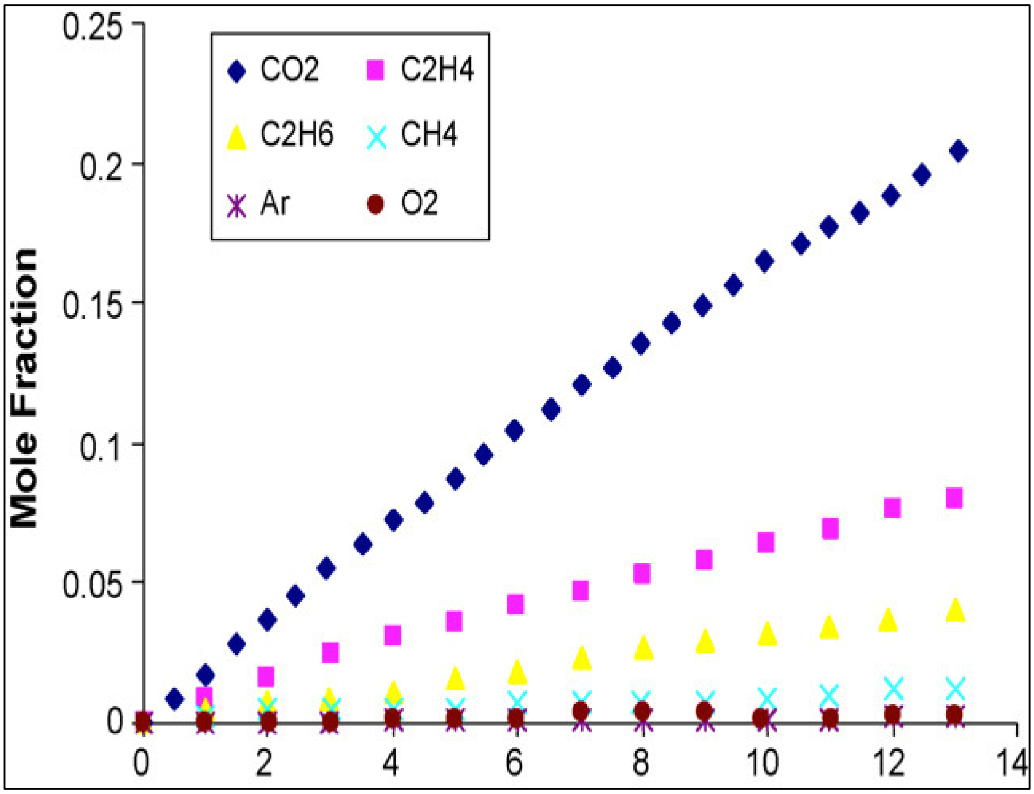

Figure 2.8. Solubilities of $CO_2$, $C_2H_4$, $C_2H_6$, $CH_4$, Ar and $O_2$ in [bmim][$PF_6$] at 25 °C [115].

In proportion to the structural features and absorption mechanisms, the ionic liquids can be classified into two categories, conventional ionic liquids and task-specific ionic liquids. The conventional ionic liquids could absorb less amount of $CO_2$ as compared to task-specific ionic liquids because of the physical interactions between $CO_2$ and ionic liquids [118, 119]. Apparently, most conventional room temperature ionic liquids portray a typical behaviour of physical solvent [120-124].

Amongst other conventional ionic liquids, imidazolium-based cation ionic liquids possess highest $CO_2$ solubility and selectivity for $CO_2$ relative to $N_2$ and $CH_4$ [125-128]. Kamps *et al.* [129] presented solubility data of $CO_2$ in [bmim][$PF_6$] at temperatures range of 293 to 393 K. As reported in the pressure region investigated, the solubility pressure practically increases linearly with increasing amount of the gas in the liquid. This is the distinctive behavior of gas dissolution in ionic liquid which is purely a physical phenomenon, with no chemical reaction.

More imidazolium ionic liquids such as 1-butyl-3-methylimidazolium bis(trifluoromethylsulfonyl)imide ([bmim][$NTf_2$]), 1-hexyl-3-methylimidazolium bis(trifluoromethylsulfonyl) imide ([hmim][$NTf_2$]), 1-octyl-3-methylimidazolium bis(trifluoromethylsulfonyl)imide ([omim][$NTf_2$]), and 2,3-dimethyl-1-hexylimidazolium bis(trifluoromethylsulfonyl)imide ([hmmim][$NTf_2$]) are studied as solvents for $CO_2$ capture [130-135].

Solubilities on phosphonium ionic liquids; tributyl-tetradecyl-phosphonium mesylate ([$P_{444,14}$][$MeSO_3$]) and trihexyl-tetracyl-phosphonium dodecyl-benzene-sulfonate ([$P_{666,14}$][LABS]), hydroxyl ammonium ionic liquids; 2-hydroxy-ethyl-ammonium formate (HEF), 2-hydroxy-ethyl-ammonium acetate (HEA), 2-hydroxy-ethyl-ammonium lactate (HEL), tri-(2-hydroxy-ethyl) ammonium acetate (THEAA), tri-(2-hydroxy-ethyl) ammonium lactate (THEAL), 2-(2-hydroxy-ethoxy) ammonium formate (HEAF), 2-(2-hydroxy-ethoxy) ammonium acetate (HEAA), 2-(2-hydroxy-ethoxy) ammonium lactate (HEAL) and guanidine ionic liquids 1,1,3,3-tetramethyl-guanidium lactate (TMGL) were reported by Yuan *et al.* [136]. The results showed that all these ionic liquids are good sources for capture $CO_2$. For instance, at 15 bar of $CO_2$ partial pressure, the $CO_2$ solubility in 1-butyl-3-methylimidazolium hexafluorophosphate ([bmim][$PF_6$]) was about 23 mol % [137].

Blanchard *et al.* [138] determined the solubility of $CO_2$ in a series of imidazolium-type ILs including 1-*n*-butyl-3-methylimidazolium hexafluorophosphate ([bmim][$PF_6$]), 1-*n*-octyl-3-methylimidazolium hexafluorophosphate ([omim][$PF_6$]), 1-*n*-octyl-3-methylimidazolium tetrafluoroborate ([omim][$BF_4$]), 1-*n*-butyl-3-methyl imidazoliumnitrate ([bmim][$NO_3$]), 1-ethyl-3-methylimidazolium ethylsulfate ([emim][$EtSO_4$]) and *n*-butylpyridinium tetrafluoroborate ([*N*-bupy][$BF_4$]) in the pressure region from 0.1 to 10 MPa. The reported solubility of $CO_2$ follows the sequence of [bmim][$PF_6$]/ [omim][$PF_6$] > [omim][$BF_4$] > [N-bupy][$BF_4$] > [bmim][$NO_3$] > [emim][$EtSO_4$] (refer to Figure 2.9). The work concludes that the $CO_2$ solubility depends on the nature of both cation and anion species.

Furthermore, imidazolium-based ionic liquids have less than one-third the heat capacity of water (1.30 $J\ g^{-1}\ K^{-1}$ as compared to 4.18 $J\ g^{-1}\ K^{-1}$), or less than one-half on a volume basis (1.88 $J\ cm^{-3}\ K^{-1}$ as compared to 4.18 $J\ cm^{-3}\ K^{-1}$). However, generally, the absorption of $CO_2$ in the conventional ionic liquids is very limited because of its physical nature of interactions, although it is relatively higher than the solubility of $CO_2$ in the conventional organic solvents such as heptane, ethanol, benzene and others. The equilibrium solubility of $CO_2$ in these conventional ionic liquids is about 0.10 – 0.15 wt% at room temperature and atmospheric pressure, which is obviously too low for industrial application for $CO_2$ capture [139-141].

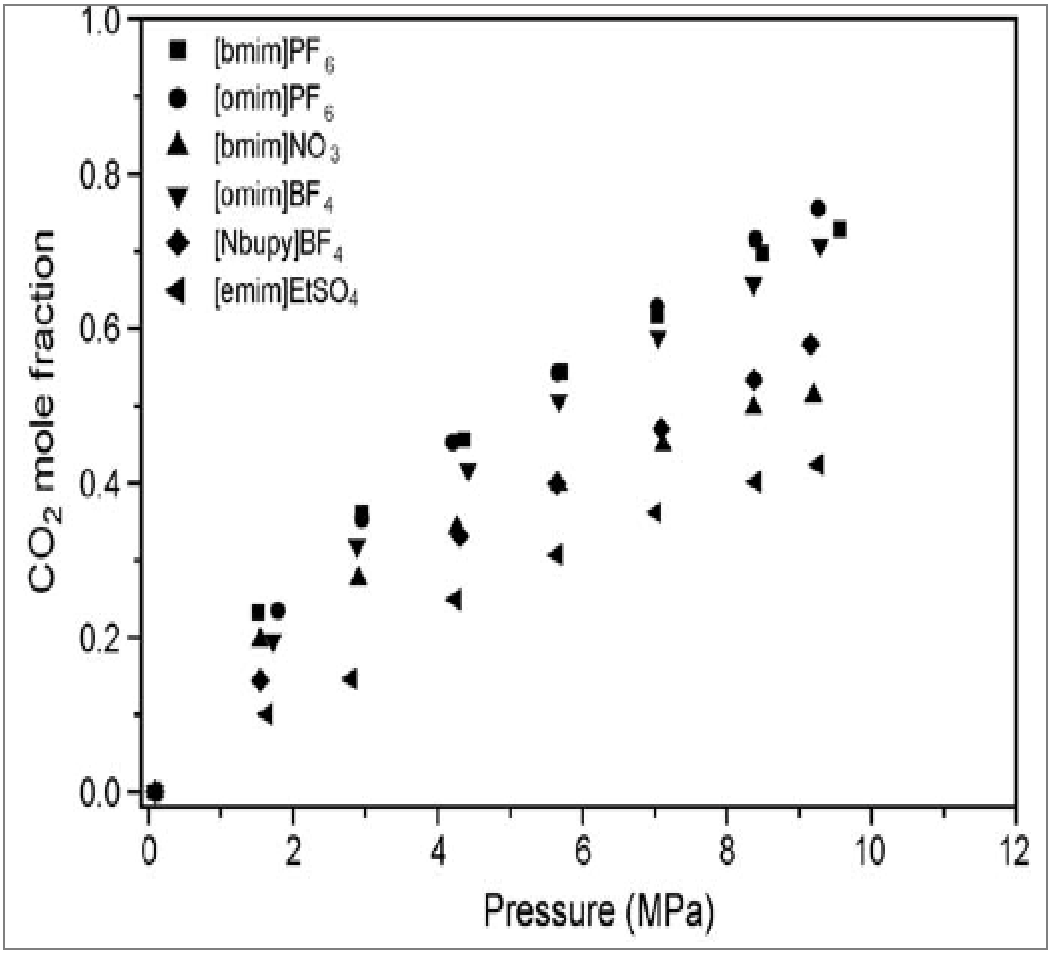

Figure 2.9. Relationship between the solubility of $CO_2$ and pressure for six different types of conventional ionic liquids [138].

### 2.4.2 Task-specific ionic liquids in $CO_2$ absorption

Considering the very limited capability of the conventional ionic liquids in the absorption of $CO_2$, it is essentially necessary to explore novel ionic liquids with the specific function for the absorption of $CO_2$. Due to the unique ‘‘self-designable’’ characteristics of ionic liquids, modification on the cation has been suggested either by introducing a long chain alkyl group or an ether linkage to create greater “free volume” or by incorporating a $CO_2$ - philic carbonyl functional group

[142-149].

Thus, alkaline group such as –$NH_2$ can be attached to the structure of cation or anion of ionic liquids while still keeping the merits of the ionic liquids [150]. The task-specific ionic liquids with alkaline groups are believed to sequester larger amount of $CO_2$ than that of conventional ionic liquids because of the chemical interactions or reactivity between $CO_2$ and alkaline groups of ionic liquids [151]. The designed task-specific ionic liquids obviously can break the limitation of the conventional ionic liquids and tackle the disadvantages of the commercially applied absorbents such as aqueous amines.

Besides task specific ionic liquids, the fluoroalkyl anion-based are the one presenting the highest $CO_2$ solubility. Although both anion and cation influence the $CO_2$ solubility, the anion has the strongest influence [152-156]. The presence of fluoroalkyl groups, known to be "$CO_2$ - philic", makes OTf anion-based ionic liquids compounds for $CO_2$ solubilities.

However, this behavior is yet poorly understood and while some authors emphasize the role of the interactions between the $CO_2$ and the fluroalkyl anion, others identify the large free volume of the ionic liquid as the main factor responsible for the higher solubility [157-159]. On the other hand, the alkyl chain length of the cations, also influences the $CO_2$ solubility, indicating an entropic, rather than enthalpic, effect is present [160]. For some studied cation, the data available seems to indicate that the longer the alkyl chain, the higher the free volume, and consequently the larger the solubility [161].

Bates *et al.* [162] reported a task-specific ionic liquid, 1-*n*-propylamine-3-butylimidazolium tetrafluoroborate [pabim][$BF_4$], for $CO_2$ capture. The saturated concentration of $CO_2$ in [pabim][$BF_4$] reaches a level of 7.4 wt%. The proposed reaction mechanism is shown in Figure 2.10 [162], which is basically the same as the amines currently used as $CO_2$ absorbents. $CO_2$ molecule attacks the free electron-pair of N atom and forms a new $NHCOO^-$ group, simultaneously the $NH_2$ group of another [pabim]$^+$ accepts one $H^+$ and becomes $–NH_3^+$ group, which accounts for the saturation molar ratio of 1:2 between $CO_2$ and [pabim][$BF_4$].

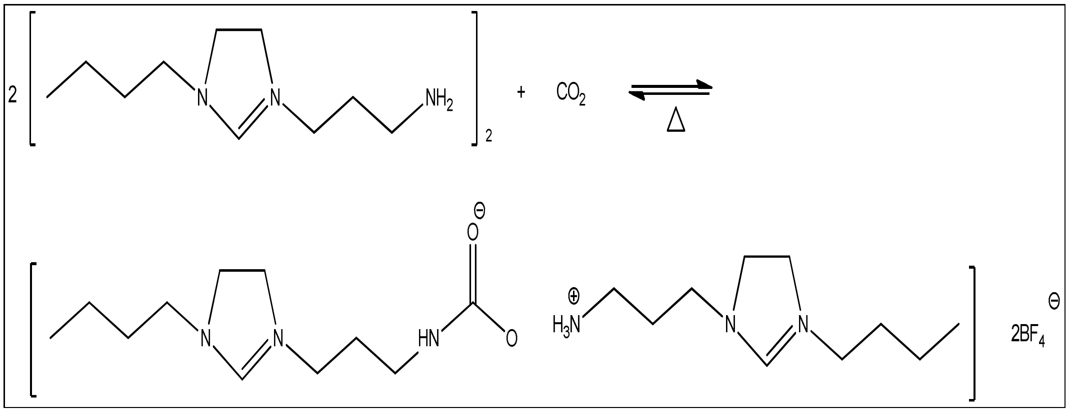

Figure 2.10. Proposed reaction mechanism between [pabim][$BF_4$] and $CO_2$ [162].

As with other solvent-based processes, the recovery of the dissolved $CO_2$ from the ionic liquid can be achieved by increasing the temperature thereby reducing the $CO_2$ solubility and/or reversing the absorption reaction. Anthony *et al.* [163] compared the ionic liquids [bmim][$PF_6$] and [bmim][$BF_4$] with a 30 wt% MEA solution as a $CO_2$ capture solvent. The energy demand for these specific ionic liquids used was estimated to be too high because the ionic liquids used were not task specific for $CO_2$ capture.

However, Gutowski *et al.* [164] suggested that a task specific ionic liquid could be competitive with a 30 wt% MEA solution for capturing $CO_2$. In contrast to conventional ionic liquids, where the absorption of $CO_2$ is mainly based on physical dissolution, task specific ionic liquids have the potential to capture larger amounts of $CO_2$ using chemical interactions between $CO_2$ and reactive groups. It would emerge that the $CO_2$ capture performance is essentially influenced by the ionic liquid's anion.

However, the task-specific ionic liquids and its derivatives do not emerge to be utterly viable for industrial processes, because there are drawbacks associated with their use in $CO_2$ capture. These functionalized ionic liquids are more viscous in their unreacted states compared to the conventional ionic liquids, and their corresponding $CO_2$ adducts are intractable tars, thus limiting the utility of task-specific ionic liquids as neat solvents for $CO_2$ capture.

Russel, Etter & Ward [165] utilized the advantage of hydrogen-bond sites on guanidinium cations and substituted sulfonate anions in the preparation of material *i.e.* guanidinium trifluoromethanesulfonate, $C_2H_6F_3N_3O_3S$, containing infinite hydrogen-bonded sheets (refer to Figure 2.11).

The precise topology of these motifs can be modified through an appropriate substitution of the anion. Moving from molecular to ionic motifs simply requires deprotonation of the acid which creates an asymmetric anion with a carboxylate 'tail' (with strong hydrogen-bond acceptors) and a carboxylic 'head', acting as a powerful hydrogen-bond donor.

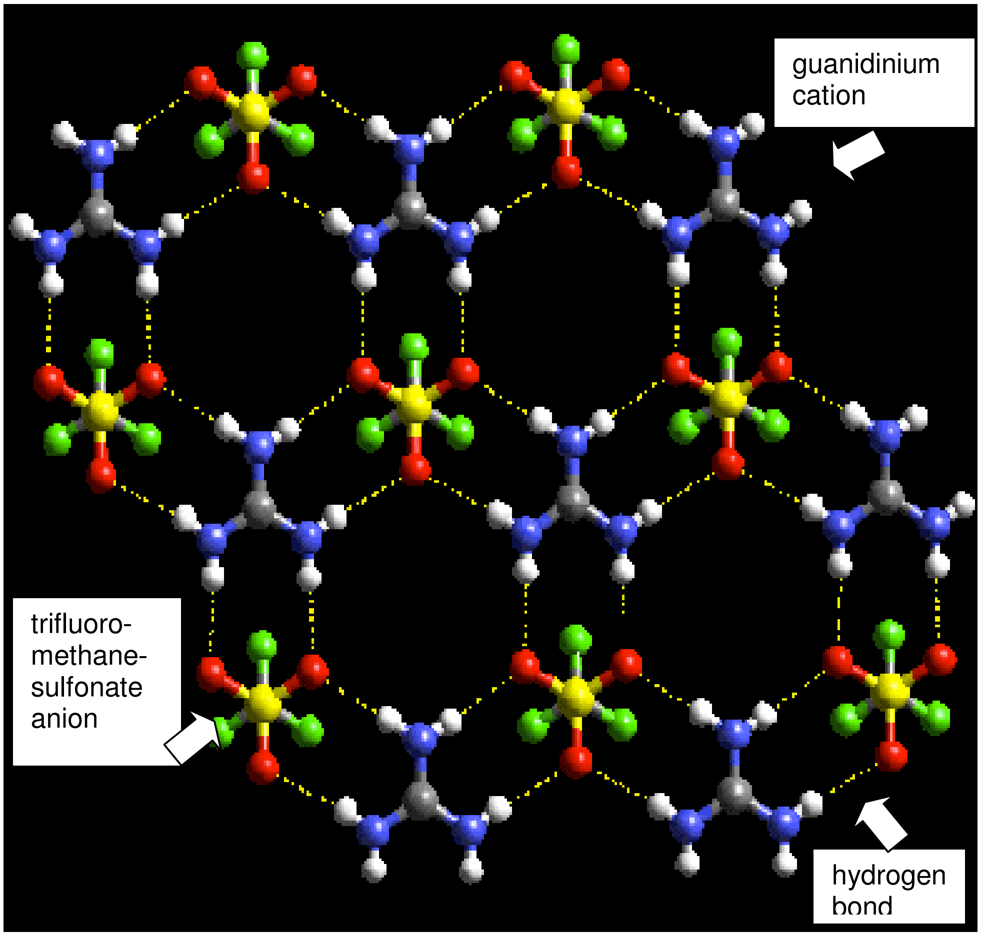

Figure 2.11. An infinite hydrogen-bonded sheet in guanidinium trifluoromethanesulfonate [165].

Typically, monoanions of dicarboxylic acids have a propensity to form infinite chains through a very short and near-linear O---H..-O hydrogen bond between the 'head' and 'tail' of adjacent anions. Two O--H...O interactions between neutral species are thereby replaced with one O--H...O interaction between anions, but the overall structural outcome is unchanged; a 1-D motif.

An additional bonus is given by the fact that this chain is inherently polar, which may have useful implications for the physical properties of the resulting material. The next step involves combining 1-D elements into 2-D features in a reliable manner. In these anions there are several hydrogen-bond acceptors available, so by introducing a donor group on the anion, preferably positioned so that it can provide a link between neighbouring chains, it should be possible to create infinite anionic layers [166].

## 2.5 The $CO_2$ solubility study

There are a number of techniques to quantitatively determine the $CO_2$ loading in the solvent capture such as closed cell (static) method, chromatography, pressure change measurement, volumetric, wet chemistry and gravimetry [167-169]. The volumetric method is based on the standard Association of Analytical Communities, AOAC method, where the liquid sample is acidified with a 2 M HCl solution to release the $CO_2$ gas, which can be directly measured using a burette.

Haji-Sulaiman *et al.* [170] proposed a technique to determine the concentration of all species in an equilibrium system of $CO_2$ – alkanolamine - $H_2O$ based on titration with a strong base NaOH. This method has claimed by them as simple to perform and has been found to be reliable. Using those values, they were able to estimate the equilibrium constant at infinite dilution for the formation of carbamate at different temperatures and assessed their variations with ionic strength.

Another technique is a headspace gas chromatography [171]. This technique is based on synthetic method and allows for the determination of the total pressure required to dissolve a known amount of gas in a known amount of liquid at a given temperature and liquid-phase composition.

Navaza *et al.* [172] employed a photographic method based on bubble diameter determination. The bubble diameter was measured based on capturing images of the bubbles along the height of the column and from the bottom to top. Photographs of different bubble column zones were analyzed, taking into account the possible influence of mass transfer accompanying of chemical reaction upon the bubble size along the liquid phase height.

Screening tests of the absorption performance are usually done based on two principal parameters *i.e.* partial pressure of the studied gas and also the temperature.

(a) Effect of pressure

Generally, for a gaseous solute, pressure also affects solubility, but only the partial pressure of the gas that is dissolved. Henry's Law, P = kC, where P is the partial pressure of the solute in the gas above and k is a constant with the dimensions of pressure divided by concentration, expresses this relationship. As the partial pressure of the gas increases, its solubility increases. The spontaneous release of dissolved gas is a result of a rapid decrease in the partial pressure of the gas and the resulting decrease in solubility.

Soriano *et al.,* [173, 174] mentioned in their articles that $CO_2$ absorption in aqueous alkanolamine solutions depends on partial pressure driving force from gas to liquid. In the liquid phase, absorbed acid gas will lead to an increase of the acid gas partial pressure. Also, acid gas vapor pressure at a given loading and temperature is a function of the strength and type of amine.

(b) Effect of temperature

Solubility can be affected by temperature. The solvent's capacity for absorbing acid gases increases as the temperature is decreased. A decrease in temperature can reduce the circulation rate, thus reducing operating costs. Also, the amount of light hydrocarbon or $H_2$ and CO may be reduced significantly. The solubility of $CH_4$, $H_2$, and CO show little change with temperature, so the absorption of acid gas is more selective.

Usually the only parameter available for control in the column temperature is the lean alkanolamine temperature. Since the $CO_2$ reaction with MDEA is kinetically controlled, the hotter the column the faster the reaction rate. However, once the lean amine temperature reaches about 135 to 140 F, the decrease in solubility of the $CO_2$ in the amine solution will usually become the overriding factor and the net $CO_2$ pickup will begin to decrease. Lower solubility for such exothermic processes resulted from the increment in temperature.

## 2.6 Modelling for $CO_2$ solubilities

Design of gas-treating operations demands knowledge of the vapour-liquid equilibria (VLE) of the aqueous acid gas-alkanolamine system. An account of vapour-liquid equilibria data is needed so that the design engineer can assertively and systematically interpolate and extrapolate the available data. Unfortunately, process simulation and design of gas-treating operations have been hindered by the lack of a correlation for accurately representing thermodynamic properties of concentrated aqueous electrolyte solutions. Design calculations are, therefore, often based upon empirical methods.

Emerging number of recent research in vapour-liquid equilibrium of alkanolamine - $H_2O$ - $CO_2$ systems has led to more semi-empirical excess Gibbs energy models or activity coefficient models developed and reported in literatures. The models were applied in the system to analyze and correlate the data for prediction of $CO_2$ solubility in alkanolamine - $H_2O$ - $CO_2$ systems under a wide range of operating conditions.

Several models are available to analyze the solubility of $CO_2$ in an aqueous solution of alkanolamine and to predict the equilibrium $CO_2$ loading. Among the models that have been widely applied are Kent – Eisenberg [175], Pitzer [176], the electrolyte NRTL model of Chen and Evans [177], the model of Deshmukh-Mather [178], Meissner and Tester [179], Bromley [180], Cruz and Renon [181], Ball *et al.,* [182], Chen *et al.,* [183] and Christensen *et al.* [184].

The Chen and Evans model used a combination of Debye - Hückel theory and the electrolyte - NRTL equation to calculate the activity coefficients. This model was applied by Austgen *et al*., [185] amongst others. The Deshmukh and Mather model employed the Guggenheim equation to represent activity coeffcients and is much simpler to handle when compared to the previous model. It is a more rigorous thermodynamic model to predict the gas loading in aqueous solutions of alkanolamine, which used the same chemical reaction in the liquid phase as in the Kent Eisenberg model. Instead of assuming activity coefficients to be unity, activity coefficients except water are calculated by an extended expression of the Debye-Hückel theory.

Sander *et al.,* [186] developed an excess Gibbs energy model to represent the salt effect on the VLE of mixed solvents systems. Mock *et al.,* [187] extended Chen's model to represent the salt effect on mixed solvent VLE. Chen and co-workers completed this extension to represent activity coefficients of both ionic and molecular species in mixed solvent systems [188].

Kent Eisenberg Model is the simplest model where the non-idealities that are presented in the system are combined with the K values. This relatively simple model correlates with the data fairly well [189]. Kent Eisenberg (1976) [175], proposed a model that neglected activity coefficients and used apparent equilibrium constants in the equations of chemical equilibria where all activity coefficients and fugacity coefficients are assumed to be in unity (ideal liquid and vapour phase). The chemical reaction equilibrium is defined in the liquid phase. The equilibria constants of the amine dissociation reaction and carbamate formation reaction are regressed based on the experimental acid gas solubility data in the aqueous amine system [190]. This approach is typically to represent $H_2S$ and $CO_2$ equilibrium partial pressures over aqueous solutions of MEA and DEA.

Since the systems are, in fact, highly non-ideal, Kent Eisenberg (1976) suggested that the concentration-based equilibrium constants of the amine protonation and/ or the carbamate formation should be fitted to the given experimental data [191].

Even though this approach succeeds in predicting the equilibrium $CO_2$ partial pressures and loadings, it would be unlikely to predict the concentrations of each species in the systems accurately because of the non-idealities of the systems. Accurate predictions of the system species, especially those of the unreacted $CO_2$ and amine, are essential for the design and simulation of absorbers and strippers used in the gas treating units.

Pitzer model uses an extension of the Guggenheim's equation, which gives a better estimation of the long range ion-ion electrostatic forces and short range ion-ion interactions [192]. This model has been shown to be valid for ionic strengths typical of those encountered in the industry. However its application is generally limited to aqueous systems with single solvents. The solute-solute binary interaction parameters are unknown functions of the solvent composition. The model contains a large number of binary and ternary temperature dependent adjustable parameters, which are difficult to estimate [193].

Shiflett *et al.* [194] used RK (Redlich-Kwong) type of cubic equations of equations of state (EOS) to analyze the experimental solubility data of pure ionic liquid [bmim][acetate].

The above-mentioned models require a large number of experimental VLE data in order to estimate the interaction parameters. Due to the lack of experimental data on $CO_2$ solubility in MDEA and [gua][OTf], a simple correlation is proposed in this work.

## 2.7 Physicochemical properties

Ionic liquids have been shown to possess exclusive physical and solvent properties depending on their constituent ions. They have been referred to as "tunable" solvents due to the ability to diverge the constituent ions, thereby modifying and optimizing the ionic liquids physical and solvent properties for an exclusive application. As such, the variety of cations and anions [195] that could be combined to make an ionic liquid is virtually vast.

Besides solubility data, physical properties such as density and viscosity of pure chemicals and of their mixtures over the whole composition range measured at several temperatures, are useful for a full understanding of their thermodynamic and transport properties as well as for practical chemical engineering purposes [196-198]. Solution density and viscosity are important in the mass-transfer-rate modelling of absorbers and regenerators because these properties affect the liquid film coefficient for mass-transfer. Design of related operations such as pumps and heat exchangers would also benefits from better knowledge of the physical properties of process solutions.

For both densities and viscosities, a comparison of all the data presented in the literature allows one to make some general qualitative conclusions about trends, but a detailed analysis indicates that a quantitative description is much more difficult to make. Excess thermodynamic functions and deviations of non-thermodynamics ones of mixtures are also fundamental for understanding the interactions between molecules in these types of mixtures, particularly when polar components are involved [199-202]. These functions have also been used as a qualitative and quantitative guide to predict the extend of the complex formation in this kind of mixtures.

From the experimental results of densities and viscosities, excess molar volume ($V^E$), viscosity deviation from the ideal behaviour ($\Delta_\eta$), activity coefficient ($\gamma^i$), and excess molar Gibbs function ($G^E$) were calculated [203-207]. Empiric equations for the density and viscosity of pure components as a function of a temperature and composition were applied. These equations are useful for interpolation within the studied temperature range. On the other hand, the excess thermodynamic properties and non-thermodynamic ones were fitted to a Redlich-Kister type equation using least squares to obtain their dependencies on concentration and temperature [208-210].

### 2.7.1 Density

Substantial amounts of data on the density of ionic liquids are available in the literatures (many in communications dedicated primarily to synthesis) as it is a typical property for characterizing a substance. Specifically, the density is essential for the rational design of gas treating units and for optimum gas treating processes. The data is also obligatory to model the rate of reaction and the mass-transfer rates in absorption and desorption operations [211]. The density values are also required in modeling gas absorption in binary and ternary systems.

Densities are perhaps the most straightforwardly determined physical property of material. Density is defined as “the mass of fluid per unit volume”. For a solution, it is a sum of mass concentrations of the components of that solution.

$$\rho = m / V = \sum_{i} \rho_i \qquad (2.5)$$

where;

$m$ = mass; $V$ = volume; SI unit : unit kg $m^{-3}$

### 2.7.1.1 Density of alkanolamine

The period 1992-2003 has been very rewarding for the experimental study of different thermophysical properties of aqueous solutions of alkanolamines blends that are of great interest for the purification of sour hydrocarbon gas stream.

The densities in alkanolamines appear to be the physical property least sensitive to variations in temperature. For example, as for alkanolamine such as pure MDEA and MEA, 10 K changes in temperature from 303 to 313 K results only about 0.6 and 0.9 % decrement respectively. This is dissimilar with viscosity which decreased by 41 and 34 % respectively for the same alkanolamine [212]. In addition, the impact of impurities to the density of alkanolamine appears to be far less dramatic than in the case of viscosity. Recent works indicate that the densities of alkanolamine vary linearly with weight percent of impurities. For example, 70 wt% of water in pure MDEA results in lower than 2 % decrease in density [213].

Bernal-garcía *et al.* [214] presented an atmospheric density values for (*N*, *N*-dimethylethanolamine + water) over entire composition range and at temperature from 293.15 to 363.15 K. Meanwhile, Hartono *et al.* [215] discussed the densities of aqueous diethylenetriamine (DETA) solutions for entire composition range and at temperature range between 293.15 and 363.15 K. The measured densities for both works increased with increasing DEA concentration, reached a maximum value and then decreased. The effect of increasing temperature is to decrease the density and the maximum density values were found to be shifted gradually to lower mole fraction values.

### 2.7.1.2 Density of ionic liquids

One of the reviews of density measurement of ionic liquids that has been published is by Mantz and Trulove [216]. Until 2005, the most studied liquids are those containing imidazolium and, to a lesser extent, pyridinium-based cations. Usually, the influence of the alkyl chain length in these cations on the density is studied as well as the effect of different anions (chloride, $Cl^-$, tetrafluoroborate $BF_4^-$, hexafluorophosphate $PF_6^-$, bis (trifluoromethylsulfonyl)imide $NTf_2^-$). Matsumoto *et al.*, [217] and Sun *et al.*, [218] have worked on other types of cation (ammonium, pyrrolidinium) but only at 298 K. The most frequently studied ionic liquid was 1-butyl-3-methylimidazolium hexafluorphosphate, [bmim][$PF_6$] [219].

In general, the density decreases with increasing length of an alkyl chain in a cation or anion as was documented for imidazolium-based cations [220]. The density values are often reported at a single temperature, usually 293 or 298 K.

Knowledge of the temperature dependence of this property is, however, very useful and several recent studies [221, 222] present data as a function of temperature.

They have reported an approximately linear decrease of density with temperature, corresponding to typical values [223] for the thermal expansion coefficient near $5 \times 10^{-4}$ $K^{-1}$ which is about twice higher compared to water and three times lower compared to common organic solvents (such as methanol, acetone, benzene and *n*-hexane). Gu *et al*. [224] examined also the variation of the density of ionic liquids with pressure. They came to a conclusion of an isothermal compressibility comparable with water and lower than that for organic solvents.

Similar to sensivity of alkanolamines to variation in temperatures, a 10 degree change in temperature from 293.15 to 303.15 K results in only a 0.62 % decrease in the density for [bmim][$BF_4$]. The densities of all ionic liquids always decrease with the increase of temperature due to the thermal expansion and weakening molecular interactions [225].

As mentioned, commonly, the density of ionic liquids is greater than typical organic solvent such alkanolamines. For task specific ionic liquids, it exhibits a greater density than conventional ionic liquids over a certain range of temperature. This can be shown by an amine appended imidazolium paired with tetrafluoroborate, [Am - Im][DCA] which has a greater density than [bmim][DCA] [226]. However, there are some exceptional cases whereby the density of ionic liquids (*e.g.* dialkylimidazolium dialkylphosphate) is not significantly affected by the variation of temperature, but it is influenced by the chain length of alkyl groups on the cation and/ or the anion.

The longer alkyl chain creates a larger free volume within the ionic liquids and therefore the density is decreased. Wang *et al.* [227] showed that the density is also dependant on the molar mass of cation and anion of ionic liquids. The overall density is in the decreasing trend as the organic solvent is added into ionic liquids, with increase in temperature for organic solvent and ionic liquids mixture. In addition, correlation of density with temperature is developed for specific temperature range to estimate the thermal properties of the ionic liquids.

Wang *et al.,* [228] also measured the densities, conductivities, and polarity indexes of pyrene for aqueous solutions of a series of $[C_n\text{mim}][\text{Br}]$ ($n$ = 4, 6, 8, 10, 12) and $[C_4\text{mim}][BF_4]$ at 298.15 K, and discussed the aggregation behaviours of these aqueous ionic liquids solutions. Also, García-Miaja *et al.*, [229] has presented the density for a set of binary system of ionic liquid + water as a function of temperature at atmospheric pressure.

The studied ionic liquids are 1-butyl-3-methylpyridinium tetrafluoroborate $[\text{bmpyr}][BF_4]$, 1-ethyl-3-methylimidazolium ethylsulfate $[\text{emim}][\text{EtSO}_4]$, 1-butyl-3-methylimidazolium methylsulfate $[\text{bmim}][\text{MetSO}_4]$, 1-butyl-3-methylimidazolium trifluoromethanesulfonate [bmim][OTf] and 1-ethyl-3-methylimidazolium trifluoromethanesulfonate [emim][OTf]. The results show that the thermodynamic behaviour of the studied solutions is mainly determined by the chemical structure of the anion: the sulfate-based RTILs are the most hydrophilic whereas the $BF_4$- based presents the higher hydrophobicity.

### 2.7.1.3. Density-derived thermodynamic properties

The experimental density values can be used to calculate some thermodynamic properties, such as the isobaric thermal expansion coefficient, $\alpha_p$ and the thermal pressure coefficient, $\gamma$.

The following form of the Tait equation [230];

$$\rho = \frac{\rho(\mathrm{T}, \mathrm{P} = 0.1\ \mathrm{MPa})}{\{1 - C\ ln\ ((B + \mathrm{P})/(B + 0.1))\}} \qquad (2.6)$$

where;

$$\rho = \rho(\mathrm{T}, \mathrm{P} = 0.1\ MPa) = a_1 + a_2\mathrm{T} + a_3\mathrm{T}^2 \qquad (2.7)$$

It was fitted to the density data and $a_1$, $a_2$ and $a_3$ are found by fitting to the experimental $\rho$ (T, P = 0.1 MPa). Coefficient $B$ is defined as;

$$\mathrm{B} = b_1 + b_2/\,\mathrm{T} \qquad (2.8)$$

The coefficients $C$, $b_1$ and $b_2$ are obtained by fitting the Tait equation to experimental data. The standard deviation is defined by;

$$\sigma = [\sum_{j=1}^{Np} (\rho_{\mathrm{calc}} - \rho_{\mathrm{exp}})\ i^2 / N_p - k\ ]^{1/2} \qquad (2.9)$$

where;

$N_p$ represents the number of points ($N_p$ = 96) and k is the number of adjusted parameters ($k$ = 3). The average absolute deviation *(AAD)* is fitted as;

$$AAD = 1/\, N_p \sum_{j=1}^{Np} 100\, |(\rho_{\mathrm{calc}} - \rho_{\mathrm{exp}}) \,/\, \rho_{\mathrm{exp}}| \qquad (2.10)$$

The logarithm of density of all liquids, ln $\rho$ (g cm$^{-3}$) decreased linearly with the temperature, implying a constant thermal expansivity, as defined below [231].

$$\alpha_{\mathrm{p}} = 1/\, V_m\, (\delta V_m/\, \delta \mathrm{T})_p = (-1/\rho)\, (\delta\rho/\, \delta\mathrm{T})_p = -(\delta \ln\rho/\, \delta T)_p \qquad (2.11)$$

and the following expression is derived from the Tait equation;

$$\alpha_P = -\frac{[(d\rho\,(\mathrm{T, P = 0.1})/\, d\mathrm{T})]}{\rho\,(\mathrm{T, P = 0.1})} + C\, \frac{[dB/\, d\mathrm{T}\,(\mathrm{P - 0.1})]}{[1 - C \ln(\mathrm{B + P})]\,(B + 0.1)\,(B + \mathrm{P})} \qquad (2.12)$$

where;

$$\frac{\mathrm{d}B}{\mathrm{dT}} = \frac{-\, b_2}{\mathrm{T}_2} \qquad (2.13)$$

From further studies in the experimental density data, correlations are developed to allow the calculation of the density of the alkanolamines and/ or ionic liquids as a function of concentration and temperature. Basically, the linear and polynomial correlated equations are;

$$\rho\,(kgm^{-3})\,(x^1, T) = a\,(T/\,K) + b\,(T/\,K) \times x_1 \qquad (2.14)$$

$$\rho\,(kgm^{-3})\,(x^1, T) = a\,(T/\,K) + b\,(T/\,K) \times x_1 + c\,(T/\,K) \times x_1^2 \qquad (2.15)$$

where;

$\rho$ is the density in kg m$^{-3}$, T is the temperature in K, $x_1$ is the mole fraction, and *a, b, c* are parameters.

On the basis of pure-component molar volumes together with excess molar volumes (due to interactions of various species), an expression to correlate the density of aqueous single or mixtures are developed. The density of a solution is given by its average molecular weight divided by its total molar volume;

$$\rho_{aqAm} = \frac{x_{Am} M_{Am} + xH_2O\, M_{H2O}}{V_m} \qquad (2.16)$$

$$\rho_{aqIL} = \frac{x_{IL} M_{IL} + xH_2O\, M_{H2O}}{V_m} \qquad (2.17)$$

$$\rho_{aqAm+IL} = \frac{x_{A+ILm} M_{Am+IL} + xH_2O\, M_{H2O}}{V_m} \qquad (2.18)$$

where;

$\rho$ is the solution density (g mL$^{-1}$) $V_m$ is the molar volume of the solution (mL mol$^{-1}$), and $x_i$ and $M_i$ are the mole fraction and the molecular weights, respectively, of the amine, ionic liquid and water.

Auxiliary correlation on the densities of liquid mixtures, a Redlich-Kister type equation for the excess molar volume is applied. For a binary system, the Redlich-Kister equation [232] has the form;

$$V^E_{12}\,(\text{cm}^3\,\text{mol}^{-1}) = x_1 x_2 \sum_{i=0}^{n} A_i\,(x_1 - x_2)_i \qquad (2.19)$$

where;

$A_i$ is a parameter that is temperature-dependent. The excess volume of the liquid mixture for a ternary system is assumed to be given by the following expression;

$$V^E = V^E_{12} + V^E_{13} + V^E_{23} \qquad (2.20)$$

The excess volume of the liquid mixtures can also be calculated by the measured density of the fluids;

$$V^E = V_m - \sum x_i V_i \qquad (2.21)$$

where;

the $V_m$ is the molar volume of the liquid mixture and $V_i^{\circ}$ is the molar volume of the pure fluids at the system temperature [233].

Theoretically, excess molar volume of solution is a thermodynamic property and is defined as the amount of volume which is in excess to that of an ideal solution at the same conditions of composition, temperature and pressure [234]. $V^E$ decreases with an increase of chain length. Polarity increases with an increase of chain length resulting in a decrease in $V^E$ due to the dipole - dipole interaction between unlike molecules [235].

The dependence of $V^E$ on both composition and temperature for the present mixture can be explained as a balance between positive contributions (the breaking up of the associates or molecular order present in the pure liquids and dispersive interactions between unlike molecules) and negative contributions (intermolecular interactions and geometrical fitting between the components) [236-238].

If $V^E$ is positive, then there will be more available free volume than in the ideal solution and photons will be less likely to interact with the molecules or ions constituting the compound; as a result, light will travel at a higher velocity in the medium concerned [239] and vice versa.

### 2.7.2 Viscosity

Viscosity describes a fluid's resistance to shear or flow. The resistance is caused by intermolecular friction exerted when layers of fluids endeavor to slide by one another. Viscosity information of fluids and their mixtures is imperative for the design of heat-transfer equipment, process piping, reactors, stripping columns, deodorizers, liquid-liquid extractors, distillation columns, crystallization equipment, and other units found in various chemical, oil, plant, clay, dairy and food industry [240]. In addition, it also affects other transport properties such as diffusion.

Because viscosity strongly affects flow behavior, it must be considered in engineering process calculations, analysis and design, as also an input for process simulation and optimization. There are two related measures of fluid viscosity, known as dynamic (or absolute) and kinematic viscosity. Dynamic (absolute) viscosity is a tangential force per unit area required to move one horizontal plane with respect to the other at unit velocity when maintained a unit distance apart by the fluid. Meanwhile, kinematic viscosity is the ratio of absolute or dynamic viscosity to density - a quantity in which no force is involved [241].

#### 2.7.2.1 Viscosity of alkanolamine

Bernal-Gracìa *et al.* [242] reports viscosity values for (*N*, *N*-dimethylethanolamine + water) over the entire composition range from T equals 313.15 to 353.15 K. Three different Cannon-Fenske viscosimeters are used for the viscosity measurements. Viscosity deviations are calculated using a Redlich-Kister type equation and are positive at all temperatures and compositions in that work. Also, Chowdhury *et al.* [243] showed the viscosities of the pure liquids vary as: DEA >> MDEA > EDEA > BDEA, which may be considered as a reflection of the strength of self-association of the liquids.

The diethanolamines, DEA is the most effective self-association liquid by H-bonding, followed in succession by MDEA, EDEA and BDEA, owing to their increasing order of steric effect. Such alkyl substituted alkanolamine, MDEA, it exhibits viscosity maxima in aqueous solutions at low temperatures. This indicates that the hydrophobic alkyl groups in such compounds also facilitate the formation of alkanolamine-water complexes or clathrates. Formation of such ‘association complexes’ [244] has already been considered to interpret maximum viscosity in aqueous-organic mixtures.

Kipkemboi and Easteal [245] have introduced the concept of structural promotion in the solution by gradual formation of clusters of associated species via H-bonding. Likewise, at low concentration, dissociated alkanolamine molecules also may be considered to enter into the cavities of structural networks of water. At moderate concentration, increased number of MDEA fails to be accommodated in the structural network of water, which leads to the formation of alkanolamine clusters by reorganization, surrounded by restructured water network. After reaching the maxima, this organization of alkanolamine and water starts to be disrupted forming alkanolamine structural networks in which segregated/ monomeric water molecules are trapped.

#### 2.7.2.2 Viscosity of ionic liquids

Viscosity is an important physical property of ionic liquids. A low viscosity is generally desired for an ionic liquid to be used as a solvent. This is to minimize pumping costs and increase mass transfer rates while higher viscosities may be favorable for other applications such as lubrication or in membranes.

Yet, it is known that the viscosity of ionic liquids varies widely depending on the type of cation and anion. The viscosities of ionic liquids are relatively high compared to those of common organic solvents. Organic solvents typically have viscosities ranging from 0.2 to 10 cP at room temperature [246] whereas ionic liquids display a broad range of room temperature viscosities, from 10 to a greater than $10^5$ cP at ambient temperature [247].

The viscosity is comparable with the values obtained for oils, that is to say two or three orders of magnitude higher than viscosities of traditional organic solvents. This is obviously a real disadvantage for their industrial application and it explains the quest for new ionic liquids exhibiting lower viscosity [248]. The influence of temperature on viscosity is much more important than on density: a strong decrease is observed with increasing temperature [249] making ionic liquids easier to apply at elevated temperatures.

However, apparently, the viscosity of ionic liquids is much less studied than the density and only limited data are available in the literature. Most of the studies [250-255] concern imidazolium-based ionic liquids, differing in the length and ramification of the alkyl chains. In fact, Okoturo *et al.* [256] have also studied pyrrolidium cations.

Another group has studied the physicochemical properties of aqueous solutions of imidazolium-based ionic liquids. Goomez *et al.* [275] reported dynamic viscosities and densities of (water + [hmim][Cl]) and (water + [omim][Cl]) over the entire mole fraction range from 298.15 to 343.15 K. Ge *et al.* [258] reported dynamic viscosities and densities for the binary mixtures of (water + [bmim][OTf]) over the entire mole fraction range from 303.15 to 343.15 K. Muhammad *et al.* [259] reported dynamic viscosities and densities of (water + [emim][$EtSO_4$]), (water + [emim][OTf]) and (water + [emim][TFA]) over the entire mole fraction range. Wilkes *et al.* [260] reported osmotic coefficients, mean activity coefficients, vapor pressure data, and excess Gibbs free energy $G^E$ of aqueous solutions of [$C_n$mim][Br] ($n = 3, 5, 6$).

Paulechka *et al.* [261] presents a collection of experimental viscosities for a selection of six hydrophobic and hydrophilic ionic liquids *i.e.* 1-butyl-3-methyimidazolium hexafluorophosphate [bmim][$PF_6$], 1-butyl-3-methyimidazolium tetrafluoroborate [bmim][$BF_4$], 1-butyl-3-methyimidazolium bis (trifluoromethylsulfonyl)imide [bmim][$NTf_2$], 1-ethyl-3-methyimidazoliumb [emim][$NTf_2$], 1-ethyl-3-methyimidazolium ethylsulfate [emim][$EtSO_4$] and butyltrimethylammonium bis(trifluoromethylsulfonyl)imide [$N_{4111}$][$NTf_2$]. The viscosities of dried samples are measured from 293 to 388 K and those of the water-saturated samples from 293 to 343 K.

The trends in the evolution of viscosity with the structure of the cations and the anions are in many aspects inverse to those observed for density. The $NTf_2^-$ anion lowers the viscosity as compared to the other investigated anions. Particularly the contribution of the $PF_6^-$ anion to the viscosity increase is exceptionally strong. It is also concluded that the $EtSO_4^-$ anion increases viscosity as compared to the $BF_4^-$ anion. They also anticipate that the viscosity would decrease as the size of the non-polar part of the cation becomes larger. The justification put forward by Huddleston *et al.* [262] is that it is the increase in the van der Waals interactions due to the presence of a long alkyl chain that leads to higher viscosities. However, this argument seems to come from a simple correlation of what is observed without having a strong molecular basis.

The study of Kosmulski *et al.* [263] is more profound, since it relates the behaviour of the transport properties, viscosity and diffusion, to a ratio of ionic conductivities that can be interpreted as a measure of ionic dissociation or “ionicity”. These authors observe that the “ionic dissociation” is directly related to the diffusion coefficient, and inversely related to the viscosity, and they attribute this to a preponderance of the effect of the Van der Waals interactions over electrostatic terms. Meanwhile, Okoturo *et al.* [264] has considered the structure-viscosity relationship, with the aim of understanding how the structure influences the viscosity.

Therefore, the viscosity-temperature dependence plots obtained for the RTILs were either:

i) Accurately described by the Arrhenius model (the RTILs contained less symmetrical cations without functional groups in the alkyl chain).

ii) Accurately described by the VTF model (the RTILs contained small, symmetrical cations with low molar mass). The ideal gas transition decreased with increasing size and molar mass of the cation and anion).

iii) Not accurately described by the Arrhenius and VTF models (the RTILs contained cations which (a) were less symmetric, (b) contained functional groups, (c) had higher molar mass).

### 2.7.2.3 Viscosity-derived thermodynamic properties

The viscosity deviation of the mixtures is calculated with the logarithmic additivity rule;

$$\Delta \ln \sigma = \ln (\sigma_{12}) \text{ x } (x_1 \ln \sigma_1 + x_2 \ln \sigma_2) \quad (2.22)$$

where;

$\sigma_{12}$ is the viscosity of the mixture, $\sigma_1$ and $\sigma_2$ are the viscosities of water and alkanolamine/ ionic liquid, respectively, and $x_1$, $x_2$ are mole fractions.

The excess Gibbs energies of activation for viscous flow are obtained by using the following equation [265];

$$\Delta G^E = RT\ [\ln (\sigma V/\ hN_A)\ \mathrm{x}\ (x_1 \ln (\sigma_1 V_1/\ hNA) + (x_2 \ln (\sigma_2 V_2/\ hN_A))] \qquad (2.23)$$

where;

$R$ is the gas constant, $T$ is the absolute temperature, $\sigma_1$, $\sigma_2$ and $V_1$, $V_2$ are the viscosities and the molar volumes of pure water/ and pure alkanolamine, respectively, $h$ is Plank constant, and $N_A$ is Avogadro's number.

The viscosity deviation values and the excess free energies are fitted to the Redlich-Kister equation [266, 267].

$$Y^E = x_2\ (1 - x_2) \sum A_n\ (1 - 2x^2)^n \qquad (2.24)$$

where;

$Y^E$ represents the viscosity deviation or excess Gibbs energy of activation for viscosity flow, $x_2$ is the mole fraction of the alkanolamine/ ionic liquid, and $A_n$ are the coefficients of the fitting polynomials.

The fitted curve corresponds to the Herschel-Bulkley Model:

$$\tau = \tau Y + K\ \gamma^n \qquad (2.25)$$

Experimental data for viscosity of ionic liquids is still scarce and limited to a few classes of well-researched ionic liquids. More viscosity data and better understanding of this property are required for developing ionic liquids for a specific purpose.

## 2.8 Summary

Recent concept of using ionic liquids for $CO_2$ capture is gaining interest due to their unique characteristics, *i.e.* wide liquid range, thermal stability, negligible vapour pressure, tunable physicochemical character and high $CO_2$ solubility. An important drawback much discussed in the case of ionic liquids is their high viscosity. However, by choosing an appropriate combination of cation and anion, the viscosities can be adjusted over an acceptable range of 50 to 10,000 cP.

For $CO_2$ capture at high temperatures and high pressures, such as integrated gasification with combined cycle (IGCC) pre-combined capture, ionic liquids viscosity is less of a concern for its sharp decrease at elevated temperatures, though thermodynamic of $CO_2$ absorption untowardly dictates poor abatement performances. Therefore, among the paths pursued in recent research works are on the use of ionic liquids for carbon dioxide capture involving room temperature ionic liquids, task specific ionic liquids or supported ionic liquid-liquid membranes.

To extend, the capacity of aqueous task specific ionic liquids and blended mixtures of MDEA solutions to absorb $CO_2$ have been focusing in this work. Essential characteristics of the systems such density and viscosity have also been compiled.

# Chapter 3: METHODOLOGY

---

## 3.1 Introduction

This chapter provides details of the materials involved, solutions preparation, experimental techniques and data analysis used throughout the course of this work.

## 3.2 Materials

Guanidinium trifluoromethanesulfonate ([gua][OTf], purity ≥ 98.5 %) and pure *N*-methylethanolamine (MDEA, purity ≥ 98 %) were purchased from Merck, respectively. Both chemicals were of analytical grade and used without further purification. Purified carbon dioxide ($CO_2$, purity ≥ 99.995 %) and oxygen-free nitrogen ($N_2$, 99 % purity) were supplied by Malaysian Oxygen Berhad (MOX). Standard solution of hydrochloric acid (HCl, 1.0 N) for titration was obtained from Fisher Chemicals. Sodium hydroxide (NaOH, 99 % purity), barium chloride ($BaCl_2$, 99 % purity), and sodium bicarbonate ($NaHCO_3$, 99 % solid) were also obtained from Merck. The structures of the [gua][OTf] and MDEA are shown in Figure 3.1(a) and 3.1 (b), respectively.

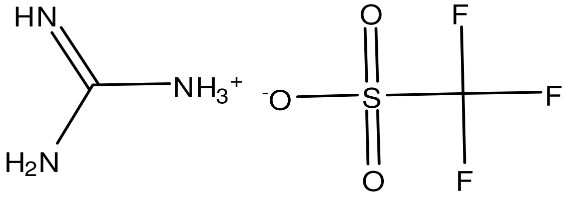

Figure 3.1(a). Structure of guanidinium trifluoromethanesulfonate, ([gua][OTf]) with molecular weight 209.15 g mol$^{-1}$.

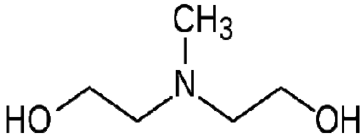

Figure 3.1 (b). Structure of *N*-methyldiethanolamine, (MDEA) with molecular weight 119.16 g mol$^{-1}$.

## 3.3 Solutions preparation

Aqueous mixtures of various compositions of the mixtures were all prepared gravimetrically with a precision of ± 0.0001 g, using analytical balance (GR 200, A&D, Tokyo, Japan). All the prepared solutions were stirred until homogenized and stored inside dark bottles to avoid degradation of the solutions resulting from light exposure.

### 3.3.1 Density

Compositions of the solutions used for the density measurement are shown in Table 3.1. For the aqueous binary systems, 1 and 4 M of MDEA and [gua][OTf] were prepared. Meanwhile, the aqueous ternary systems were prepared by mixing various concentration of [gua][OTf] and MDEA. Different compositions of MDEA and [gua][OTf] with a total concentration of 4 M were also prepared.

Table 3.1. Composition of the binary and ternary systems for density studies.

| System | Solution | Concentration of MDEA (mol dm$^{-3}$) | Concentration of [gua][OTf] (mol dm$^{-3}$) |
|---|---|---|---|
| Binary | 4M0G | 4.003 ± 0.001 | 0 |
| | 1M0G | 1.002 ± 0.001 | 0 |
| | 0M4G | 0 | 4.002 ± 0.001 |
| | 0M1G | 0 | 1.003 ± 0.001 |
| Ternary | 4M2G | 4.003 ± 0.001 | 2.003 ± 0.001 |
| | 4M1G | 4.001 ± 0.001 | 1.002 ± 0.001 |
| | 3M1G | 3.003 ± 0.001 | 1.003 ± 0.001 |
| | 2M2G | 3.001 ± 0.001 | 1.004 ± 0.001 |
| | 1M3G | 2.002 ± 0.001 | 2.002 ± 0.001 |

### 3.3.2 Viscosity

Compositions of the blended solutions of MDEA – [gua][OTf] are shown in Table 3.2. Concentrations for binary systems ranged from 0.1 to 1 M of the aqueous [gua][OTf]. These later will be compared with 1 M MDEA aqueous solution. There were also 4 M MDEA and [gua][OTf]. For the blended MDEA – [gua][OTf], solutions with addition 0.1 to 2 M [gua][OTf] to 4 M MDEA were prepared.

Table 3.2. Compositions of the binary and ternary system for viscosity study.

| System | Solution | Concentration of MDEA (mol dm$^{-3}$) | Concentration of [gua][OTf] (mol dm$^{-3}$) |
|---|---|---|---|
| Binary | 4M0G | 4.005 ± 0.001 | 0 |
| | 1M0G | 1.002 ± 0.001 | 0 |
| | 0M4G | 0 | 4.003 ± 0.001 |
| | 0M1G | 0 | 1.002 ± 0.001 |
| | 0M0.9G | 0 | 0.900 ± 0.001 |
| | 0M0.7G | 0 | 0.702 ± 0.001 |
| | 0M0.5G | 0 | 0.503 ± 0.001 |
| | 0M0.3G | 0 | 0.301 ± 0.001 |
| | 0M0.1G | 0 | 0.102 ± 0.001 |
| Ternary | 4M2G | 4.004 ± 0.001 | 2.002 ± 0.001 |
| | 4M1G | 4.002 ± 0.001 | 1.003 ± 0.001 |
| | 4M0.9G | 4.002 ± 0.001 | 0.904 ± 0.001 |
| | 4M0.7G | 4.003 ± 0.001 | 0.701 ± 0.001 |
| | 4M0.5G | 4.001 ± 0.001 | 0.503 ± 0.001 |
| | 4M0.3G | 4.001 ± 0.001 | 0.303 ± 0.001 |
| | 4M0.1G | 4.001 ± 0.001 | 0.102 ± 0.001 |

### 3.3.3 Solubility of $CO_2$ at high pressure

Table 3.3 shows the composition of the binary and ternary systems used for the solubility $CO_2$ study at high pressures. Different concentration of MDEA, and [gua][OTf] were prepared.

Table 3.3. Compositions of the aqueous and blended MDEA – [gua][OTf] systems.

| Solution | Concentration of MDEA (mol dm$^{-3}$) | Concentration of [gua][OTf] (mol dm$^{-3}$) |
|---|---|---|
| 4M0G | 4.012 ± 0.002 | 0 |
| 4M1G | 4.008 ± 0.002 | 1.005 ± 0.001 |
| 1M0G | 1.003 ± 0.002 | 0 |
| 0M1G | 0 | 1.006 ± 0.001 |

### 3.3.4 Solubility of $CO_2$ at low pressure

Table 3.4 shows the composition of binary and ternary systems used for the solubility study of $CO_2$ at low pressure. A total concentration of 4 M solutions were prepared which constitute of MDEA and [gua][OTf] denoted as 3M1G, 2M2G and 1M3G. Other than that, the effect of the addition of 1 M [gua][OTf] to 4 M MDEA was included. Furthermore, the solubility results between 1 M [gua][OTf] and 1 M MDEA and also between 4 M [gua][OTf] and 4 M MDEA were compared.

## 3.4 Validation of system preparations

The aqueous MDEA were prepared by adding distilled water to the weighted pure MDEA in a volumetric flask. After stirring, the concentrations were determined by titration with 1.0 M HCl standard solution. All aqueous MDEA solution concentrations used were found to be within 1 % of the desired concentration.

Similarly, the blended MDEA - [gua][OTf] systems were prepared by adding distilled water to the weighed pure MDEA and [gua][OTf] in a volumetric flask prior to stirring. The concentration of blended systems was determined by titration with 1.0 M HCl standard solution. All blended systems used were found to be within 2 % of the desired concentration. This indicated that the presence of ionic liquid does not affect the titration results.

Table 3.4. Compositions of the aqueous and blended MDEA – [gua][OTf] systems.

| Solution | $CO_2$ partial pressure (kPa) | Concentration of MDEA/ (mol $dm^{-3}$) | Concentration of [gua][OTf] (mol $dm^{-3}$) |
|---|---|---|---|
| 4M1G | 10 | 4.105 ± 0.002 | 1.008 ± 0.001 |
| | 50 | 4.133 ± 0.002 | 1.011 ± 0.001 |
| | 100 | 4.095 ± 0.002 | 1.004 ± 0.001 |
| 4M0G | 10 | 4.117 ± 0.002 | 0 |
| | 50 | 4.012 ± 0.002 | 0 |
| | 100 | 4.011 ± 0.002 | 0 |
| 3M1G | 10 | 3.080 ± 0.002 | 1.005 ± 0.001 |
| | 50 | 3.100 ± 0.002 | 1.002 ± 0.001 |
| | 100 | 3.096 ± 0.002 | 1.003 ± 0.001 |
| 2M2G | 10 | 1.986 ± 0.002 | 2.001 ± 0.001 |
| | 50 | 2.006 ± 0.002 | 2.000 ± 0.001 |
| | 100 | 2.013 ± 0.002 | 2.004 ± 0.001 |
| 1M3G | 10 | 1.054 ± 0.002 | 3.003 ± 0.001 |
| | 50 | 1.021 ± 0.002 | 3.002 ± 0.001 |
| | 100 | 1.004 ± 0.002 | 3.005 ± 0.001 |
| 1M0G | 10 | 1.009 ± 0.002 | 0 |
| | 50 | 1.028 ± 0.002 | 0 |
| | 100 | 1.044 ± 0.002 | 0 |
| 0M4G | 10 | 0 | 4.007 ± 0.001 |
| | 50 | 0 | 4.002 ± 0.001 |
| | 100 | 0 | 4.004 ± 0.001 |
| 0M1G | 10 | 0 | 1.003 ± 0.001 |
| | 50 | 0 | 1.009 ± 0.001 |
| | 100 | 0 | 1.003 ± 0.001 |

## 3.5 Experimental procedures

### 3.5.1 Density measurement

A digital oscillating glass U-tube density meter (density/ specific gravity meter DMA 4500, Anton Paar, Graz, Austria) was used to measure the densities of the binary and ternary systems. A built-in platinum thermometer in the density sensor was used to determine the solution temperature (with accuracy ± 0.1 K) at the temperature range of 273.2 to 363.2 K. The density meter was equipped with automatic viscosity correction under dry argon and the accuracy of all density measurements was found to be ± 0.001 g $cm^{-3}$.

Calibration was performed periodically under atmospheric condition, in accordance with the manufacturer specifications, using doubled-distilled, freshly degassed water and dry air. All measurements for each sample were performed in triplicate, and the values were reported as an average.

The measurements were taken at atmospheric pressure and temperatures of 303 to 363 K, with 10 K increment**.** The density data obtained are also used to convert the $CO_2$ solubility from volume to weight basis.

### 3.5.2 Viscosity measurement

The viscosity measurement was carried out using R/S+ rheometer (Brookfield, USA). The rheometer differed from a standard viscometer such that it was a controlled stress (or controlled torque) instrument rather than a controlled rate (RPM) instrument. R/S+ rheometer provides many benefits such as a very broad viscosity measurement range and the ability to measure flow properties of delicate high viscosity gels. Schematic diagram of this coaxial cylinder is shown in Figure 3.2.

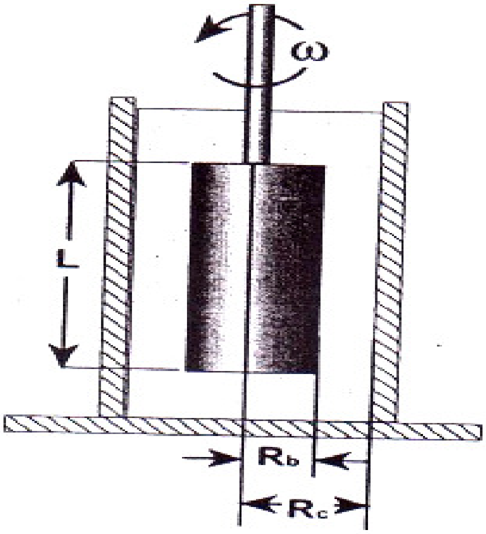

Figure 3.2. Schematic diagram of coaxial cylinder for viscosity measurement

The viscosity was determined using Equation 3.1, 3.2 and 3.3;

Viscosity (poise), $\eta = \tau / \gamma$ (3.1)

Shear stress (dynes/ cm$^2$), $\tau = M / (2\pi R_b^2 L)$ (3.2)

Shear rate (sec$^{-1}$), $\gamma = 2R_c^2 / (R_c^2 - R_b^2)\ \omega$ (3.3)

where;

$\omega$ =: angular velocity of spindle (rad/ sec)

[ = $(2\pi/ 60)\ N$ ] , $N = RPM$

$R_c$ = radius of container (cm)

$R_b$ = radius of spindle (cm)

$M$ = torque input by instrument (dyne-cm)

$L$ = effective length of spindle (cm)

The instrument was calibrated using standard viscosity oil, which was recommended by the manufacturer. Temperature of the solution was maintained within ± 0.1 K. The viscosities were measured with accuracy less than 1 %. All measurements for each sample were performed in triplicate, and the values were reported as an average. The measurement was taken at atmospheric pressure and temperature range of 303 to 363 K, with10 K increment.

### 3.5.3 Solubility of $CO_2$ at high pressure

#### 3.5.3.1 $CO_2$ Absorption set-up

Figure 3.3 illustrates a schematic diagram of the stirred cell reactor, which was used for the $CO_2$ absorption experiment. The cell was equipped with a welded stirrer assemble, a thermocouple, an inlet gas tube and air vent tube. The thermocouple had the accuracy of ± 0.1 K. Figure 3.4 shows a complete schematic process flow diagram of $CO_2$ absorption setup at high-pressure. Operation was initially started by purging the air out from the gas reservoir by introducing sufficient flow of $CO_2$ throughout the system. The gas reservoir tank was loaded with purified $CO_2$ from the storage tank before it was heated and pressurized to the required condition.

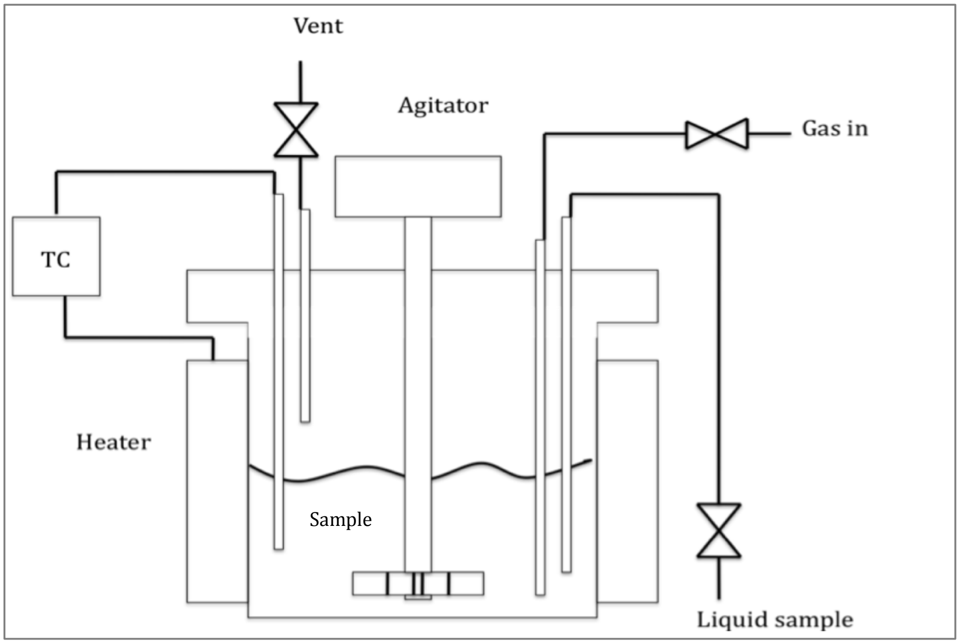

Figure 3.3. A diagram of stirred cell reactor.

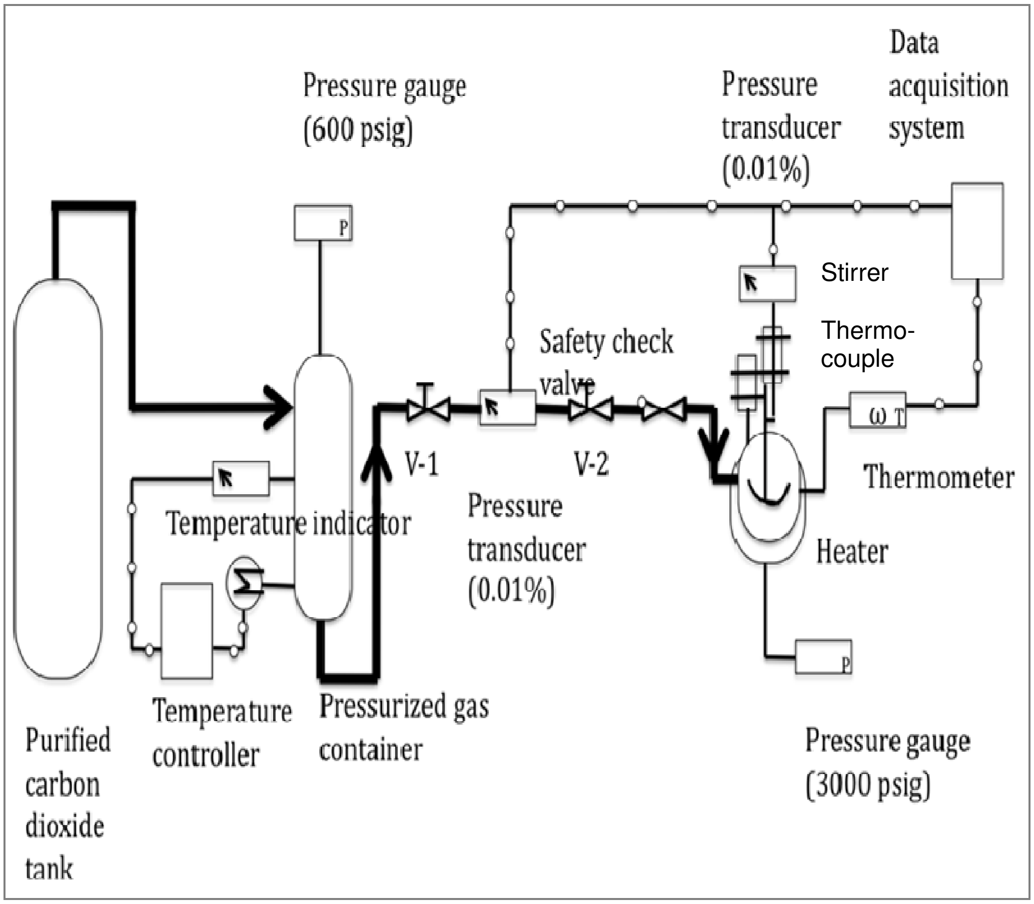

Figure 3.4. A schematic process flow diagram of the high pressure system.

A known volume of fresh sample was filled in the cell reactor prior to being sealed. The sample was stirred while the $CO_2$ gas was continuosly introduced into the system until equilibrium was reached. Following the contact of $CO_2$ with the solutions, the total systems' pressure dropped gradually, and equilibrium was considered reached after the pressure in the cell reactor remained constant for at least half an hour. A decrease in the pressure within the gas reservoir corresponded to a decrease in amount of $CO_2$. Both temperatures of gas container and reactor were kept constant, throughout the process.

### 3.5.3.2 $CO_2$ loading calculation techniques

During the experiment, all parameters were kept constant except for the pressure. By using the volume, pressure and temperature values, the moles of $CO_2$ in the gas phase can be determined. The initial and equilibrium pressures were recorded to compute the differences in moles throughout the absorption of which the solubility was expressed as per mole of total solvent. The solubility was calculated using Equation 3.4 as follows;

$$\alpha = \frac{\left[\frac{(P_{Ti} - P_{Vi}) * V_{gc}}{zRT}\right] - \left[\frac{(P_{Tf} - P_{vf}) * (V_{gc} + (V_{cell} - V_{sol}))}{zRT}\right]}{n_{total}} \qquad (3.4)$$

where;

$P_T$ = total pressure

$P_V$ = vapor pressure

$V_{gc}$ = volume of gas container

$V_{cell}$ = volume cell

$V_{sol}$ = volume solution

$i$ = initial condition

$f$ = final condition.

$n_{total}$ = summation of moles of MDEA and/ or the other absorbents in the liquid phase

### 3.5.4 Solubility of $CO_2$ at low pressure

#### 3.5.4.1 $CO_2$ Absorption set-up

The double jacket stirred cell reactor was equipped with a pressure transducer, a thermocouple, a magnetic stirrer, and a pH meter, which was linked to a data acquisition system. The temperature in the reactor was measured using a J-type thermocouple and controlled by an RC20 LAUDA water circulator. The temperature accuracy was about ± 0.1 K. A pressure transducer was used to record the total pressure in the reactor. A pH probe, which was linked to Metrohm$^R$ 719S auto titrator, was used to monitor pH of the system.

Another Metrohm$^R$ 716 DMS titrator was used to determine the final amine concentration. Both auto titrators were controlled by Tinet$^R$ 2.4 software. The gas flow rate into the reactor was measured using a set of Brooks$^R$ gas mass flow meters (model 5850E for $N_2$ and 5850C for $CO_2$), which was controlled by a four channel Brooks's mass flow controller (model 0154E).

Table 3.5 shows the specification of the double jacket cell reactor.

Table 3.5. Specification of double jacket cell reactor

| Specification | Value |
|---|---|
| Height | 85 mm |
| Internal diameter | 60 mm |
| Liquid holdup volume | 50 Ml |
| Material of construction | Resistant glass |

A schematic diagram of the experimental set-up used in this work is shown in Figure 3.5, the same experimental set up has been used by previous investigators in this laboratory, Benamor [268] and Si Ali [269].

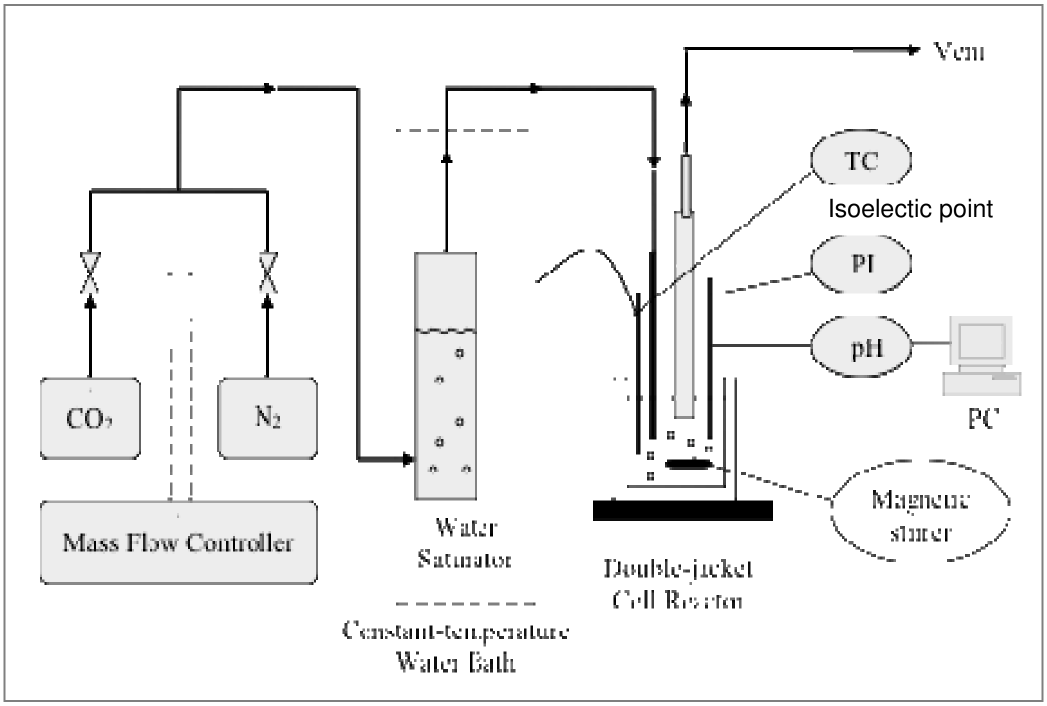

Figure 3.5. Schematic diagram of the experimental set-up.

The operating parameters for the $CO_2$ absorption at low pressure are summarized in Table 3.6.

Table 3.6. Operating parameters for the $CO_2$ absorption experiment.

| | |
|---|---|
| Temperature | 303.2 K |
| Ratio of $CO_2$ flow rate to total gas flow rate | 10%, 50%, 100% |
| Total gas flow rate | 2000 mL/ min |
| Operating pressure | 1 atm |

For a typical run, an aliquot sample of about 50 mL of the system was charged into the cell reactor and the cell temperature was set by using water bath. The gas, which was a blend of $N_2$ and $CO_2$, was mixed in the desired proportion by using Brooks mass flow controller and then was fed into the bottom section of the reactor. The gas was initially passed through a water saturator to avoid the possibility of water entrainment from the reactor that would eventually change the concentration of the system. Exhaust gas was also first gone through a condenser before being vented to the atmosphere. The condenser was used to re-condense any volatile species that might escape with the exhaust gas.

The reaction of $CO_2$ with the solvent causes a decrease in alkalinity. The variation of pH solution was continuously recorded by a computer-controlled auto titrator (Metrohm 719 DMS Titrino). The auto titrator was incorporated with the MET (Measurement Equivalence-point Titration) technique for the determination of the endpoint of pH. The pH decreased gradually due to the absorption of $CO_2$ into aqueous solution. A typical pH *versus* time curve is shown in Figure 3.6.

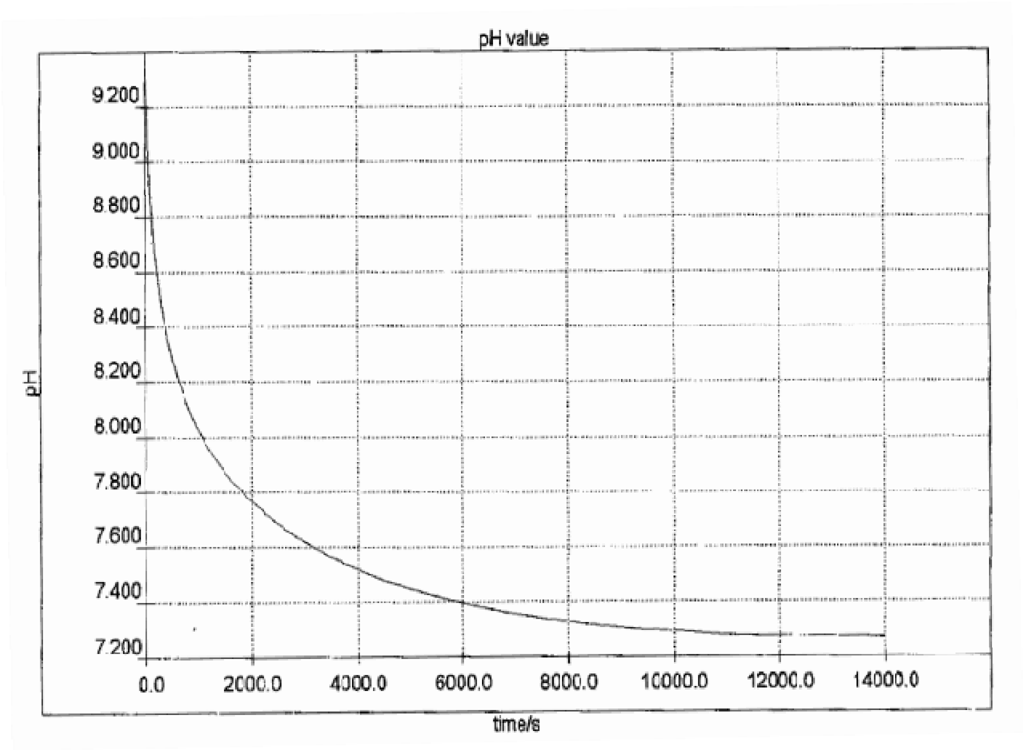

Figure 3.6. Typical pH curve of the solution during the reaction of alkanolamine and $CO_2$.

### 3.5.4.2. Determination of amine concentration

The amine concentration was determined at the beginning and at the end of each experiment to ensure that the concentration remained unchanged. This is done by titration of 10 mL sample with 1 M standard HCl. A typical titration curve is shown in Figure 3.7.

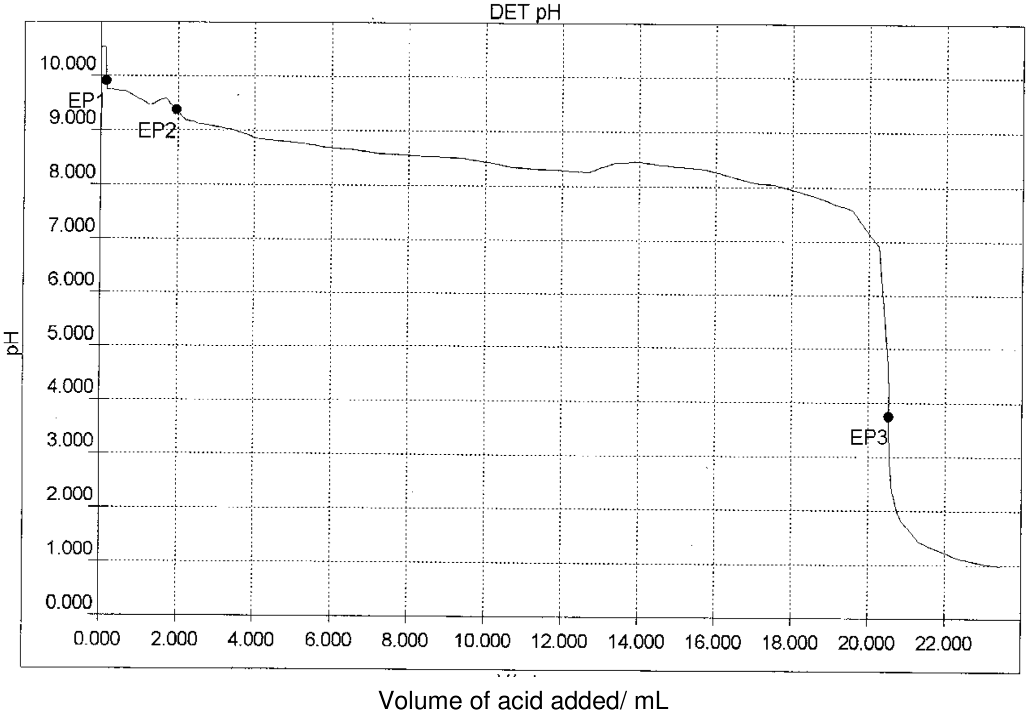

Figure 3.7. Typical titration curve of alkanolamine solution, using 1 M standard solution of HCl.

### 3.5.4.3. Determination of $CO_2$ loading

In order to obtain the $CO_2$ loading of the sample after the reaction, 5 mL sample of carbonated solution was taken through the sample point and mixed with 50 mL solution of 0.5 M $BaCl_2$ and 0.5 M NaOH. NaOH was used to convert all the free dissolved gas into non-volatile ionic species, and $BaCl_2$ was added to precipitate all the $CO_2$ existed in the carbonated solution. The mixtures were then stirred for about three hours at temperature of 343 K and atmospheric pressure. Then the sample was cooled down to room temperature before it was filtered and washed thoroughly to eliminate all traces of NaOH on the sample.

The white crystalline solid residue, $BaCO_3$ was precipitated with Glass micro fiber filter paper GF/ C, Whatman, to ensure the entire solid carbonate was collected during the filtration process. The solid $BaCO_3$ was then mixed with 300 mL of distilled water and was stirred for 3 hours to ensure the solid to be fully dissolved. Later it was titrated with the standard solution of 1 M HCl using computer-controlled auto titrator (Metrohm 716 DMS Titrino).

A typical titration curve is shown in the Figure 3.8. The data obtained were used in the calculation of $CO_2$ loading. This method of determining $CO_2$ loading *was* verified by conducting similar experiment on a sample containing a known amount of $NaHCO_3$. In order to ensure the accuracy of the data, the tests were repeated three times for each sample.

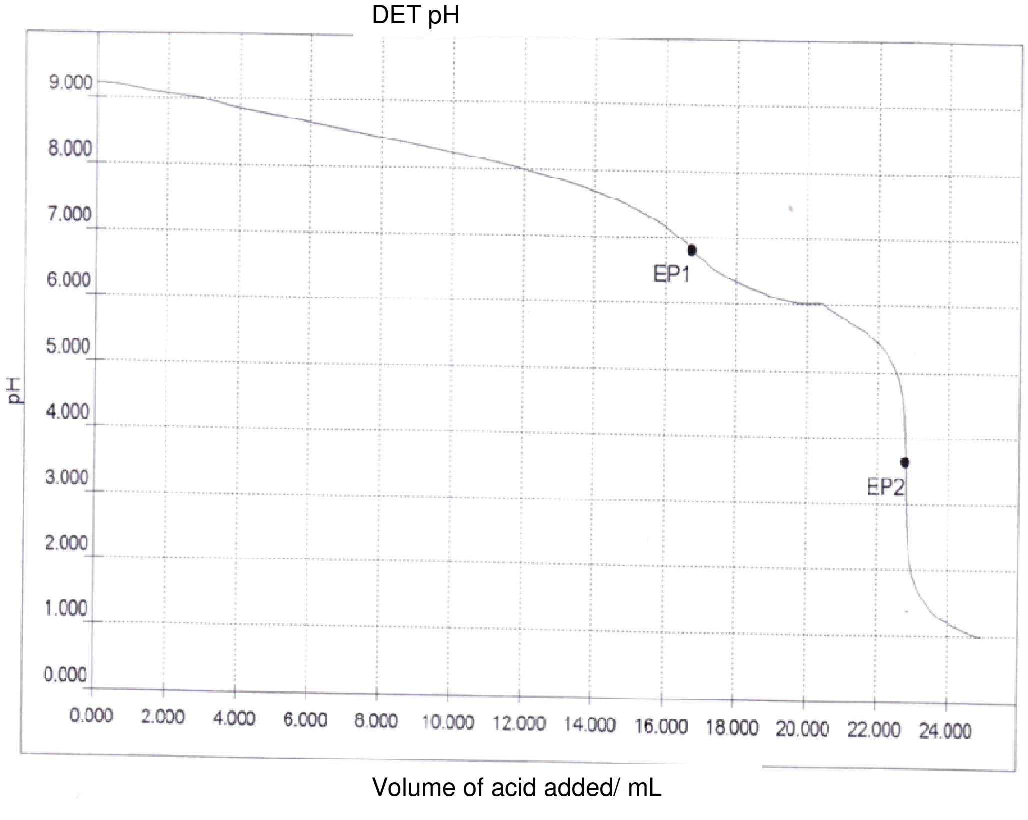

Figure 3.8. Titration curve of carbonated solution, using a solution of 1 M HCl.

### 3.5.4.4. Calculation

The volume of HCl used to neutralize the basic species in the solution is determined from the end points using the first derivative of the titration curve. The $CO_2$ loading of the solution is defined as total mol of $CO_2$ absorbed per mol of MDEA. It is calculated by using the following Equation 3.5;

$$CO_2 \text{ loading, } \alpha_{CO2} = \frac{V_{HCl} \text{ x } M_{HCl}}{2\,(M_{MDEA})(V_{sample})} \quad (3.5)$$

where;

$\alpha$ = $CO_2$ loading in mol of $CO_2$ per mol of amine

$V_{HCl}$ =Volume of HCl needed to neutralized the basic species in mL

$V_{sample}$ = Volume of sample taken for analysis in mL

$M$ = Molarity of the alkanolamine solution in mol per litre.

The detailed derivation of Equation 3.5 is given in Appendix.

# Chapter 4: DENSITY

## 4.1 Introduction

This chapter explores the density of various binary and ternary blends of MDEA - [gua][OTf]. The atmospheric densities have been taken at wide temperature range of 293 to 333 K with the increment of 10 K. This measurement has been done to determine the changing in densities at different temperatures and concentrations of MDEA and [gua][OTf].

## 4.2 Validation of the density measurement

To establish the accuracy of density meter calibration, the density of pure MDEA was determined and compared with the reported values of Henni *et al.* [197] and Esther *et al.*, [267]. The comparison of measured densities for pure MDEA between this work and the available literature values are shown in Figure 4.1. The agreement was good between them with an average absolute deviation from Equation 4.1 in the density of pure MDEA of 0.20 %.

$$AAD = 1/N \sum_{i=1}^{N} \frac{(X_{\exp} - X_{\mathrm{lit,\,i}})}{X_{\mathrm{lit,\,i}}} \quad \mathrm{x} \quad 100 \qquad (4.1)$$

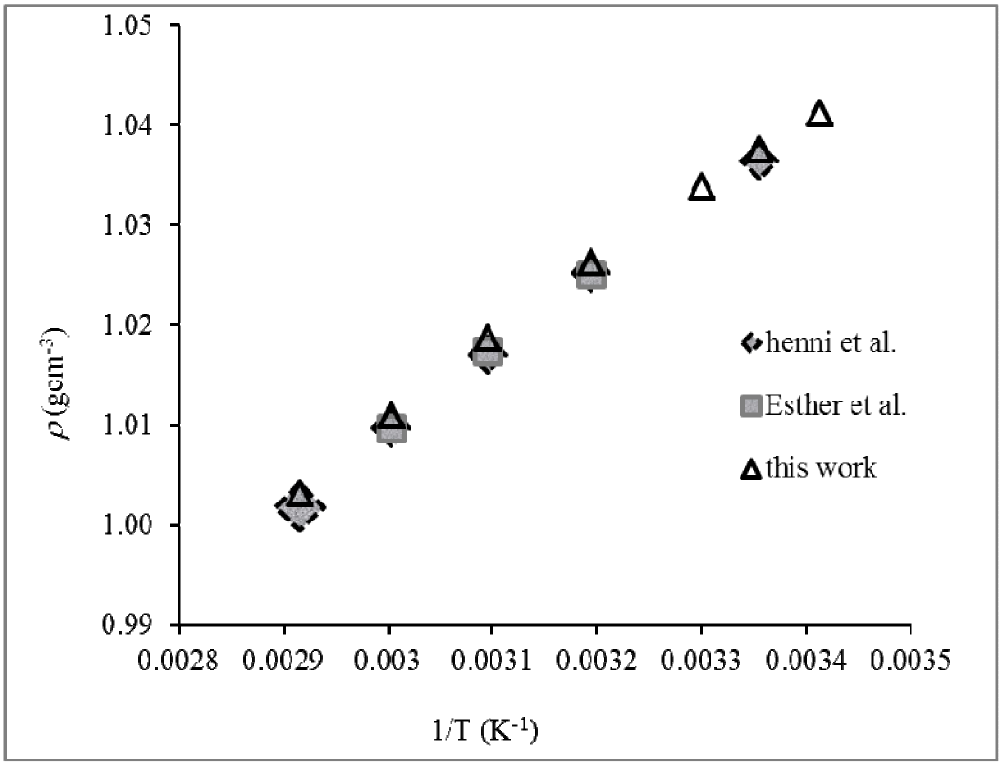

Figure 4.1. Comparison of densities for pure MDEA with literatures [197, 267].

### 4.3 Effect temperature and concentrations

Experimentally measured densities of the binary and ternary (MDEA – [gua][OTf]) systems throughout the whole temperature range from 298 to 363 K were plotted in Figure 4.2 and 4.3. The density curves showed a quasi-linear decrease in values for all binary and ternary systems of MDEA - [gua][OTf]. In regard, the density of binary 1 M [gua][OTf] ionic liquid system (0M1G) was higher by 7.26 % than that corresponding to binary 1 M MDEA system (1M0G) in the range of temperature considered. Similarly, the density varies 6.52 % between 0M4G and 4M0G. The density values of the binary systems studied followed this sequence: 0M4G > 0M1G > 4M0G > 1M0G.

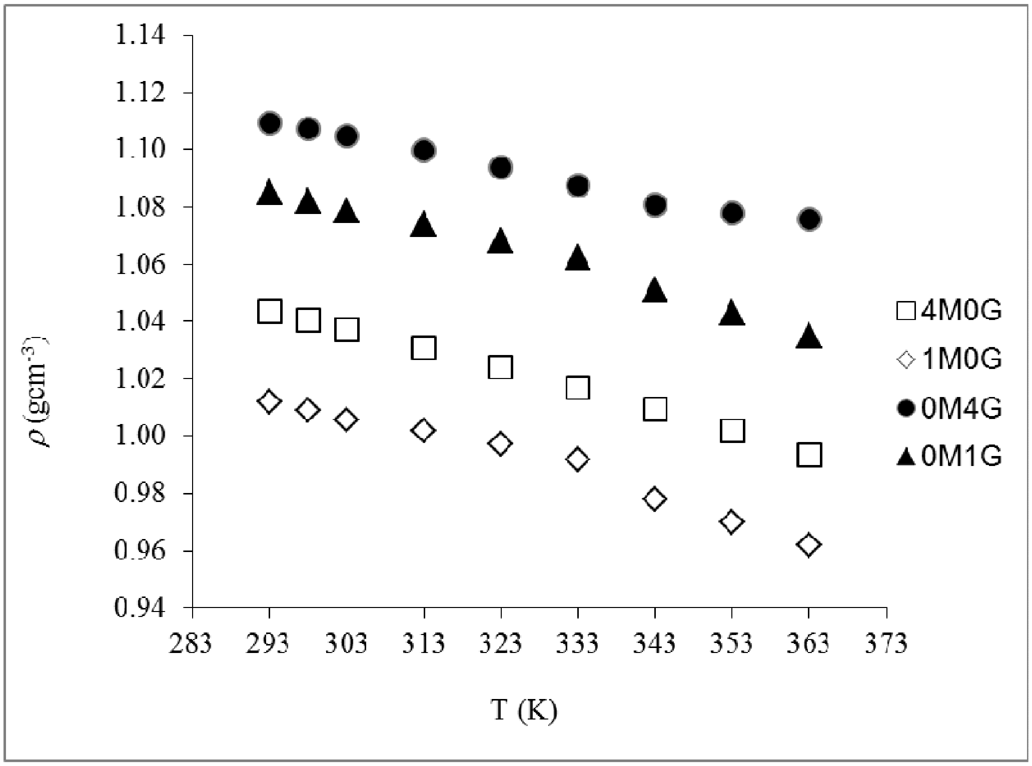

Figure 4.2. Density of binary systems 4M0G, 1M0G, 0M4G, 0M1G at various temperatures.

By observing Figure 4.3, the sequence followed the order of 4M2G > 4M1G > 1M3G > 2M2G > 3M1G. Composition of [gua][OTf] highly influenced the density of the systems compared to MDEA. This has been proved by the density of which 1M3G was higher than that of 2M2G and 3M1G. The divergence of 1 M [gua][OTf] gave substantial increment between 4M1G and 4M2G. This was due to the high molecular weight of [gua][OTf] which is 209.15 g mol$^{-1}$.

All systems showed that the density linearly decreased with increasing temperatures. This indicated that the kinetic energy of molecules and volume between molecules are increased when temperature is increased. Therefore, the interactions between molecules decreases, so the contraction in volume decreases and this led to the decreasing of density with increase in temperature.

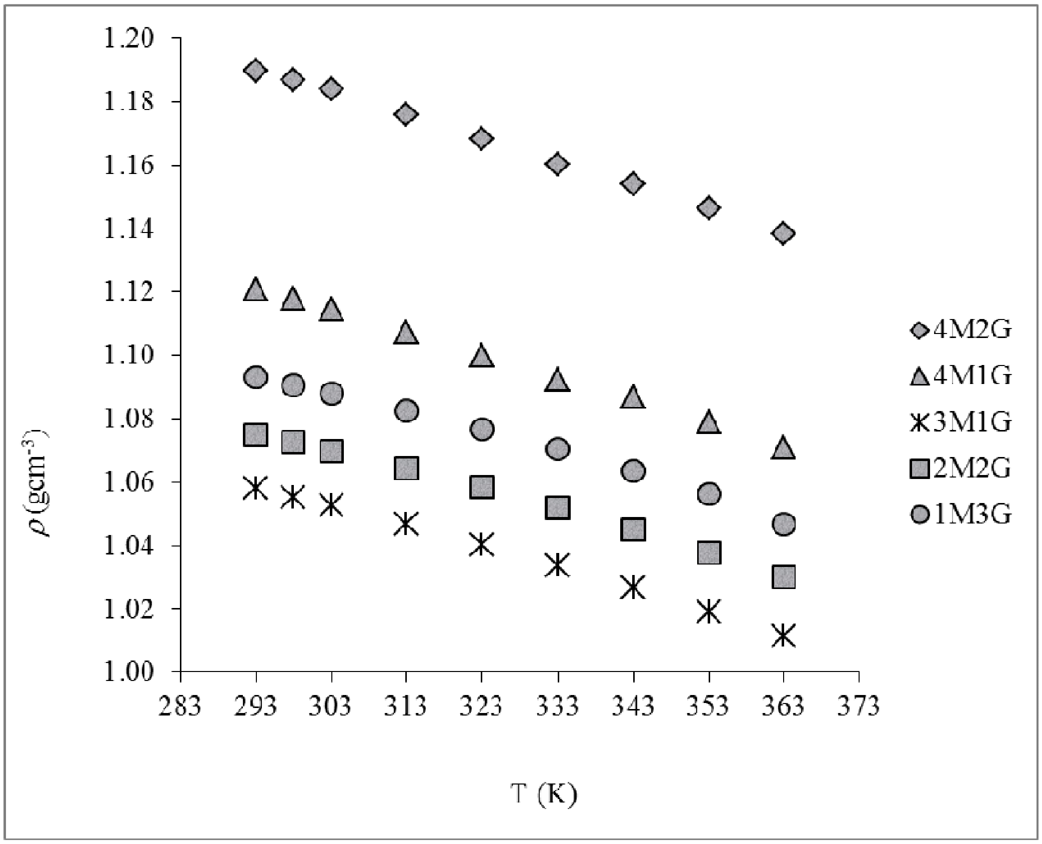

Figure 4.3. Density of ternary systems 4M2G, 4M1G, 3M1G, 2M2G, 1M3G at different temperatures.

In specified volume, amount of water contained in a mixture solutions decreased as concentration increased. It is known that water in the blend of MDEA – [gua][OTf] appeared to act as a diluent, and thus lower the density of the system.

## 4.4 Comparison of studied binary and ternary systems with literature

Ionic liquids are generally denser than either organic solvents or water, with typical values of densities ranging from 1 to 1.6 g $cm^{-3}$. Jacquemin *et al.* [199] has studied the effect of the presence of water on the densities and viscosities for the six common ionic liquids ((1-butyl-3 methylimidazolium hexafluorophosphate ([bmim][$PF_6$]), 1-butyl-3-methylimidazolium tetrafluoroborate ([bmim][$BF_4$]), 1-butyl-3-methylimidazolium bis (trifluoromethylsulfonyl) imide ([bmim][$NTf_2$]), 1-ethyl-3-methylimidazolium bis (trifluoromethylsulfonyl)imide ([emim][$NTf_2$]), 1-ethyl-3-methylimidazolium ethylsulfate ([emim][$EtSO_4$]) and butyltrimethylammonium bis(trifluoromethylsulfonyl)imide ([$N_{4111}$][$NTf_2$]).

As compared to the studied binary and ternary systems of guanidinium trifluoromethanesulfonate, [gua][OTf] and MDEA for which the densities at 293 to 353 K, range from 0.96 to 1.19 g $cm^{-3}$, the density of six dried ionic liquids vary higher typically from 1.16 to 1.52 g $cm^{-3}$ for temperature from 293 to 353 K. Figure 4.4, 4.5, 4.6 and 4.7 showed the densities of binary and ternary systems (4M0G, 1M0G, 0M4G and 0M1G) are relatively lower than dried and water-saturated ionic liquids due to the different composition and presence of water and MDEA.

However, the observed difference for dried and water-saturated is from 1 to 2 % which is almost negligible from the practical point of view. This suggested the minor change in density with water content between the dried and water-saturated ionic liquids as reported by Jacquemin *et al.* [199] appears to be largely independent of temperature.

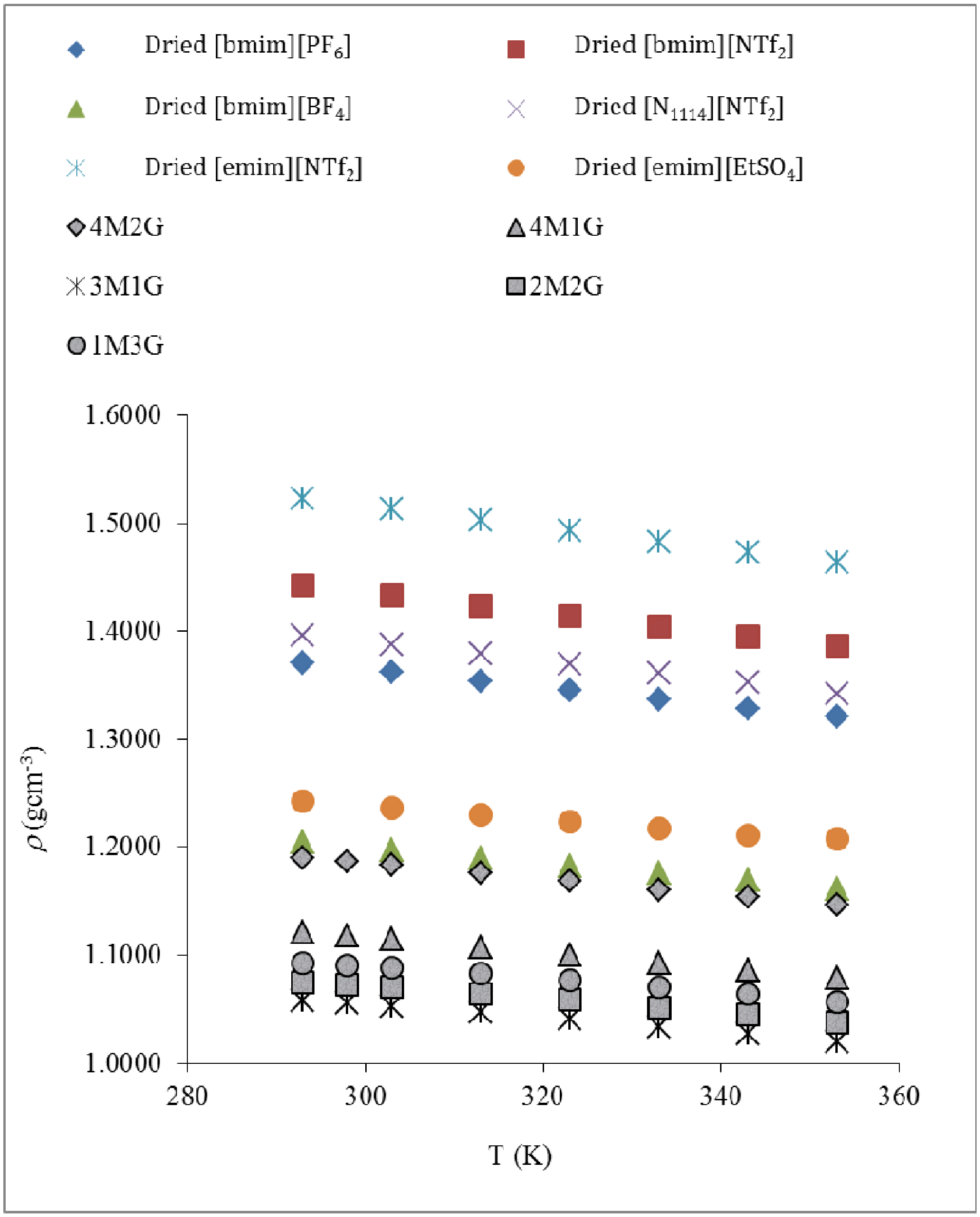

Figure 4.4. Comparison in density between the binary system from this work *i.e.* 4M0G, 1M0G, 0M4G and 0M1G, and the dried ionic liquids *i.e.* [bmim][PF$_6$], [bmim][BF$_4$], [bmim][NTf$_2$], [emim][NTf$_2$], [emim][EtSO$_4$] and [N$_{4111}$][NTf$_2$] [199].

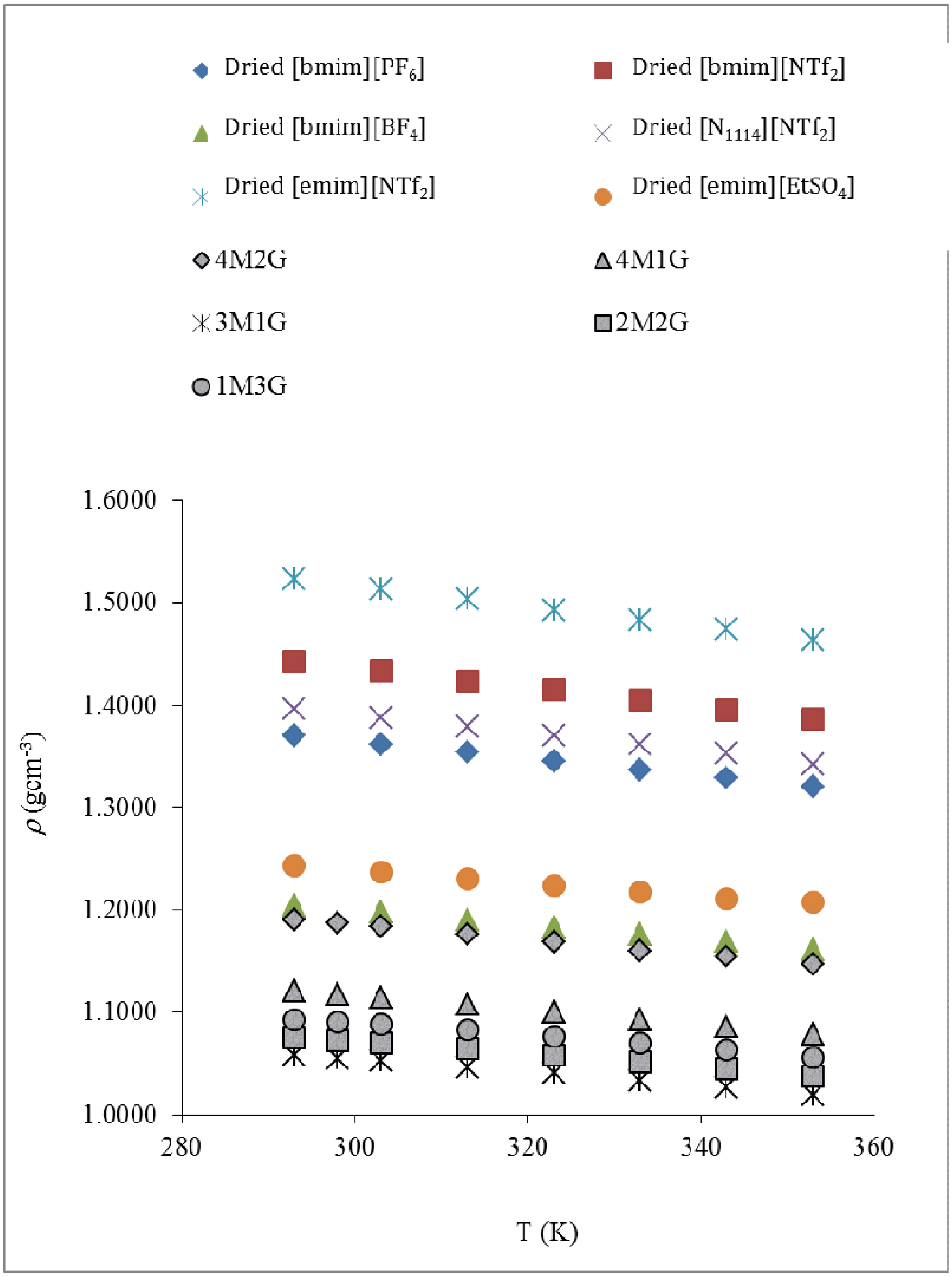

Figure 4.5. Comparison in density between the ternary system from this work *i.e.* 4M2G, 4M1G, 3M1G, 2M2G and 1M3G, and the dried ionic liquids *i.e.* [bmim][PF$_6$], [bmim][BF$_4$], [bmim][NTf$_2$], [emim][NTf$_2$], [emim][EtSO$_4$] and [N$_{4111}$][NTf$_2$] [199].

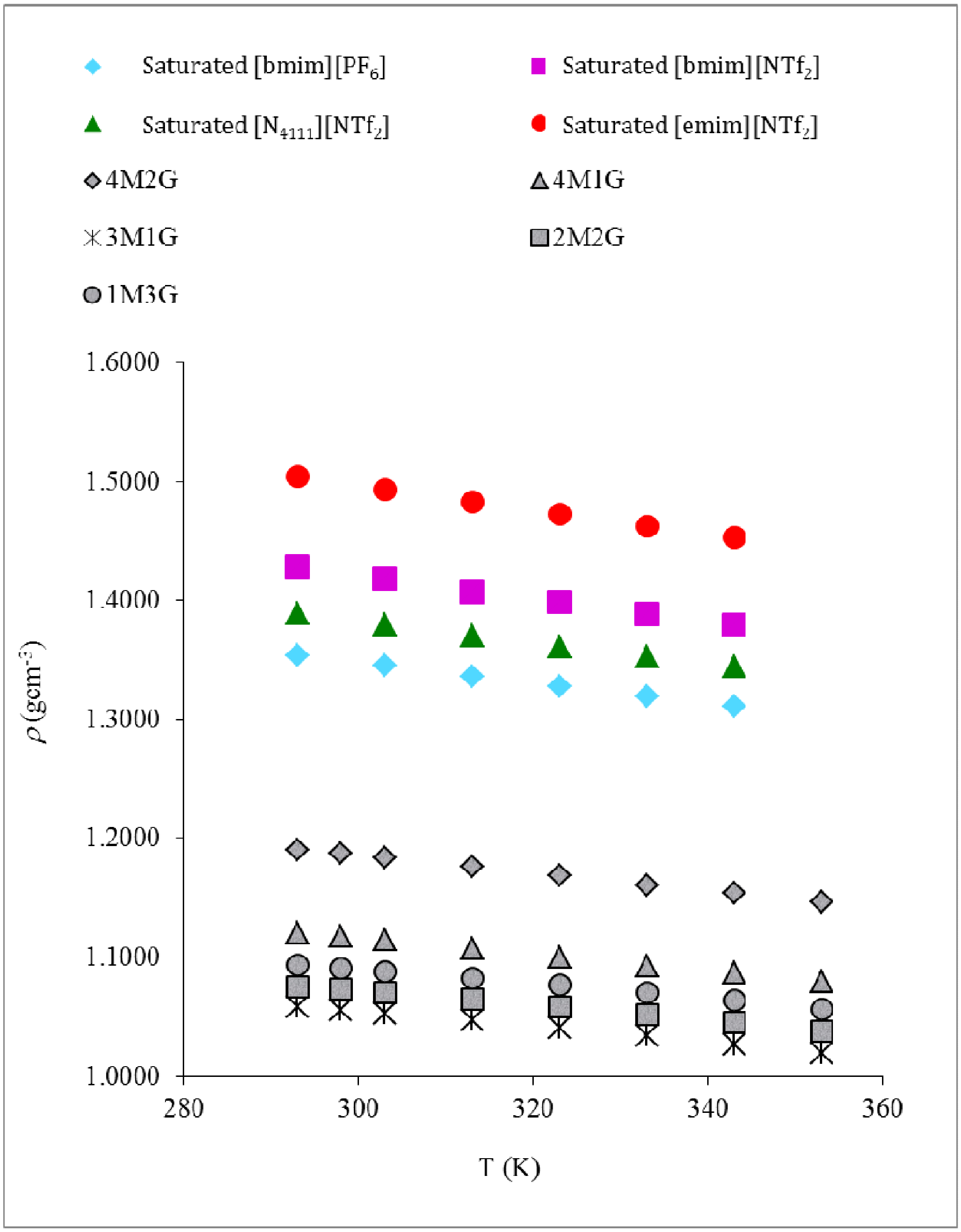

Figure 4.6. Comparison in density between the binary system from this work *i.e.* 4M0G, 1M0G, 0M4G and 0M1G, and the water-saturated ionic liquids *i.e.* [bmim][$PF_6$], [bmim][$BF_4$], [bmim][$NTf_2$], [emim][$NTf_2$], [emim][$EtSO_4$] and [$N_{4111}$][$NTf_2$] [199].

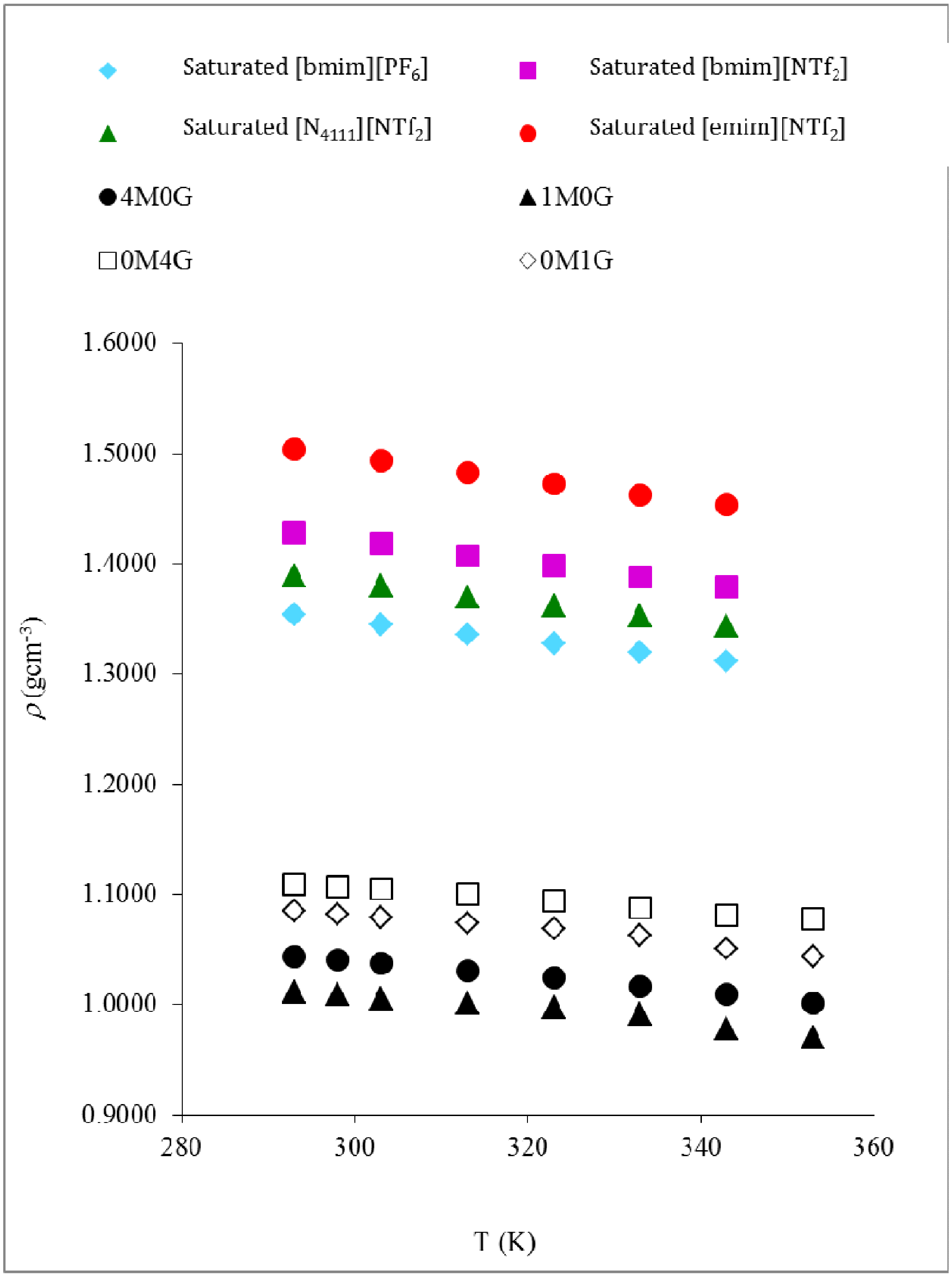

Figure 4.7. Comparison in density between the ternary system from this work *i.e.* 4M2G, 4M1G, 3M1G, 2M2G and 1M3G, and the water-saturated ionic liquids *i.e.* [bmim][$PF_6$], [bmim][$BF_4$], [bmim][$NTf_2$], [emim][$NTf_2$], [emim][$EtSO_4$] and [$N_{4111}$][$NTf_2$] [199].

The studied aqueous binary ([gua][OTf] - $H_2O$) was also compared with aqueous [hmim][Br] [196] and aqueous [BuPy][$BF_4$] [231] with composition of ionic liquid were 0.5, respectively. Figure 4.8 shows that the aqueous binary ([gua][OTf] - $H_2O$) has lower densities compared to aqueous [hmim][Br] and aqueous [BuPy][$BF_4$] at the same temperature range.

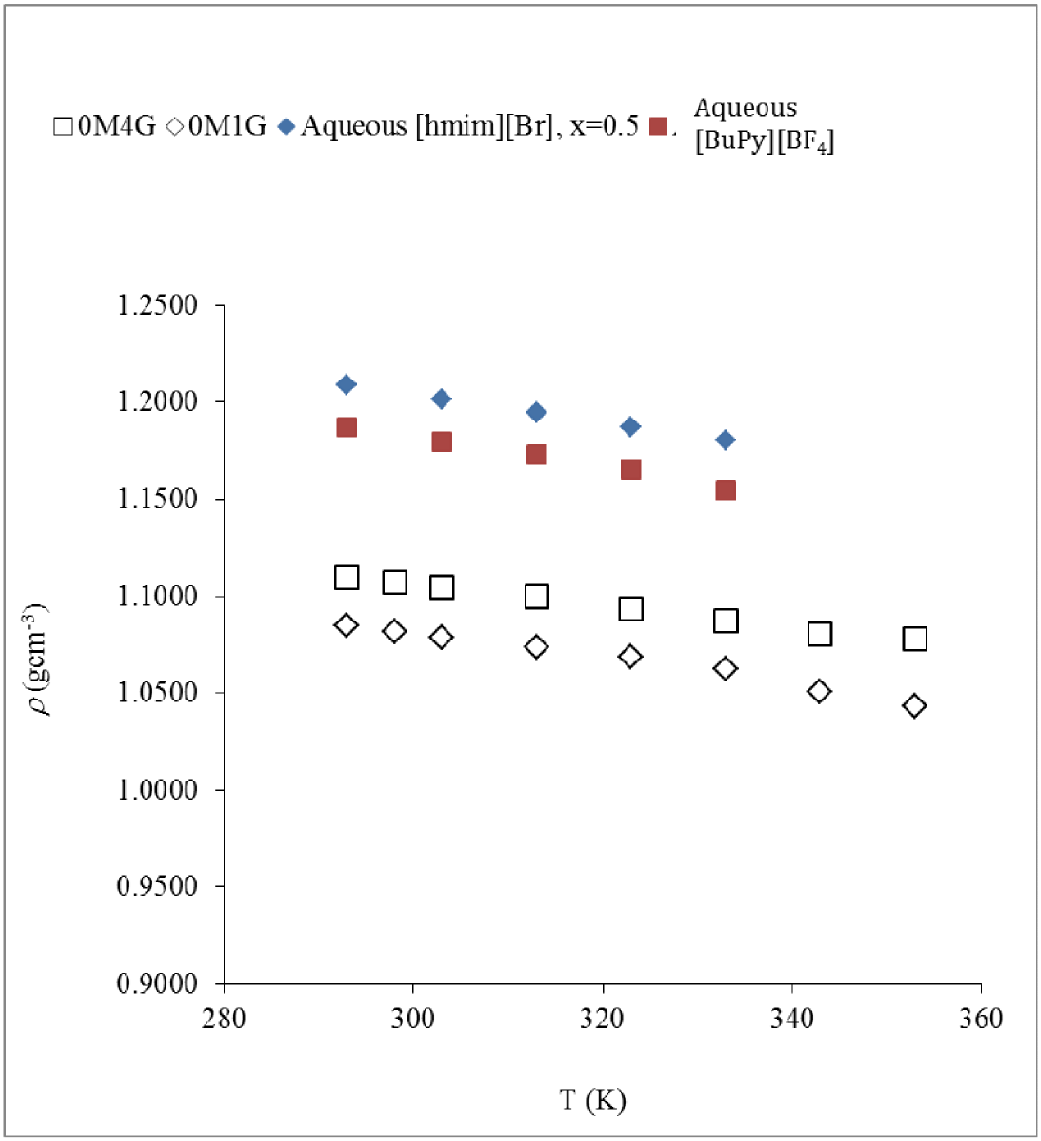

Figure 4.8. Comparison in density between aqueous binary ([gua][OTf] - $H_2O$) *i.e.* 0M1G and 0M4G with aqueous [hmim][Br] [196] and aqueous [BuPy][$BF_4$] [231].

## 4.5 Correlations of density as function of temperature, concentration of MDEA and [gua][OTf]

A correlation relating the binary and ternary blended systems of MDEA – [gua][OTf] with temperature from 293 to 363 K can be expressed using the following linear equation (Equation 4.2) [232, 234]:

$$\rho\ (\text{g cm}^{-3}) = [\beta\ ((\text{g cm}^{-3})\ \text{K})\ \text{x}\ T\ (\text{K})] + \alpha\ (\text{g cm}^{-3}) \qquad (4.2)$$

The characteristic parameters, $\alpha$ and $\beta$ were determined from *y* - intercept and slope of plotting a linear graph of density *versus* temperature at different concentration. The values of $\alpha$ and $\beta$ are summarized in Table 4.1.

From Table 4.1, 0M1G exhibited highest $\alpha$ value followed by 4M2G and pure MDEA. As for aqueous MDEA binary systems, the $\alpha$ value increased as the concentration of MDEA increased. Meanwhile, the $\alpha$ value decreased as the concentration of [gua][OTf] increased.

It was observed that there was an increment trend for the ternary systems as the $\alpha$ value increased from 1M3G < 2M2G < 3M1G < 4M1G < 4M2G. The $R^2$ values obtained for all systems were very close to unity, which further enhanced the precision of correlation in Equation 4.2 to be used as estimation for the densities within temperature range from 293 to 363 K.

Table 4.1. The correlated parameters for densities at various concentrations.

| System | Sample | $\beta$ (x $10^{-4}$ g $cm^{-3}$K) | $\alpha$ (g $cm^{-3}$) | $R^2$ |
|---|---|---|---|---|
| Binary | 4M0G | - 7.10 | 1.252 | 0.9980 |
| | 1M0G | - 7.06 | 1.221 | 0.9714 |
| | 0M4G | - 5.19 | 1.261 | 0.9872 |
| | 0M1G | - 7.08 | 1.294 | 0.9961 |
| Ternary | 4M2G | - 7.40 | 1.408 | 0.9992 |
| | 4M1G | - 7.11 | 1.330 | 0.9990 |
| | 3M1G | - 6.44 | 1.283 | 0.9917 |
| | 2M2G | - 6.38 | 1.263 | 0.9962 |
| | 1M3G | - 6.62 | 1.253 | 0.9970 |
| Pure MDEA | Pure MDEA | - 7.61 | 1.264 | 0.9999 |

A quadratic equation relating characteristic parameter, $\beta$ with concentration of [gua][OTf] is expressed as below:

$$- \beta \times 10^{-4} = a\,([\text{gua}][\text{OTf}])^2 + b\,[\text{gua}][\text{OTf}] + c \qquad (4.3)$$

where;

*a, b* and *c* are the coefficients for the Equation 4.3 and are tabulated in Table 4.2.

Table 4.2. Coefficients values of *a*, *b* and *c* at different concentrations of MDEA.

| Concentration of MDEA, M | Coefficient | | |
|---|---|---|---|
| | *A* | *b* | *C* |
| 4.0 | 0.14 | -0.13 | 7.05 |
| 2.0 | - | -0.15 | 7.06 |
| 0 | - | -0.63 | 7.71 |

The quadratic equations relating coefficients *b* and *c* with concentration of MDEA are shown below:

$b$ = -0.0575 [MDEA]$^2$ + 0.355 [MDEA] – 0.63

$c$ = 0.08 [MDEA]$^2$ – 0.48 [MDEA] + 7.71

By substituting $b$ and $c$ obtained into Equation 4.3:

$$-\beta \text{ x } 10^{-4} = 0.14 ([\text{gua}][\text{OTf}])^2 + (-0.0575 [\text{MDEA}]^2 + 0.355 [\text{MDEA}] – 0.63) ([\text{gua}][\text{OTf}]) + (0.08 [\text{MDEA}]^2 – 0.48 [\text{MDEA}] + 7.71)$$

A linear equation relating characteristic parameter, $\alpha$ with concentration of [gua][OTf] is then expressed as below:

$$\alpha = p ([\text{gua}][\text{OTf}])^2 + q [\text{gua}][\text{OTf}] + r \qquad (4.4)$$

where;

$p$, $q$ and $r$ are the coefficient for the Equation 4.4 and are tabulated in Table 4.3:

Table 4.3. Coefficients $p$, $q$ and $r$ at different concentration of MDEA.

| | Coefficient | | |
|---|---|---|---|
| Concentration of MDEA, M | *P* | *q* | *r* |
| 4.0 | 2 x $10^{-5}$ | 0.078 | 1.252 |
| 2.0 | - | 0.0107 | 1.221 |
| 0 | - | -0.011 | 1.305 |

The quadratic equation relating coefficients $q$ and $r$ with concentration of MDEA is shown below:

$q$ = 0.0057 [MDEA]$^2$ - 0.0005 [MDEA] - 0.011

$r = 0.0144\ [\mathrm{MDEA}]^2 - 0.0708\ [\mathrm{MDEA}] + 1.305$

By substituting $q$ and $r$ obtained into Equation 4.4;

$$\alpha = (2 \times 10^{-5})\ ([\mathrm{gua}][\mathrm{OTf}])^2 + (0.0057\ [\mathrm{MDEA}]^2 - 0.0005\ [\mathrm{MDEA}] - 0.011)\ ([\mathrm{gua}][\mathrm{OTf}]) + 0.0144\ [\mathrm{MDEA}]^2 - 0.0708\ [\mathrm{MDEA}] + 1.305)$$

Finally by combining Equations 4.3 and 4.4 into 4.2, density in terms of temperature, concentration of MDEA and [gua][OTf] is expressed as below;

$$\text{Density, } \rho\ (\mathrm{g\ cm^{-3}}) = [\beta\ (\mathrm{g\ cm^{-3}\ K}) \times \mathrm{T\ (K)}] + \alpha\ (\mathrm{g\ cm^{-3}}) \qquad (4.2)$$

where;

$$-\beta \times 10^{-4} = 0.14\ ([\mathrm{gua}][\mathrm{OTf}])^2 + (-0.0575\ [\mathrm{MDEA}]^2 + 0.355\ [\mathrm{MDEA}] - 0.63)\ ([\mathrm{gua}][\mathrm{OTf}]) + (0.08\ [\mathrm{MDEA}]^2 - 0.48\ [\mathrm{MDEA}] + 7.71)$$

$$\alpha = (2 \times 10^{-5})\ ([\mathrm{gua}][\mathrm{OTf}])^2 + (0.0057\ [\mathrm{MDEA}]^2 - 0.0005\ [\mathrm{MDEA}] - 0.011)\ ([\mathrm{gua}][\mathrm{OTf}]) + (0.0144\ [\mathrm{MDEA}]^2 - 0.0708\ [\mathrm{MDEA}] + 1.305)$$

Concentrations of MDEA and [gua][OTf] were in unit molar, M.

Density is calculated by using Equation 4.2 and has been compared with the experimental data. Figure 4.9 displays comparison between the calculated and experimental density for all systems.

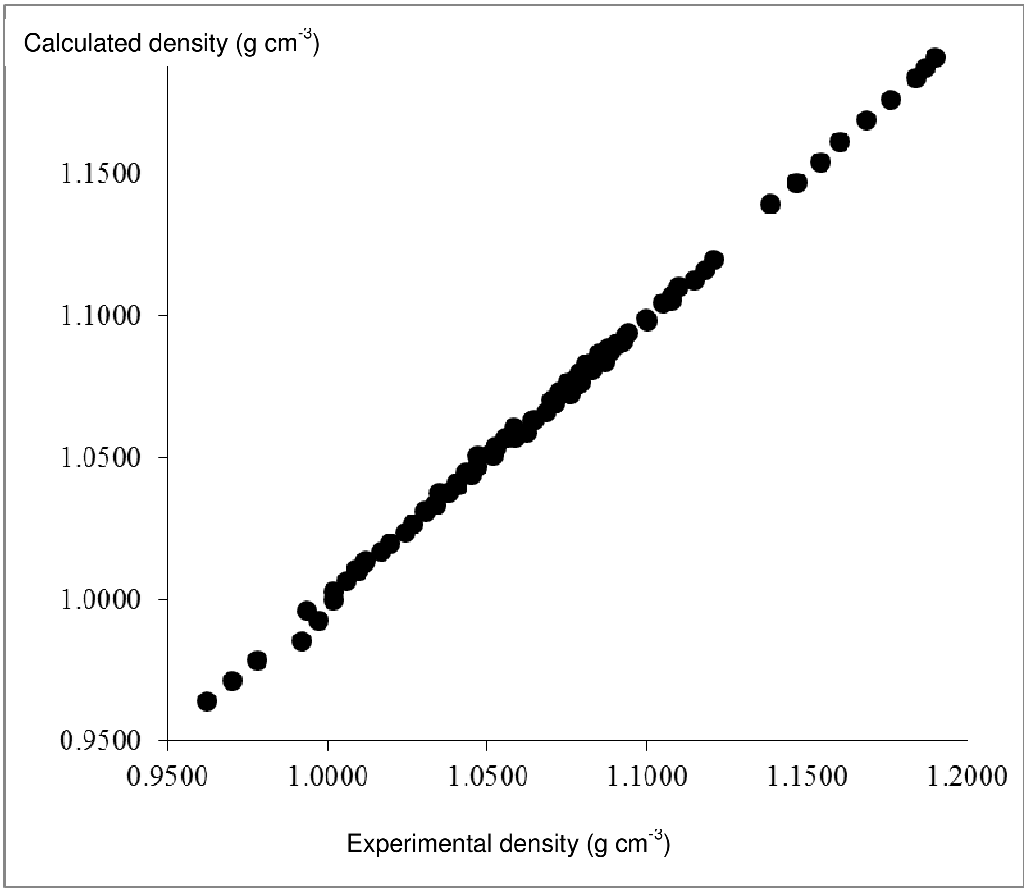

Figure 4.9. The density comparison between the calculated and the measured density

The percentages deviations of calculated densities for 4M1G, 4M0G, 3M1G and 0M1G were less than ± 1 % in temperature range from 293 to 363 K. The deviation for 1M0G was less than – 2 %. However, systems with 2 M [gua][OTf] and higher, have shown deviation up to 9.587 %.

## 4.6 Thermal expansion

Table 4.4 shows that the changes in coefficients of thermal expansion values and the variation of volume expansion of the studied systems could be considered as still dependent of temperature. Since the densities decrease linearly with temperature, it is obvious that $\alpha_p$ values are all positives but slightly increasing with temperature. Similar trends as densities are observed for the thermal expansion coefficients. The values of $\alpha_p$ increased from 6.1795 x $10^{-6}$ to 7.9184 x $10^{-6}$ $K^{-1}$ with increasing of [gua][OTf] composition in the systems.

The coefficients of thermal expansion values for the systems studied in this work were calculated based on the measured density data using Equation 4.5:

$$\alpha_p = -1 / \rho\ (\partial \rho / \partial \mathrm{T})_{\mathrm{p}} = -\ \beta / (\alpha + \beta \mathrm{T}) \qquad (4.5)$$

where;

$\alpha_p$ is the coefficient of thermal expansion;

$\rho$ is the density;

T is the temperature;

$\alpha$ and $\beta$ are the correlation coefficients obtained from Equation (4.2) by fitting the measured density data.

Table 4.4. Coefficients of thermal expansion for blended binary and ternary systems of MDEA - [gua][OTf] using Equation 4.2.

| T (K) | $\alpha_p$ (x $10^{-6}$ $K^{-1}$) | | | | | | | | |
|---|---|---|---|---|---|---|---|---|---|
| | Binary | | | | Ternary | | | | |
| | 4M0G | 1M0G | 0M4G | 0M1G | 4M2G | 4M1G | 3M1G | 2M2G | 1M3G |
| 293 | 6.7652 | 7.0668 | 7.1216 | 6.6700 | 6.1795 | 6.3048 | 6.6832 | 7.1315 | 7.5025 |
| 298 | 6.7882 | 7.0918 | 7.1471 | 6.6923 | 6.1986 | 6.3247 | 6.7056 | 7.1570 | 7.5308 |
| 303 | 6.8113 | 7.1171 | 7.1727 | 6.7148 | 6.2179 | 6.3448 | 6.7282 | 7.1827 | 7.5592 |
| 313 | 6.8580 | 7.1681 | 7.2245 | 6.7602 | 6.2568 | 6.3853 | 6.7738 | 7.2347 | 7.6168 |
| 323 | 6.9054 | 7.2198 | 7.2771 | 6.8062 | 6.2962 | 6.4263 | 6.8199 | 7.2874 | 7.6753 |
| 333 | 6.9534 | 7.2724 | 7.3304 | 6.8529 | 6.3361 | 6.4679 | 6.8668 | 7.3409 | 7.7347 |
| 343 | 7.0021 | 7.3256 | 7.3846 | 6.9002 | 6.3765 | 6.5100 | 6.9143 | 7.3952 | 7.7949 |
| 353 | 7.0515 | 7.3797 | 7.4395 | 6.9481 | 6.4174 | 6.5527 | 6.9624 | 7.4503 | 7.8562 |
| 363 | 7.1015 | 7.4346 | 7.4953 | 6.9967 | 6.4589 | 6.5959 | 7.0112 | 7.5062 | 7.9184 |

## 4.7 Conclusions

The density of MDEA – [gua][OTf] demonstrates concentration and temperature dependent behaviour. The density of binary systems 4M0G, 1M0G, 0M4G, 0M1G at various temperatures were approximately in the range of 0.96 - 1.10 g $cm^{-3}$. Meanwhile, the density of ternary systems 4M2G, 4M1G, 3M1G, 2M2G, 1M3G at various temperatures were in the range of 1.05 – 1.19 g $cm^{-3}$. The density of MDEA – [gua][OTf] decreases linearly as the temperature increases and the composition of [gua][OTf] decreases. Yet, the presence of water in the systems can modify the values of thermophysical property (density) greatly.

A correlation of density as a function of concentration (unit in M) of MDEA and [gua][OTf] at temperature range of 303.2 and 333.2 K was developed and the extended coefficient was also reported. The density measurements were only carried out at temperature lower than 333 K while at higher temperatures the composition of the samples is less accurate due to the vaporization of water.

Thermal expansion has been calculated from the density data obtained previously. The values of $\alpha_p$ increased with the increase in temperatures and composition of [gua][OTf] with the values of $\alpha_p$ varied from (6.1795 to 7.9184) x$10^{-6}$ $K^{-1}$.

# Chapter 5: VISCOSITY

## 5.1 Introduction

This chapter reports on the viscosity of aqueous binary guanidinium trifluoromethanesulfonate, [gua][OTf] and aqueous ternary system of [gua][OTf] and MDEA as a function of temperature and concentration. The viscosities were taken at the temperature range of 293 to 333 K with 10 K increment and at atmospheric pressure.

## 5.2 Validation of the viscosity measurement

In order to validate the viscosity measurement, the viscosities of pure MDEA were measured and compared with values reported from literature. Viscosities of pure MDEA obtained through this work agreed well with those reported by Li *et al.* [212]. The comparison between the measured viscosities of pure MDEA and those reported in literature [212] is shown in Figure 5.1 and the average deviation was estimated to be ± 0.05 %.

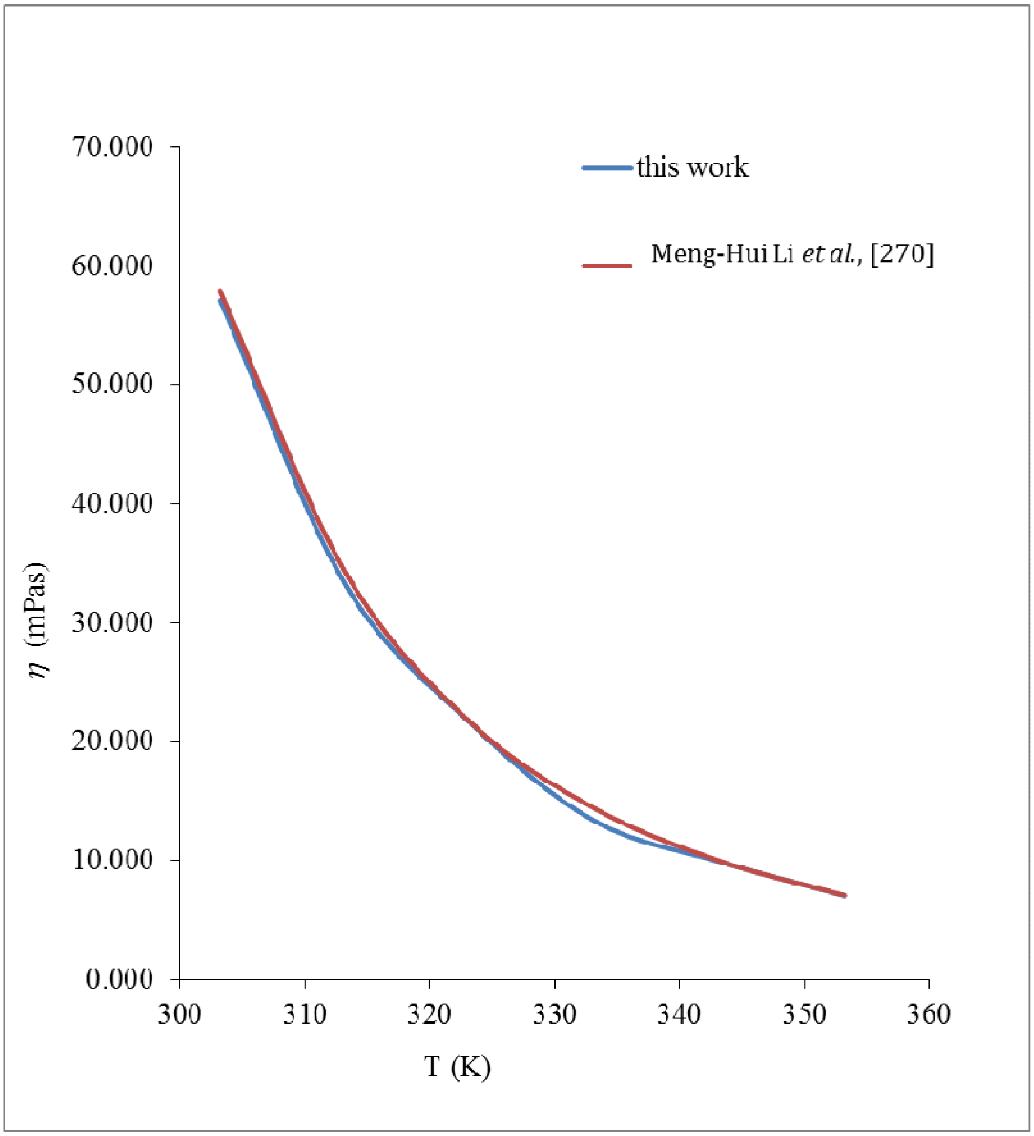

Figure 5.1. Comparison of pure MDEA with literature review [212].

### 5.3 Viscosity of binary [gua][OTf]-$H_2O$ systems

The measured viscosities of aqueous [gua][OTf] systems are summarized in Table 5.1. The results show that the viscosities of aqueous [gua][OTf] demonstrate a temperature dependent behaviour. The viscosities decrease exponentially as the temperature increase.

Figure 5.2 and 5.3 shows the viscosities of various composition of binary [gua][OTf] – $H_2O$ at temperature range between 293 and 333 K. Figure 5.3 is the scale up of Figure 5.2 for the systems with lower composition of [gua][OTf]. It can be seen from Figure 5.2 that at room temperature, there is a large difference of viscosities between the systems of different composition of [gua][OTf]. However, as the temperature approaches 333 K, the difference in the viscosities of all the systems became very small.

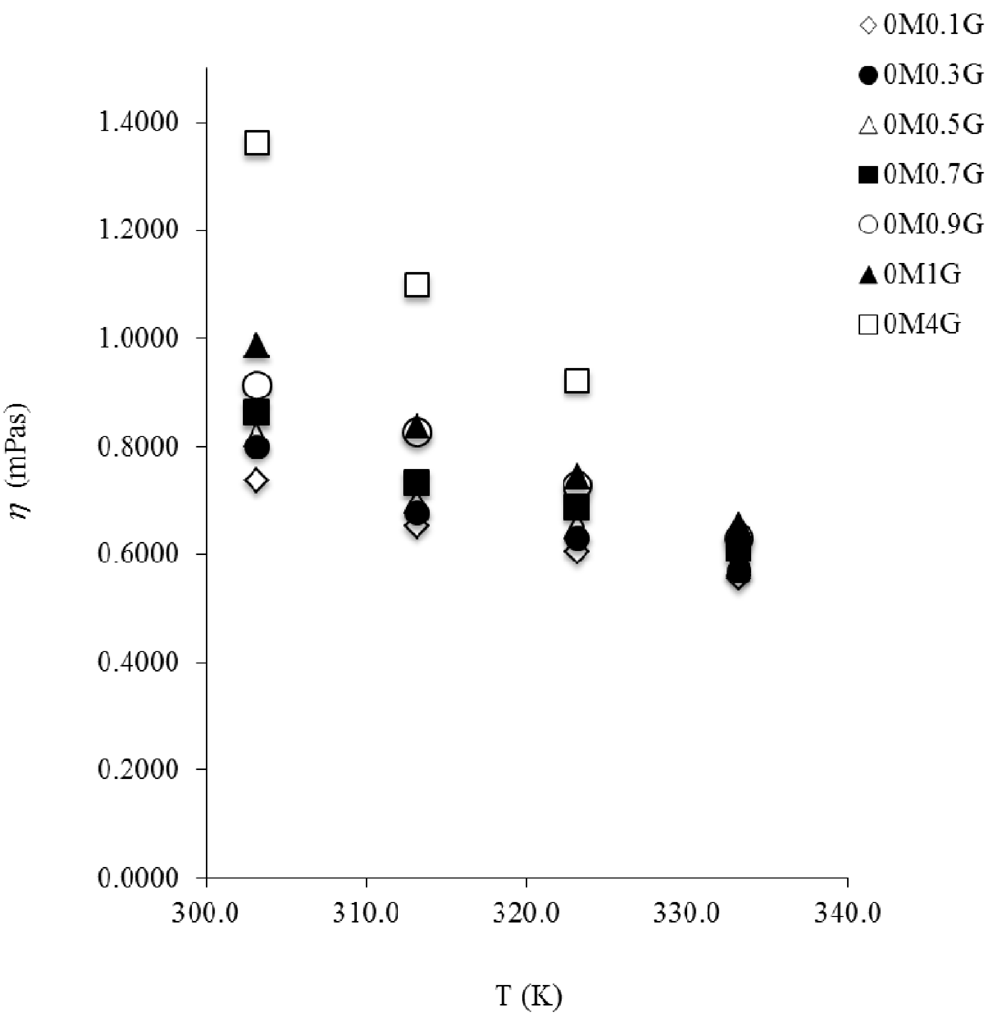

Figure 5.2. Viscosity of various concentrations of aqueous [gua][OTf].

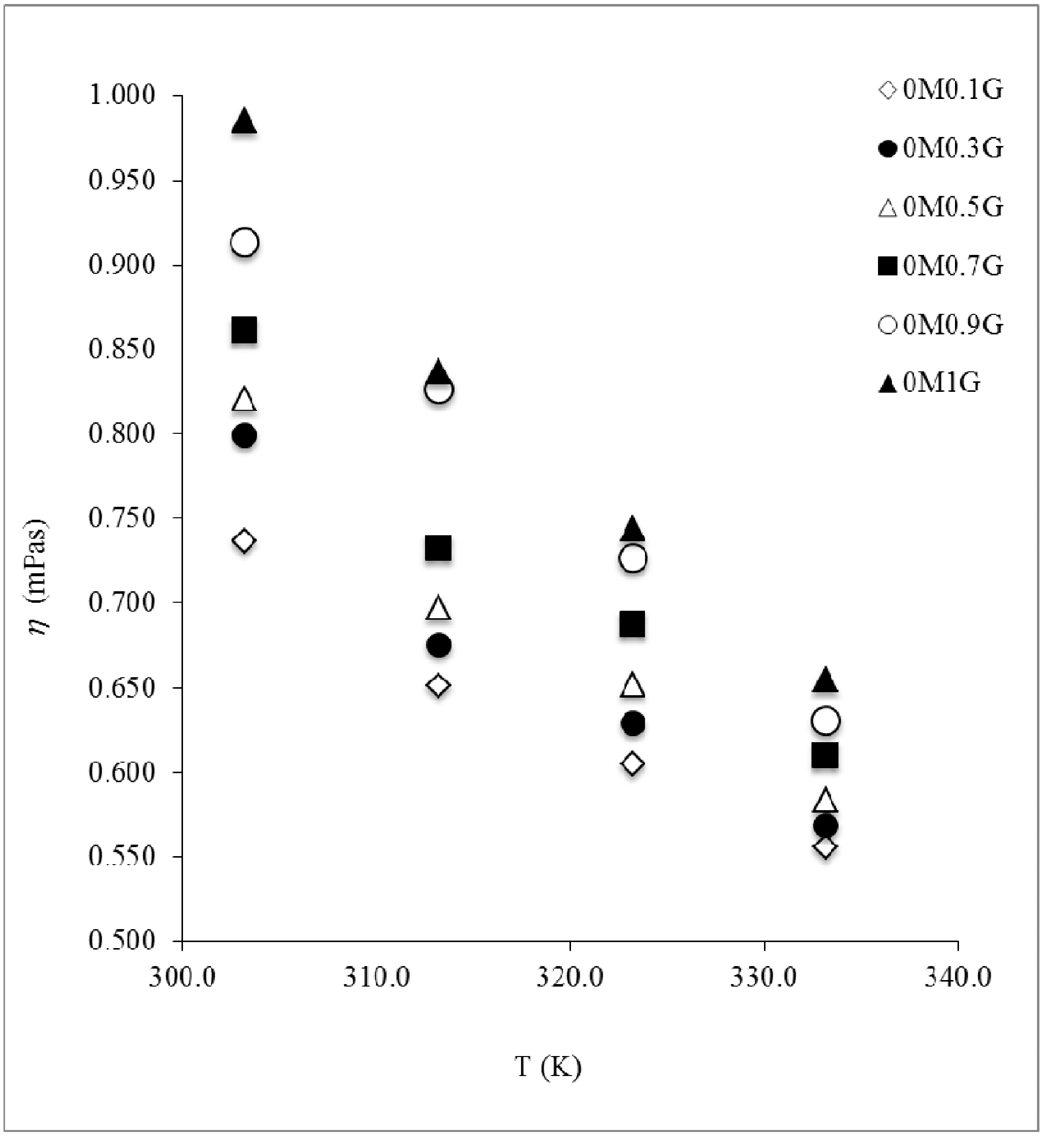

Figure 5.3. Enlargement graph (refer Figure 5.2) for viscosity of systems with concentration from 0.1 G to 1.0 G.

## 5.4 Viscosity of ternary [gua][OTf]-MDEA-$H_2O$ systems

Figure 5.4 shows that at fixed temperature the viscosity of aqueous mixture of MDEA - [gua][OTf] increase as the concentration of [gua][OTf] increase. This is due to the interactions occurring between the solute molecules *i.e.* [gua][OTf] and the organic liquid solvent, MDEA. This phenomenon could be explained by the increase of the hydrogen bonding force between [gua][OTf] and MDEA, which leads to the increase in the viscosity of the mixture.

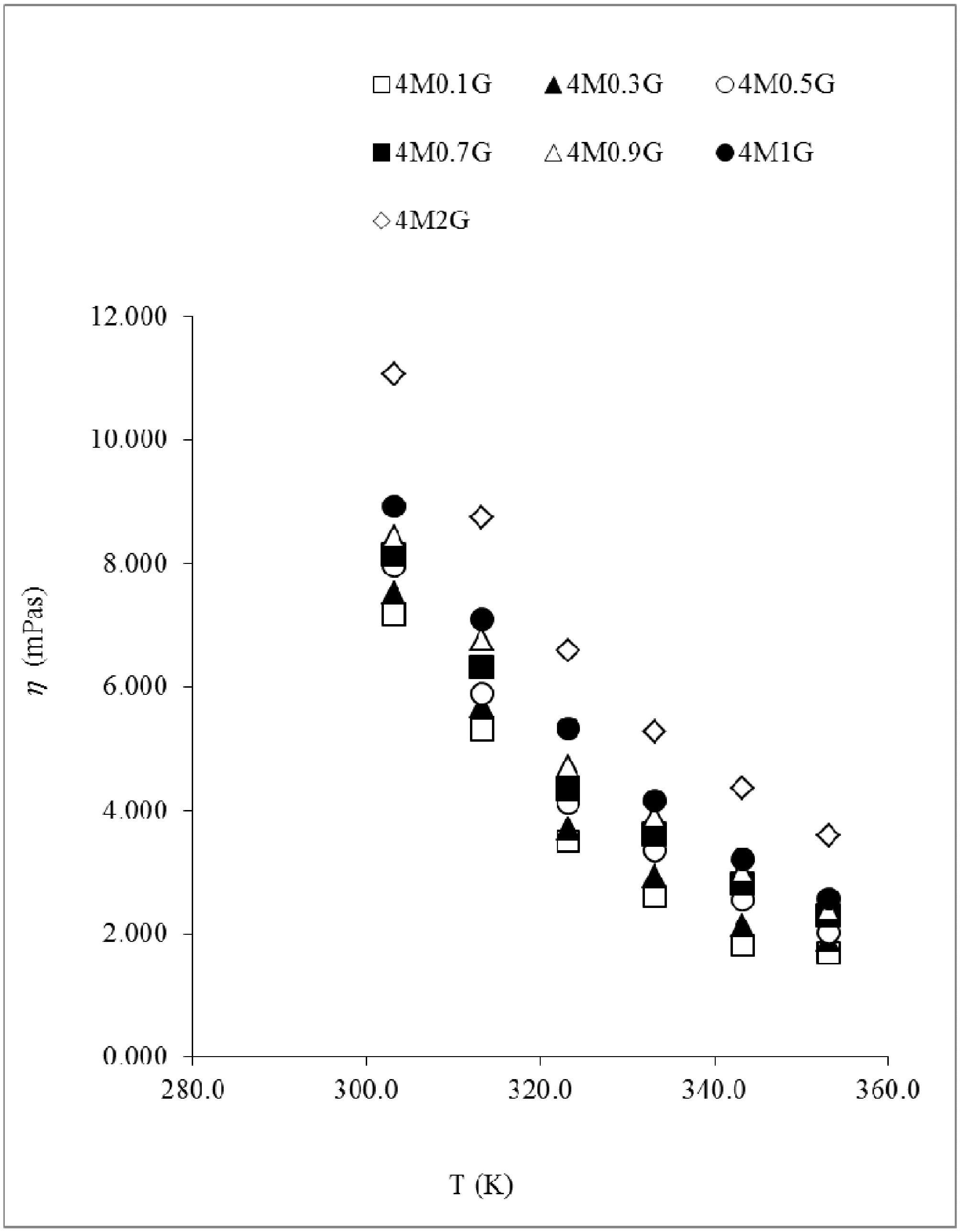

Figure 5.4. Viscosity of 4M0.1G, 4M0.3G, 4M0.5G, 4M0.7G, 4M0.9G, 4M1G and 4M2G at 303.2, 313.2, 323.2 and 333.2 K.

The study also shows that the viscosity of 1 M MDEA is higher than that of 1 M [gua][OTf] (refer Figure 5.2). Therefore, addition of [gua][OTf] into the aqueous solution of MDEA would reduce the overall viscosity of the aqueous mixtures. More over the presence of water which is known to have a low viscosity is another factor for the viscosity reduction. Some studies reported that water would accommodate in the ionic liquids structure possibly by forming hydrogen bonds with both anion and the cation. The dramatic decrease in viscosity was due to the water molecules reducing the electrostatic attractions between the ions. Thus, the overall cohesive energy of the systems is lowered.

## 5.5 Comparison of studied systems with the literature

For the ([gua][OTf] - $H_2O$) binary and ([gua][OTf] - $H_2O$ - MDEA) ternary systems it can be observed that the viscosity remains constant with increasing shear rates (from 0 to 200 $s^{-1}$). This seems to be consistent with the findings of Seddon *et al.* [223] and Huddleston *et al.* [262]. They reported a Newtonian behaviour for ionic liquids of alkylimidazolium $BF_4^-$ family (with the alkyl chain length between 4 and 8 carbons atoms) while the ionic liquids with longer alkyl chains (number of carbon atoms typically 12) are thixotropic fluids whose viscosity decreases when the shear rate is increased.

Figure 5.5 and 5.6 show the comparison between the studied systems and several dried and water saturated alkylammonium-based ionic liquids and imidazolium-based ionic liquids. These figures show that the viscosities of the studied systems are lower than that of ([bmim][$PF_6$]), ([bmim][$BF_4$]), ([bmim][$NTF_2$]), ([emim][$NTf_2$]), ([emim][$EtSO_4$]) and ([$N_{4111}$][$NTf_2$]). Jacquemin *et al.* [199] reported that the alkylammonium-based ionic liquids exhibited a higher viscosity than the imidazolium-based ionic liquids with same anion. Furthermore the viscosity of the latter ionic liquids increases with the length of the alkyl chain on the imidazolium ring.

On the contrary, one would expect that as the side-chain length increases, the overall contribution of the strong, associating, electrostatic (and hydrogen-bond) terms to the interactions diminishes, while the contribution of weaker, non-associating, dispersion forces increases, resulting in the viscosity reduction due to the size of the non-polar part of the cations. Though, this is not the case for studied systems ([gua][OTf] - $H_2O$ – MDEA).

The justification put forward by Bonhôte *et al.* [253], was that it was the increase in the Van der Waals interactions due to the presence of a long alkyl chain that leads to higher viscosities. However, this argument seems to come from a simple correlation of what was observed without a strong molecular basis. Also, the study of Tokuda *et al.* [221] was more profound, since it relates the behaviour of the transport properties, viscosity and diffusion, to a ratio of ionic conductivities that can be interpreted as a measure of ionic dissociation or "ionicity".

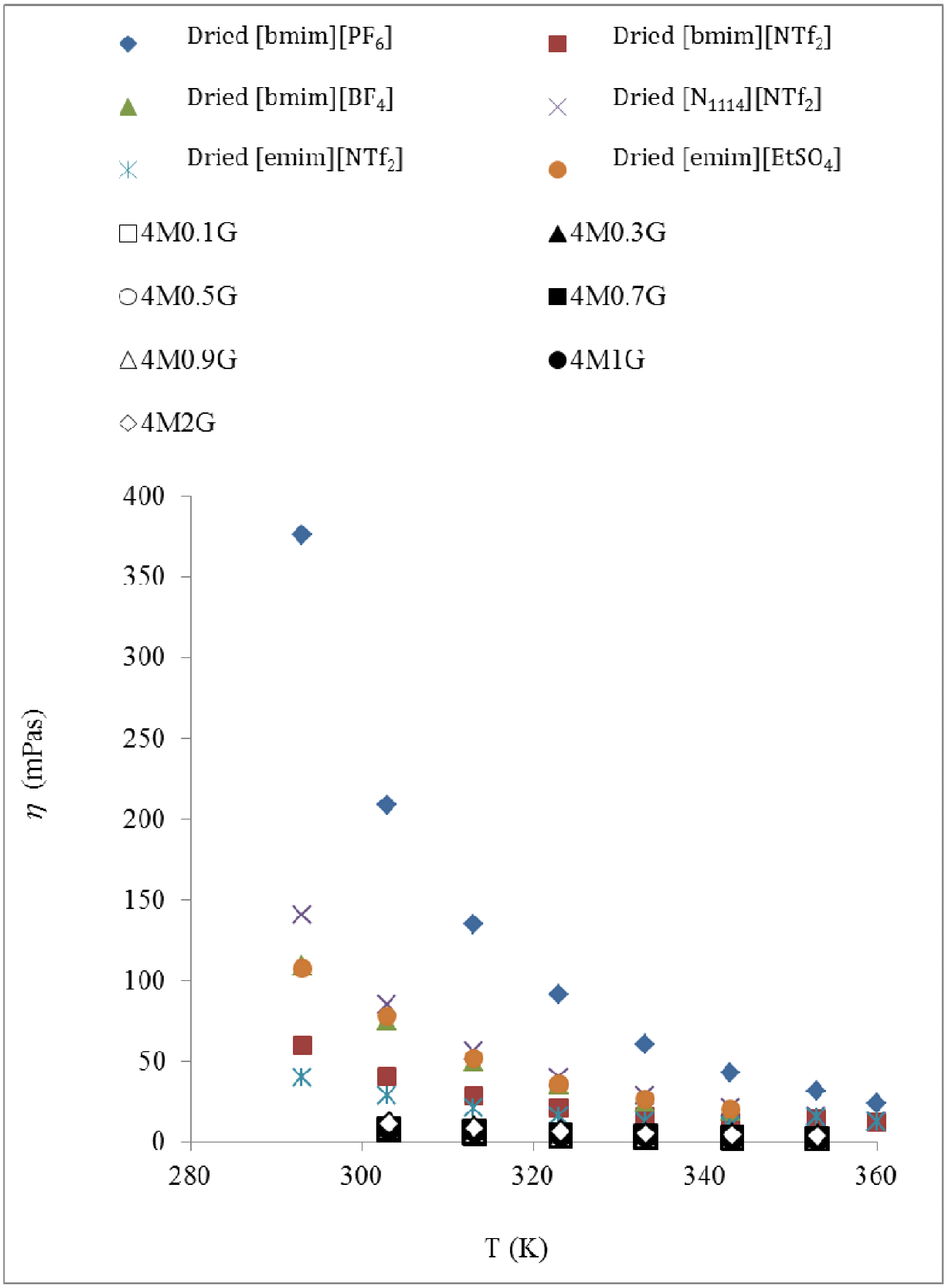

Figure 5.5. Comparison of the viscosity between ternary system *i.e.* 4M0.1G, 4M0.3G, 4M0.5G, 4M0.7G, 4M0.9G, 4M1G, 4M2G and dried ionic liquids *i.e.* [bmim][$PF_6$], [bmim][$BF_4$], [bmim][$NTf_2$], [emim][$NTf_2$], [emim][$EtSO_4$] and [$N_{4111}$][$NTf_2$] [221].

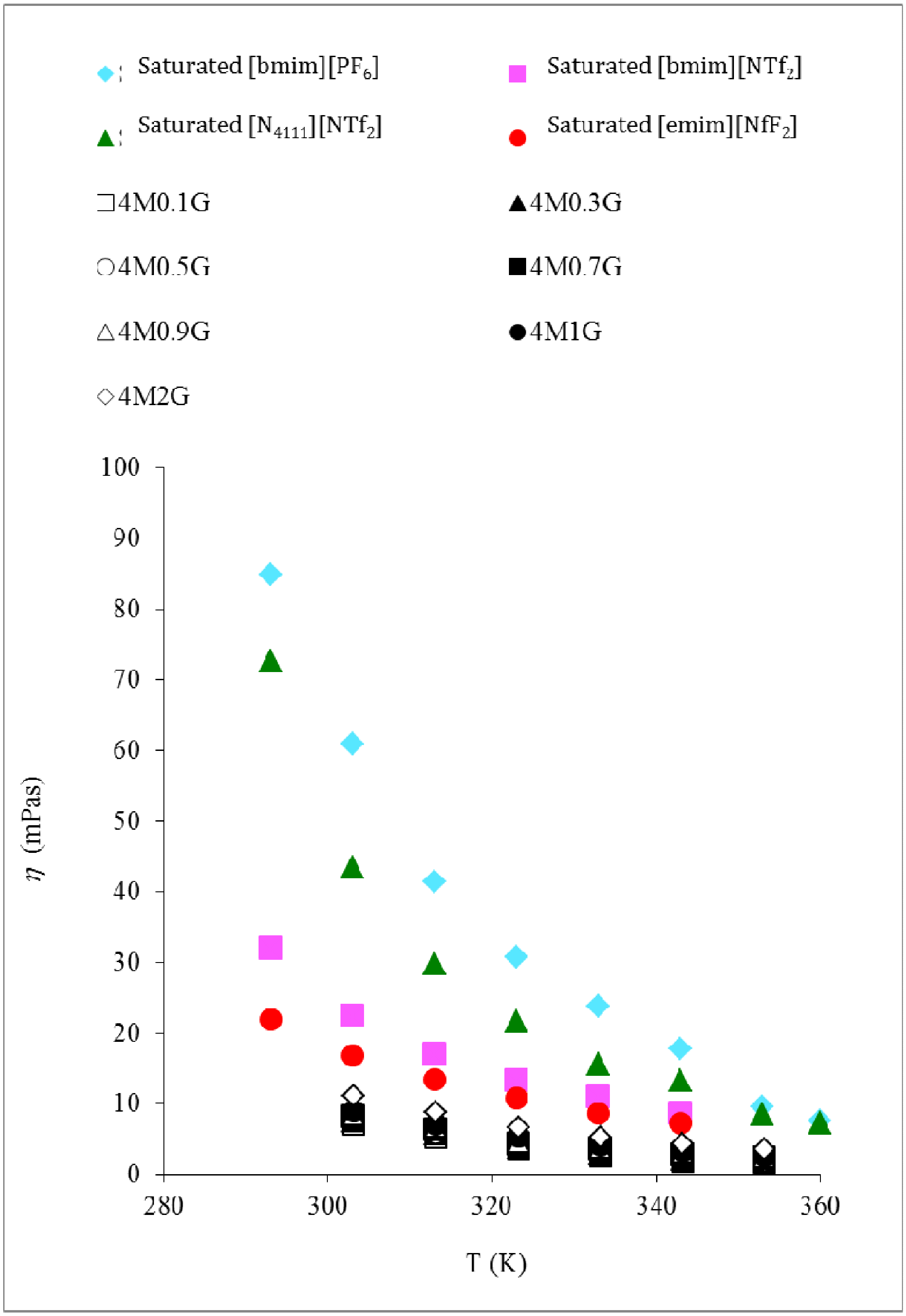

Figure 5.6. Comparison of the viscosity between ternary system *i.e.* 4M0.1G, 4M0.3G, 4M0.5G, 4M0.7G, 4M0.9G, 4M1G, 4M2G and saturated ionic liquids *i.e.* [bmim][$PF_6$], [bmim][$BF_4$], [bmim][$NTf_2$], [emim][$NTf_2$], [emim][$EtSO_4$] and [$N_{4111}$][$NTf_2$] [221].

Figure 5.7 shows the viscosity of aqueous binary [bmim][$BF_4$] [271] and aqueous binary [gua][OTf] based on mole fraction of ionic liquid at 298 K. It can be seen that the viscosity of the ionic liquid solutions depends strongly on their concentration. The viscosities of the aqueous binary [gua][OTf] system are lower than that of the aqueous binary [bmim][$BF_4$] system.

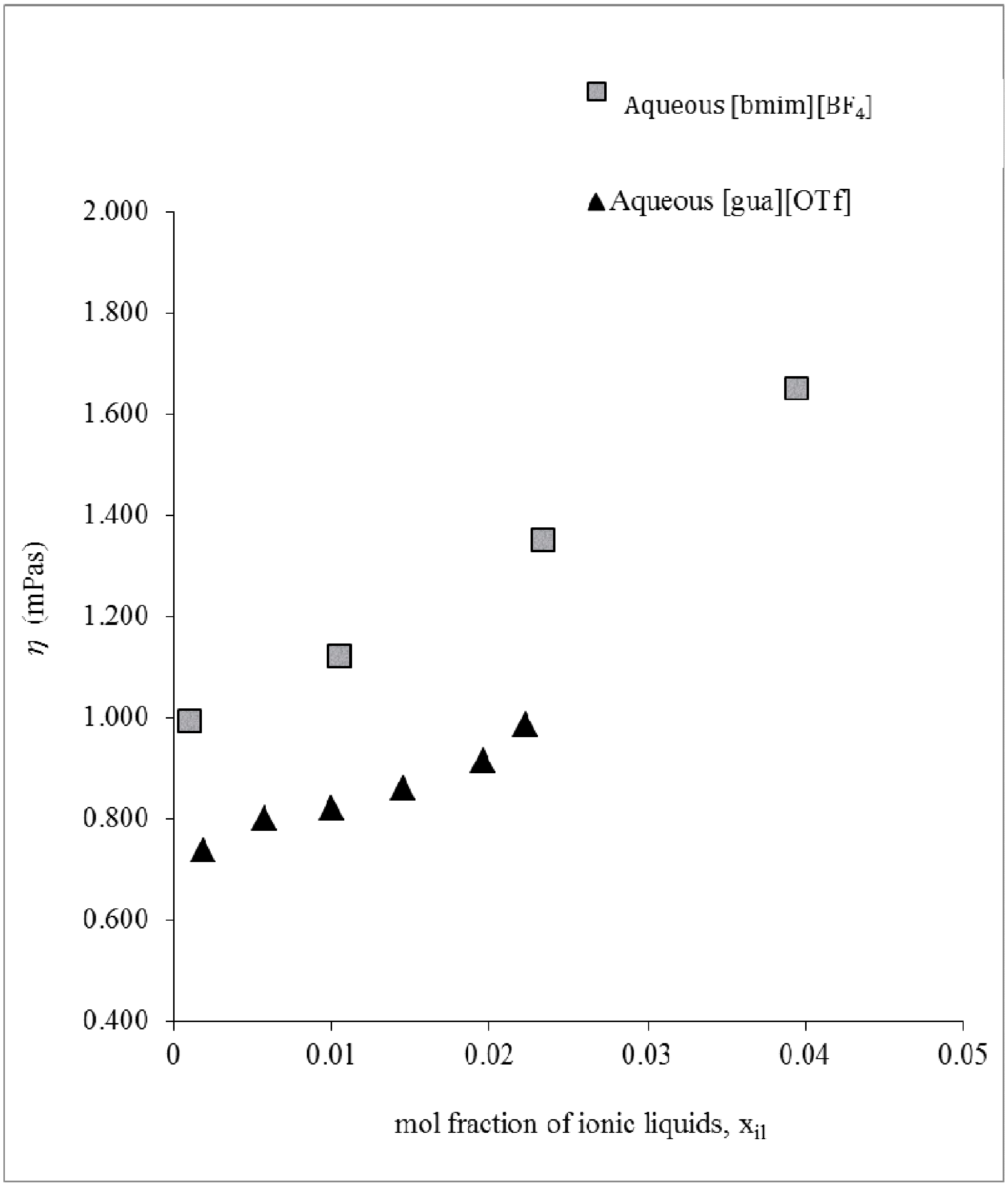

Figure 5.7. Comparison of the viscosity between the aqueous binary [bmim][$BF_4$] and aqueous binary [gua][OTf] at 298 K [256].

## 5.6 Correlation of viscosity as function of temperature, concentration of MDEA and [gua][OTf]

An extended Arrhenius-equation can be used to correlate the temperature and the viscosity. The Arrhenius equation is expressed as Equation 5.1.

$$\ln \eta = (E_a / RT) + \ln \eta_\infty \qquad (5.1)$$

where;

$\eta$ = viscosity of the system (mPas)

$Ea$ = activation energy (kJ/ mol)

$R$ = gas constant, 8.314 (kJ/ kmol K)

$T$ = absolute temperature (K)

$\eta_\infty$ = viscosity at infinite temperature (mPas)

Graph of ln $\eta$ versus 1/ T was linearly fitted where $E_a$ and $\eta_\infty$ are obtained from the gradient and *y*-intercept, respectively. The results are tabulated in Table 5.1. Table 5.2 shows that the activation energy value, $E_{a,}$ for binary systems, increases as the composition of [gua][OTf] increases. The value ranges from 7.7486 to 31.0669 kJ/ mol. Meanwhile, the activation energy values, $E_{a,}$ for ternary systems decrease as the composition of [gua][OTf] increases and the value ranges between 27.4304 and 20.2163 (kJ/ mol). The larger $E_a$ value corresponds to higher viscosity value. The $R^2$ values of all samples are closed to unity, which shows that the correlation (Equation 5.1) can be used to estimate the viscosity in the temperature range from 303.2 and 333.2 K.

Table 5.1. The correlated parameters for viscosities at various concentrations.

| System | Sample | $E_a$ (kJ/ mol) | $\eta_\infty$(x $10^2$ mPas) | $R^2$ |
|---|---|---|---|---|
| Binary | 0M0.1G | 7.7486 | 0.033746 | 0.9917 |
|  | 0M0.3G | 9.2244 | 0.020197 | 0.9757 |
|  | 0M0.5G | 9.1969 | 0.021028 | 0.9788 |
|  | 0M0.7G | 9.2776 | 0.021414 | 0.9779 |
|  | 0M0.9G | 10.4058 | 0.014942 | 0.9888 |
|  | 0M1G | 12.5201 | 0.006937 | 0.9888 |
|  | 0M4G | 16.3013 | 0.002113 | 0.9988 |
|  | 1M0G | 20.1573 | 0.000498 | 0.9723 |
|  | 4M0G | 31.0669 | 0.000030 | 0.9988 |
| Ternary | 4M0.1G | 27.4304 | 0.000134 | 0.9857 |
|  | 4M0.3G | 25.7219 | 0.000276 | 0.9880 |
|  | 4M0.5G | 24.4556 | 0.000483 | 0.9974 |
|  | 4M0.7G | 22.8926 | 0.000923 | 0.9948 |
|  | 4M0.9G | 22.6440 | 0.001079 | 0.9951 |
|  | 4M1G | 22.5866 | 0.001181 | 0.9982 |
|  | 4M2G | 20.2163 | 0.003634 | 0.9984 |

By assuming a cubic trend line to the plots, a cubic equation relating to characteristic parameter, $E_a$ with concentration of [gua][OTf] for both systems can be fitted using Equation 5.2 as follows:

$$E_a = e\,([\text{gua}][\text{OTf}])^3 + f\,([\text{gua}][\text{OTf}])^2 + g\,([\text{gua}][\text{OTf}]) + h \qquad (5.2)$$

where;

*e, f, g* and *h* are the coefficients for Equation 5.2 and the values are tabulated in Table 5.2.

Table 5.2. The coefficients *e*, *f, g* and *h* for aqueous [gua][OTf] and aqueous MDEA - [gua][OTf].

| Systems | Coefficient |  |  |  |
|---|---|---|---|---|
|  | *E* | *F* | *g* | *h* |
| Aqueous [gua][OTf] | 0.0149 | -0.4776 | 5.2212 | -18.647 |
| Aqueous MDEA- [gua][OTf] | -0.0046 | 0.3672 | -9.7896 | 88.226 |

By substituting the coefficient $e$, $f$, $g$ and $h$ into Equation 5.2, the activation energy, $E_a$ can be expressed as follows:

$$E_a = [(-268.77\ [\text{MDEA}] + 4)\ ([\text{gua}][\text{OTf}])]^3 + [(0.2112\ [\text{MDEA}] - 0.4776\ ([\text{gua}][\text{OTf}])]^2 + (-3.7527\ [\text{MDEA}] + 5.2212)\ ([\text{gua}][\text{OTf}]) + 26.718\ [\text{MDEA}] - 18.647 \quad (5.2)$$

For the correlation of viscosity at infinite temperature, $\eta_\infty$, at various concentration of [gua][OTf] and MDEA can be expressed as:.

$$\eta_\infty \text{ x } 10^2 = i\ ([\text{gua}][\text{OTf}])^3 + j\ ([\text{gua}][\text{OTf}])^2 + k\ ([\text{gua}][\text{OTf}]) + m \quad (5.3)$$

where;

*i, j, k* and *m* are the coefficients for the Equation 5.3 and the values are tabulated in Table 5.3.

Table 5.3. The coefficients; *i, j, k* and *m* for aqueous [gua][OTf] and aqueous MDEA - [gua][OTf].

| Systems | Coefficient | | | |
|---|---|---|---|---|
| | *I* | *j* | *k* | *M* |
| Aqueous [gua][OTf] | -0.2006 | 0.3279 | -0.1679 | 0.0472 |
| Aqueous MDEA-[gua][OTf] | -0.0027 | 0.0047 | -0.001 | 0.0002 |

The linear equation, which relates the coefficients, *i*, *j*, *k* and *m* with concentration of MDEA are shown as follows:

$i$ = 19.954 [MDEA] + 4

$j$ = 23.83 [MDEA] + 4

$k$ = -12.184 [MDEA] + 4

$m$ = -84.742 [MDEA] + 4

By substituting the coefficients $i$, $j$, $k$ and $m$ into Equation 5.3, the infinite viscosity, $\eta_\infty$can be expressed as:

$$\eta_\infty \text{ x } 10^2 = (19.954\ [\text{MDEA}] + 4)\ [\text{gua}][\text{OTf}]^3 + (23.83\ [\text{MDEA}] + 4)\ [\text{gua}][\text{OTf}]^2 + (-12.184\ [\text{MDEA}] + 4)\ [\text{gua}][\text{OTf}] + (-84.742\ [\text{MDEA}] + 4) \qquad (5.3)$$

By substituting Equation 5.2 and 5.3 into 5.1, the extended Arrhenius Equation as a function of temperature, concentration of MDEA and [gua][OTf] can be expressed as follows:

$$\ln \eta = (E_a / RT) + \ln \eta_\infty \qquad (5.1)$$

where:

$$E_a = (-268.77\ [\text{MDEA}] + 4)\ [\text{gua}][\text{OTf}]^3 + (0.2112\ [\text{MDEA}] - 0.4776)\ [\text{gua}][\text{OTf}]^2 + (-3.7527\ [\text{MDEA}] + 5.2212)\ [\text{gua}][\text{OTf}] + (26.718\ [\text{MDEA}] - 18.647)$$

$$\eta_{\infty} \times 10^2 = (19.954\,[MDEA] + 4)\,[gua][OTf]^3 + (23.83\,[MDEA] + 4)\,[gua][OTf]^2 + (-12.184\,[MDEA] + 4)\,[gua][OTf] + (-84.742\,[MDEA] + 4)$$

Concentration of MDEA and [gua][OTf] are in unit molar, M.

Figure 5.8 shows the comparison between the calculated viscosity data using Equation 5.1 and the measured viscosity data for all systems. The percentages deviations of calculated and experimental viscosities for 1M0G and 4M0G were less than ± 1.5 % in temperature range from 293 to 353 K. The deviation for ternary systems MDEA - [gua][OTf] *i.e.* 4M0.1G, 4M0.3G, 4M0.5G, 4.M0.7G, 4M0.9G, 4M1G and 4M2G were between ± 1.5 - 3.5 %. Binary systems of [gua][OTf] – $H_2O$ *i.e.* 0M0.1G, 0M0.3G, 0M0.5G, 0M0.7G and 0M0.9, 0M1G and 0M4G showed higher deviation in viscosities up to 8.442 %.

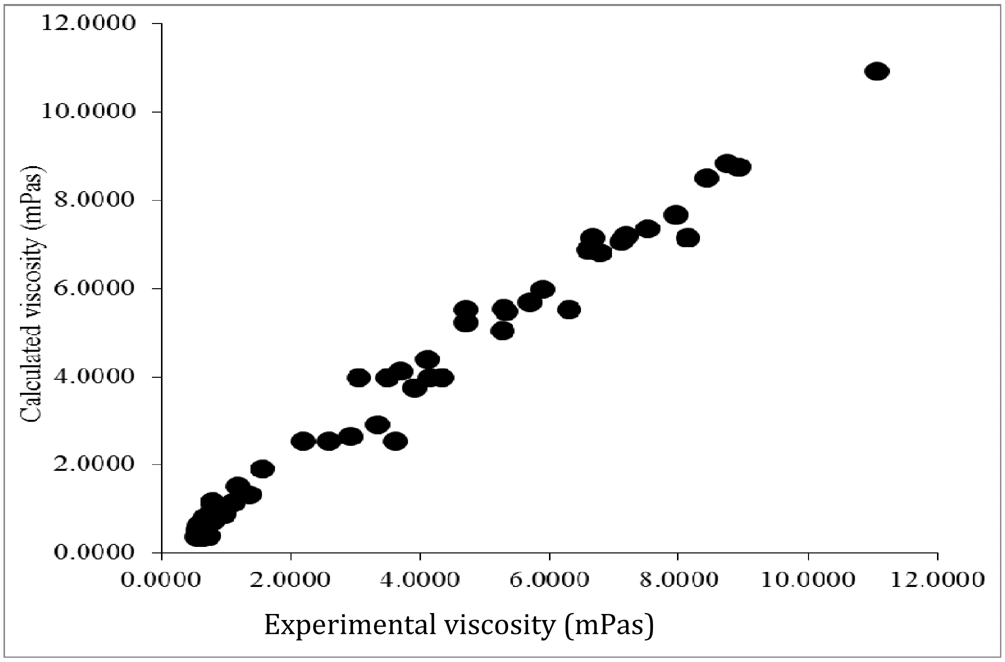

Figure 5.8. The comparison between the calculated and the measured viscosities for all the studied systems.

## 5.7 Conclusion

Similar to the density, the viscosity results indicate that the mixture of MDEA – [gua][OTf] demonstrates concentration and temperature dependent behaviour. The viscosities of MDEA – [gua][OTf] decreased linearly with increase in temperature but decreased as composition of [gua][OTf] in the system increased. The change in the slope with respect to temperatures for binary ([gua][OTf] - $H_2O$) and ternary ([gua][OTf] - $H_2O$ - MDEA) system is relatively barely visible. A correlation of viscosity as a function of the concentration of MDEA and [gua][OTf] at temperature range from 303.2 to 333.2 K was determined.

# Chapter 6: $CO_2$ ABSORPTION AT HIGH PRESSURES

## 6.1 Introduction

This chapter was aimed to examine the ability of aqueous [gua][OTf] and aqueous mixture of MDEA – [gua][OTf] systems in capturing $CO_2$ from the pressure range of 500 to 3000 kPa. The $CO_2$ solubility was measured at several temperatures (303.2, 323.2 and 333.2 K). All data were reported loading capacity (mol $CO_2$/ total mol system (MDEA + [gua][OTf] + $H_2O$)) as a function of partial pressure of $CO_2$ at the corresponding temperature. Correlation for the solubility of $CO_2$ was also developed. The (extended) Henry's law was successfully applied to correlate the solubility and the pressure. Table 6.1 summarizes various systems, which were used in this study.

Table 6.1. Various compositions of the systems used in this work.

| Sample | Concentration of MDEA (mol dm$^{-3}$) | Concentration of [gua][OTf] (mol dm$^{-3}$) |
|---|---|---|
| 4M0G | 4.012 ± 0.002 | 0 |
| 4M1G | 4.008 ± 0.002 | 1.005 ± 0.002 |
| 1M0G | 1.003 ± 0.002 | 0 |
| 0M1G | 0 | 1.006 ± 0.002 |

## 6.2 Validation of the experimental procedures

The validation of the experimental procedure for $CO_2$ solubility study was conducted using 4 M MDEA systems at 333.2 K to ensure the accuracy of the procedures and measurement used in this work. These data and also the data reported in literature [272] are shown in Table 6.2 and are plotted in Figure 6.1. As can be seen from Table 6.2 and Figure 6.1, both data are in good agreement.

Table 6.2. The comparison of $CO_2$ loading obtained between this study and the data extracted from the literature [272] at 333.2 K for 4 M MDEA.

| George *et al.* [272] | | this work | |
|---|---|---|---|
| $P_{CO2}$ (kPa) | $\alpha_{CO2}$ (mol $CO_2$/ total mol system) | $P_{CO2}$ (kPa) | $\alpha_{CO2}$ (mol $CO_2$/ total mol system) |
| 205 | 0.669 | - | - |
| 335 | 0.773 | 369 | 0.639 |
| 694 | 0.896 | - | - |
| 852 | 0.920 | 821 | 0.832 |
| 1159 | 0.957 | - | - |
| 1357 | 0.975 | 1383 | 0.934 |
| 1497 | 0.973 | - | - |
| 1791 | 1.005 | 1706 | 0.961 |
| - | - | 2422 | 1.092 |
| - | - | 2877 | 1.124 |
| 3363 | 1.083 | - | - |

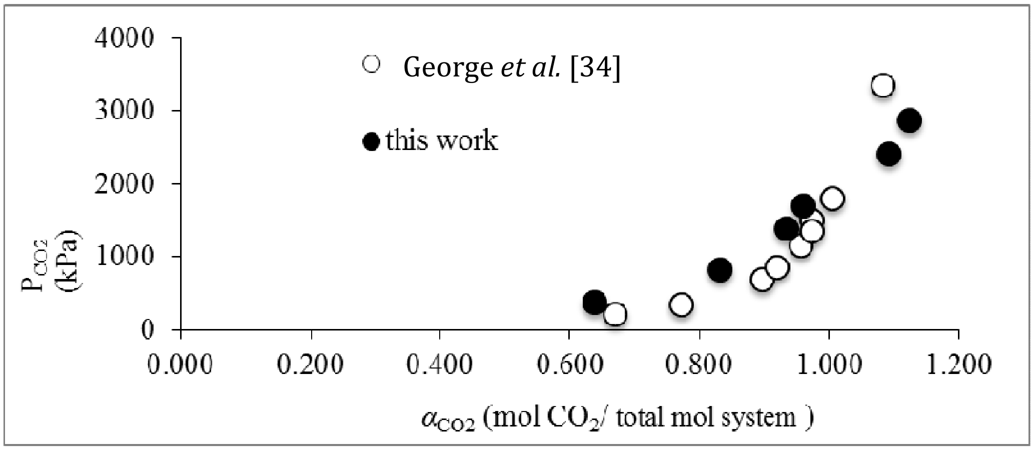

Figure 6.1. Comparison of solubility data for $CO_2$ at 333.2 K in 4 M MDEA between published data [272] and this work.

## 6.3 Effect of temperature on the solubility of $CO_2$

Figure 6.2 to 6.13 illustrate the effect of temperature on $CO_2$ loading at various $CO_2$ partial pressure (500 - 3000 kPa) and concentrations of MDEA and [gua][OTf]. In general, all figures show a complete agreement to the expected trend in which the equilibrium loading decreases as the temperature increases. The reduction in $CO_2$ solubility in those figures indicates that the solubility of $CO_2$ was lower at higher temperature.

It was possible to affirm that an exothermic process is involved as heat was given off during the dissolving process, and the energy released was much greater than that required to break the bonds holding the gas together which is an endothermic process. The increase of temperature inhibited the dissolving reaction since excess heat was already being produced by the reaction. Thus, the solubility of $CO_2$ decreased at higher temperatures.

According to Van't Hoff's law of dynamic equilibrium, if the temperature of a system at equilibrium is raised, the change will be favourable towards absorption of heat. With regards to this work, it was usual for the absorption process of alkanolamine to be accompanied by the evolution of heat. Thus the solubility of reaction gas usually decreases as the temperature increases.

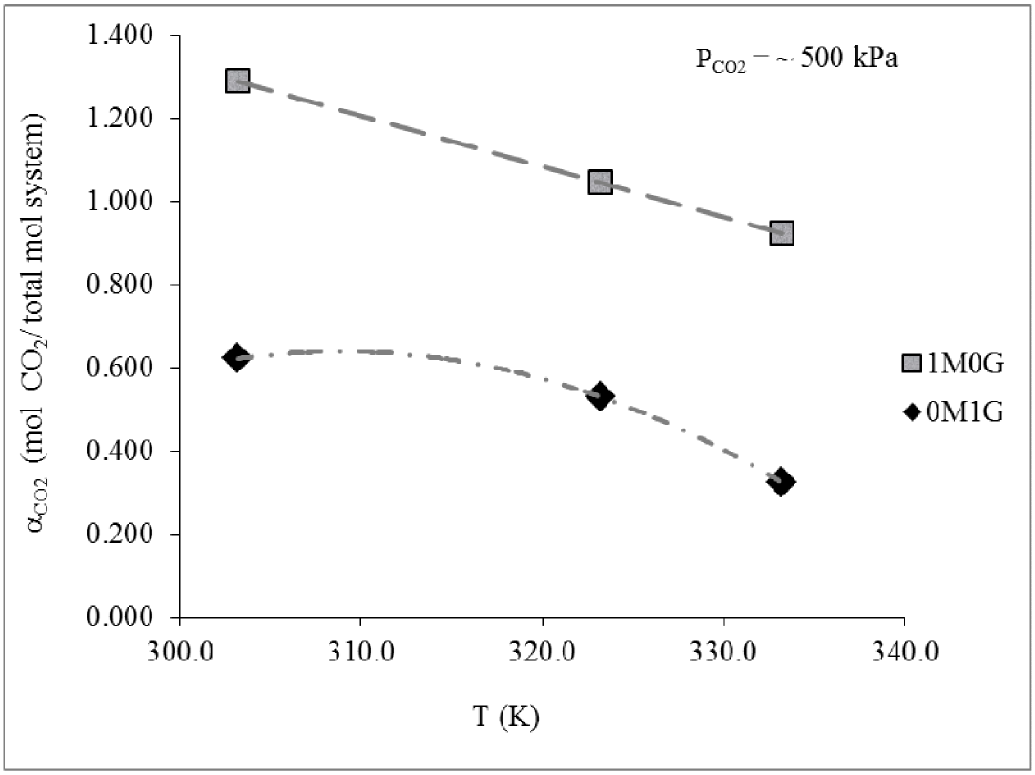

Figure 6.2. The effect of temperature on the solubility of $CO_2$ for 1M0G and 0M1G systems at 500 kPa.

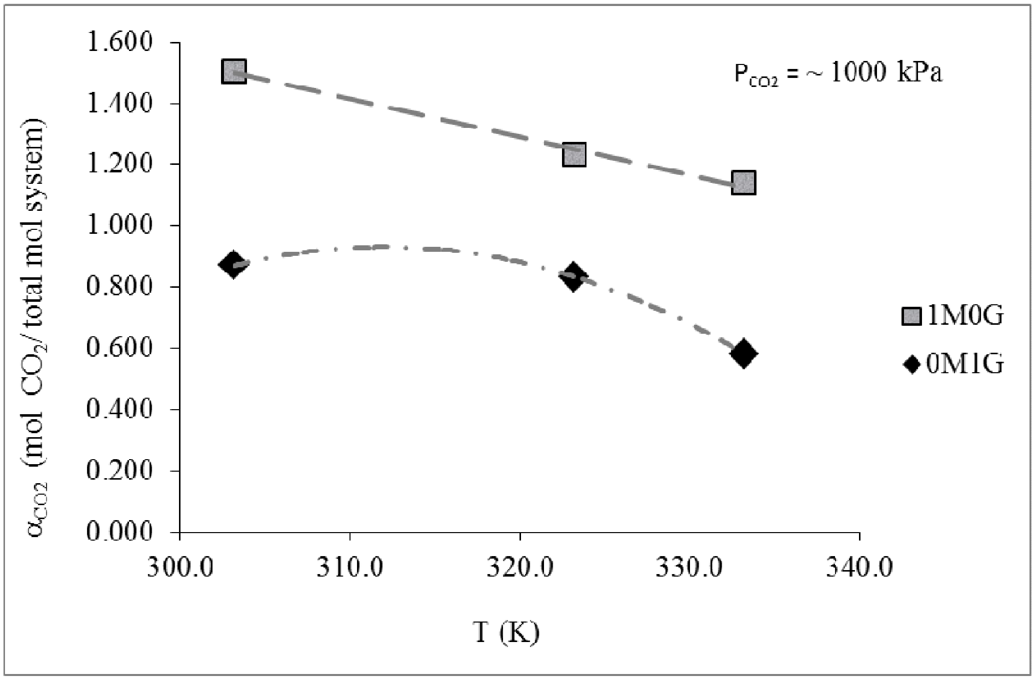

Figure 6.3. The effect of temperature on the solubility of $CO_2$ for 1M0G and 0M1G systems at 1000 kPa.

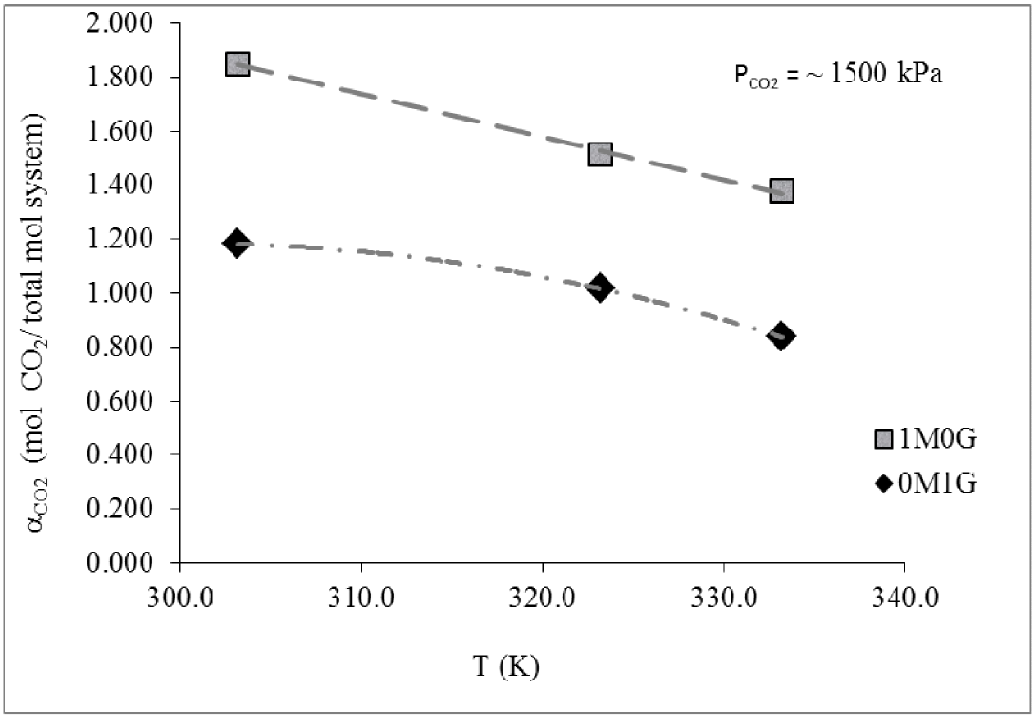

Figure 6.4. The effect of temperature on the solubility of $CO_2$ for 1M0G and 0M1G systems at 1500 kPa.

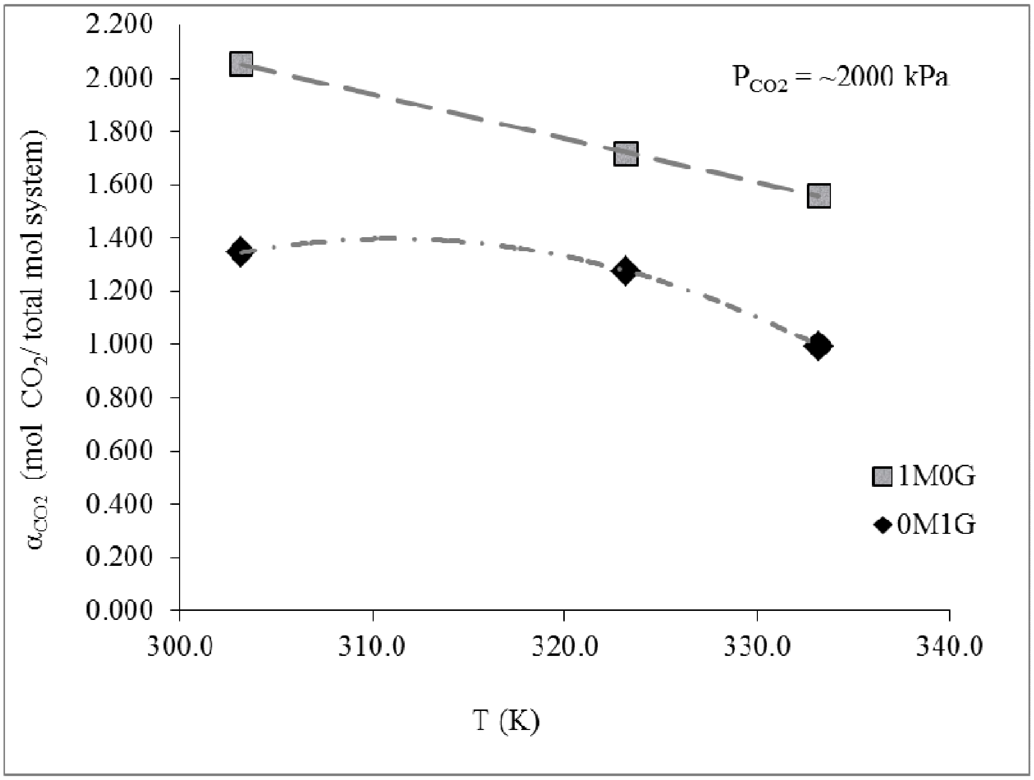

Figure 6.5. The effect of temperature on the solubility of $CO_2$ for 1M0G and 0M1G systems at 2000 kPa.

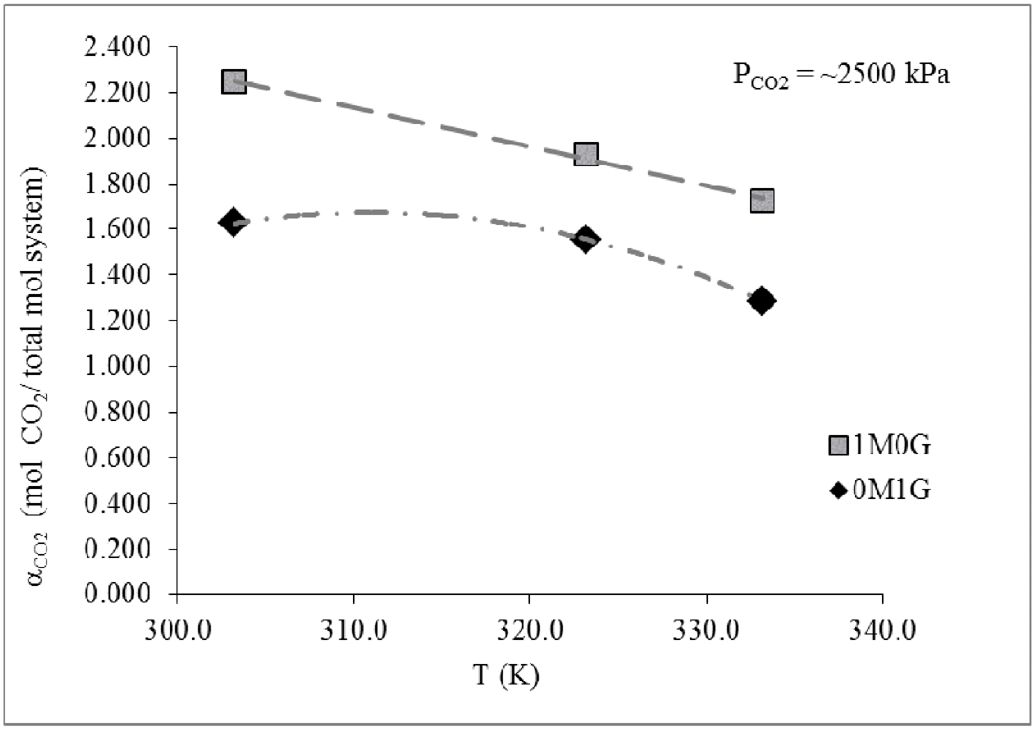

Figure 6.6. The effect of temperature on the solubility of $CO_2$ for 1M0G and 0M1G systems at 2500 kPa.

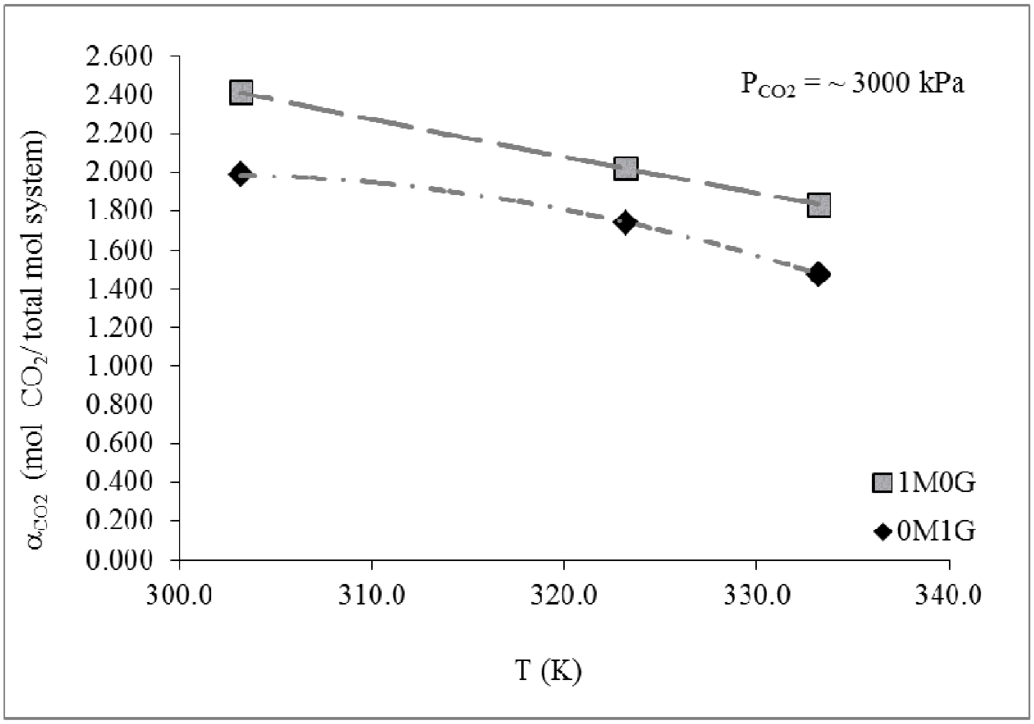

Figure 6.7. The effect of temperature on the solubility of $CO_2$ for 1M0G and 0M1G systems at 3000 kPa.

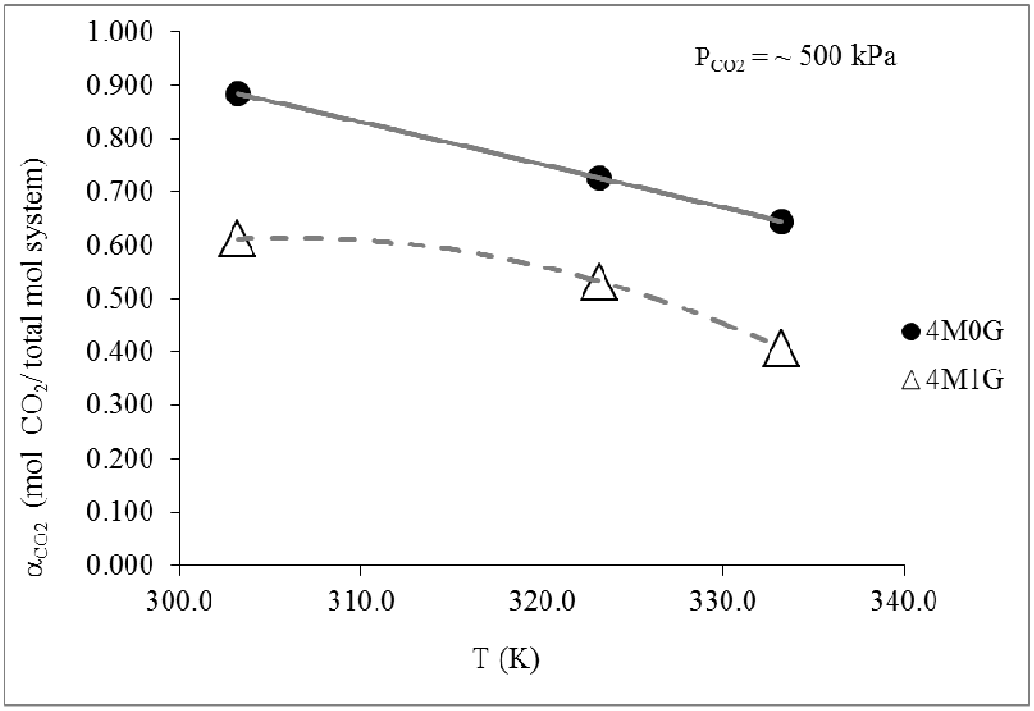

Figure 6.8. The effect of temperature on the solubility of $CO_2$ for 4M0G and 4M1G systems at 500 kPa.

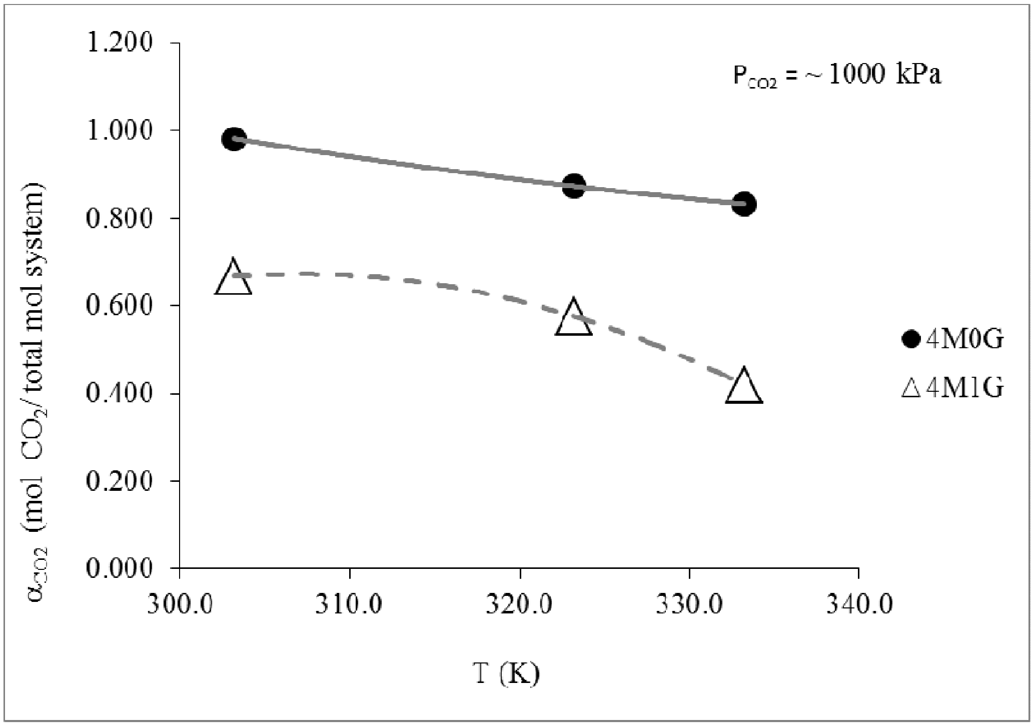

Figure 6.9. The effect of temperature on the solubility of $CO_2$ for 4M0G and 4M1G systems at 1000 kPa.

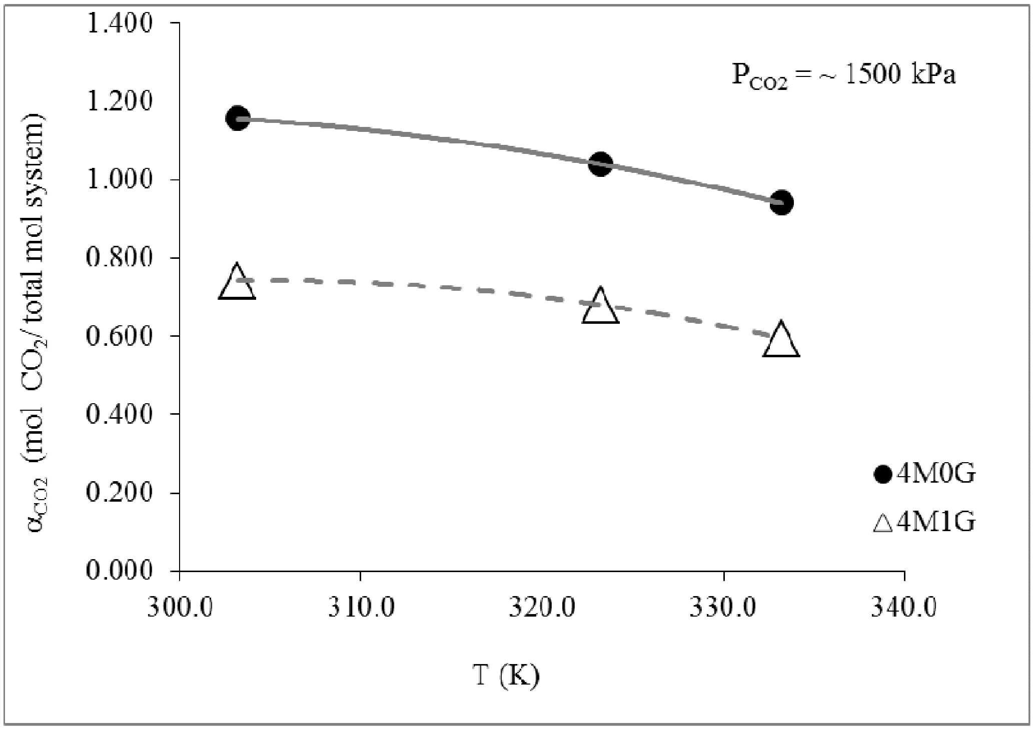

Figure 6.10. The effect of temperature on the solubility of $CO_2$ for 4M0G and 4M1G systems at 1500 kPa.

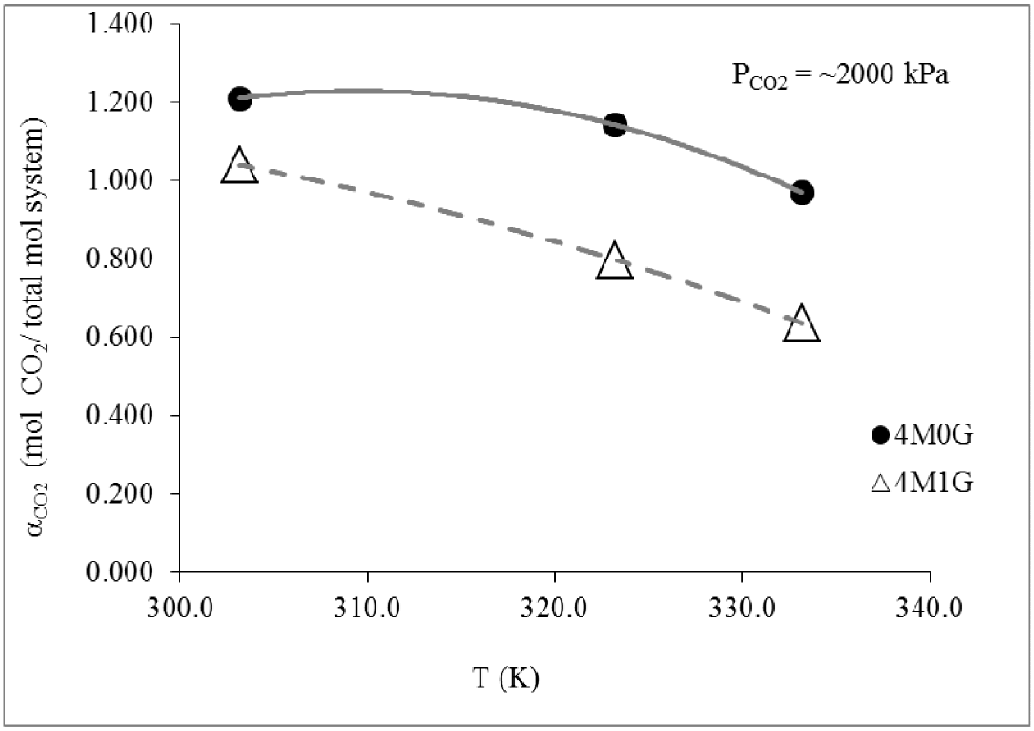

Figure 6.11. The effect of temperature on the solubility of $CO_2$ for 4M0G and 4M1G systems at 2000 kPa.

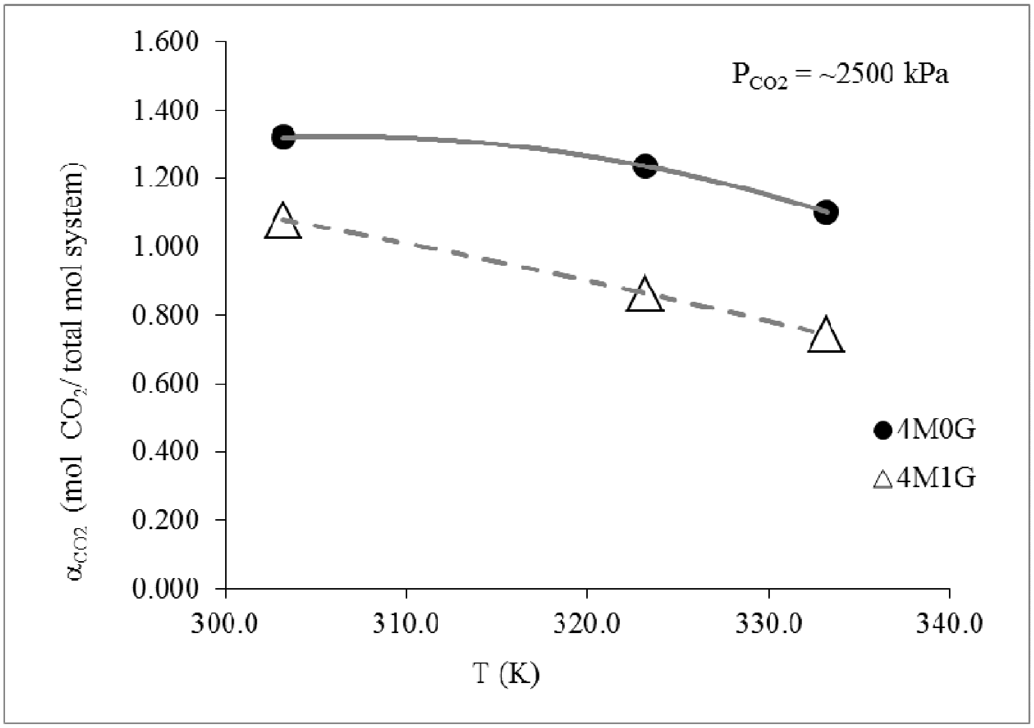

Figure 6.12. The effect of temperature on the solubility of $CO_2$ for 4M0G and 4M1G systems at 2500 kPa.

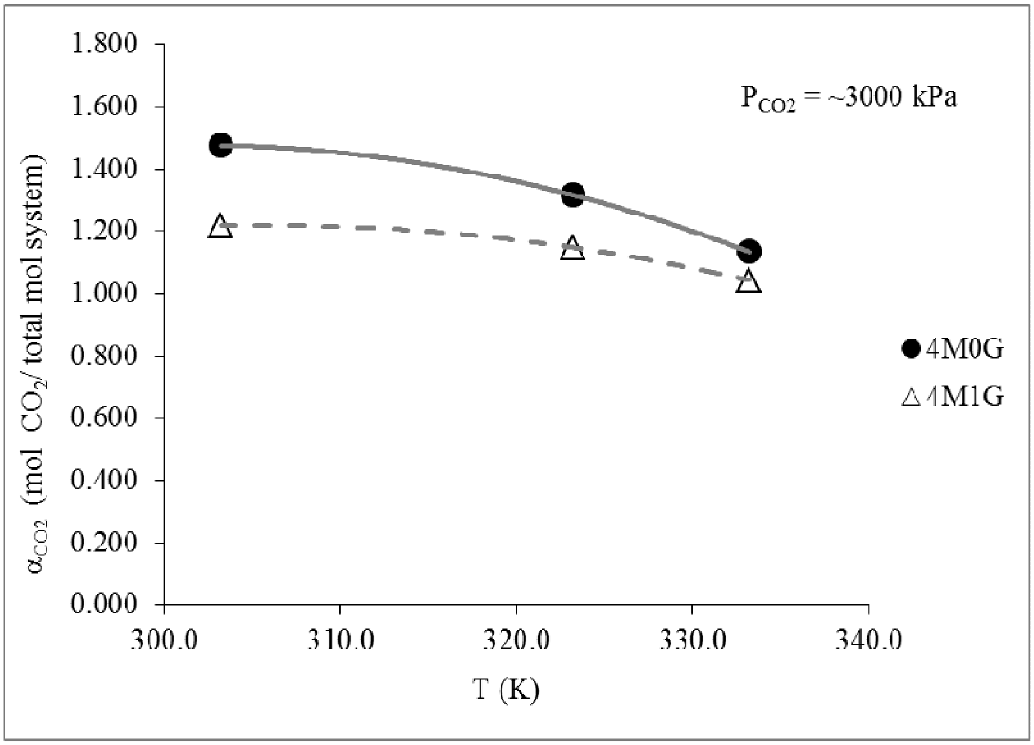

Figure 6.13. The effect of temperature on the solubility of $CO_2$ for 4M0G and 4M1G systems at 3000 kPa.

Using the idea of entropy of solution, it could be predicted that $CO_2$ should become less soluble in the binary and ternary systems with increasing temperature because they have negative entropy of solutions. The second law of thermodynamic predicts that the $CO_2$ will shift to the more disordered, highly dispersed, and therefore more probably gas state. Yet, they are also confined to a smaller volume when dissolved as compared to their volumes as gases, which would lead to lower solubility of $CO_2$ at higher temperature.

### 6.4 Effect of pressure on the solubility of $CO_2$

Figure 6.14 to Figure 6.19 shows the effect of pressure on the solubility of $CO_2$. These figures show that the $CO_2$ solubility increases as the $CO_2$ pressure increases. The pressure was varied from 500 to 3000 kPa at three different temperatures (303.2, 323.2 and 333.2 K) and for various concentrations of MDEA and [gua][OTf] in order to obtain a series of solubility data. In physical absorption, as the partial pressure of the reactant gases increases, the numbers of molecules colliding with surface of the absorbent solution also increases. Therefore, more gas could be absorbed at higher pressure.

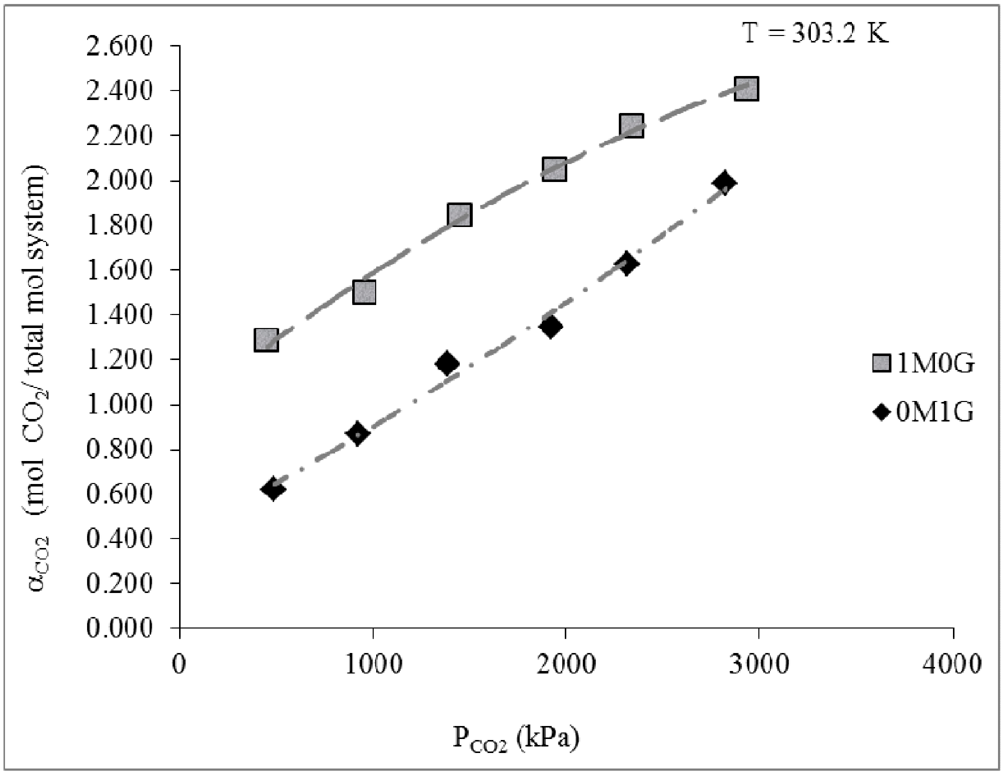

Figure 6.14. The effect of pressure on the solubility of $CO_2$ for 1M0G and 0M1G systems at T = 303.2 K.

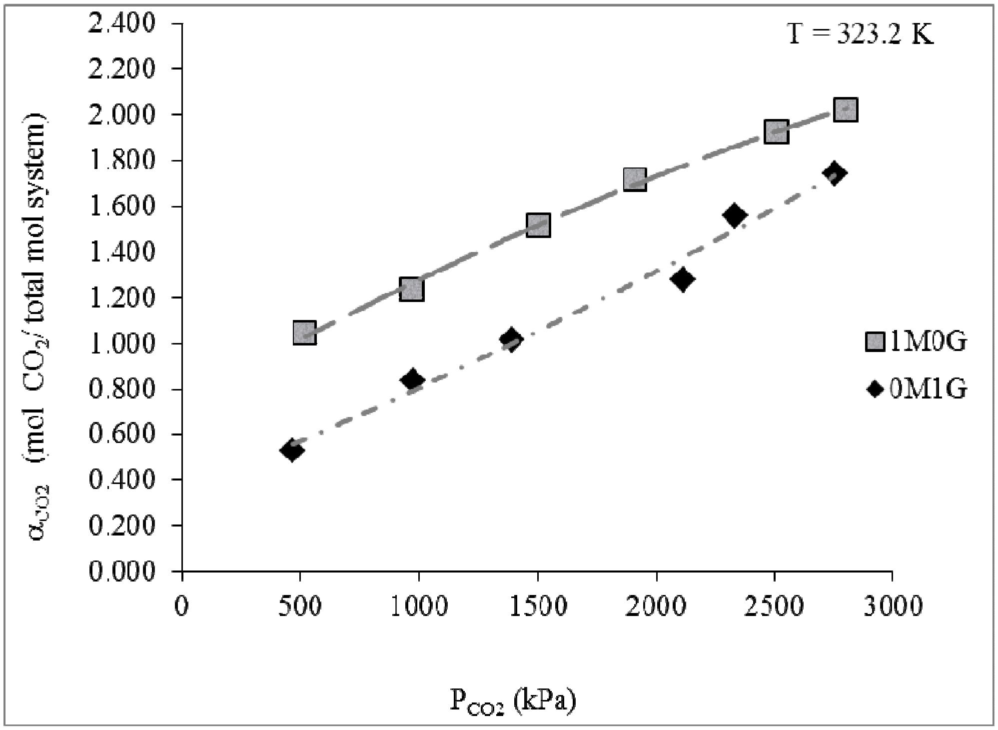

Figure 6.15. The effect of pressure on the solubility of $CO_2$ for 1M0G and 0M1G systems at T = 323.2 K.

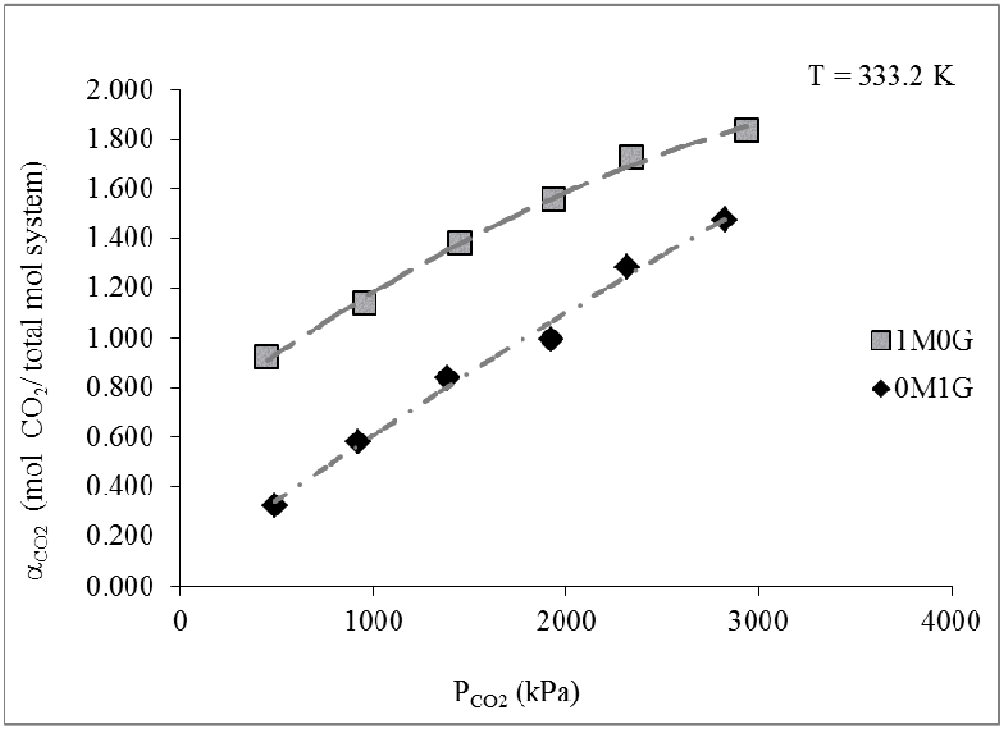

Figure 6.16. The effect of pressure on the solubility of $CO_2$ for 1M0G and 0M1G systems at T = 333.2 K.

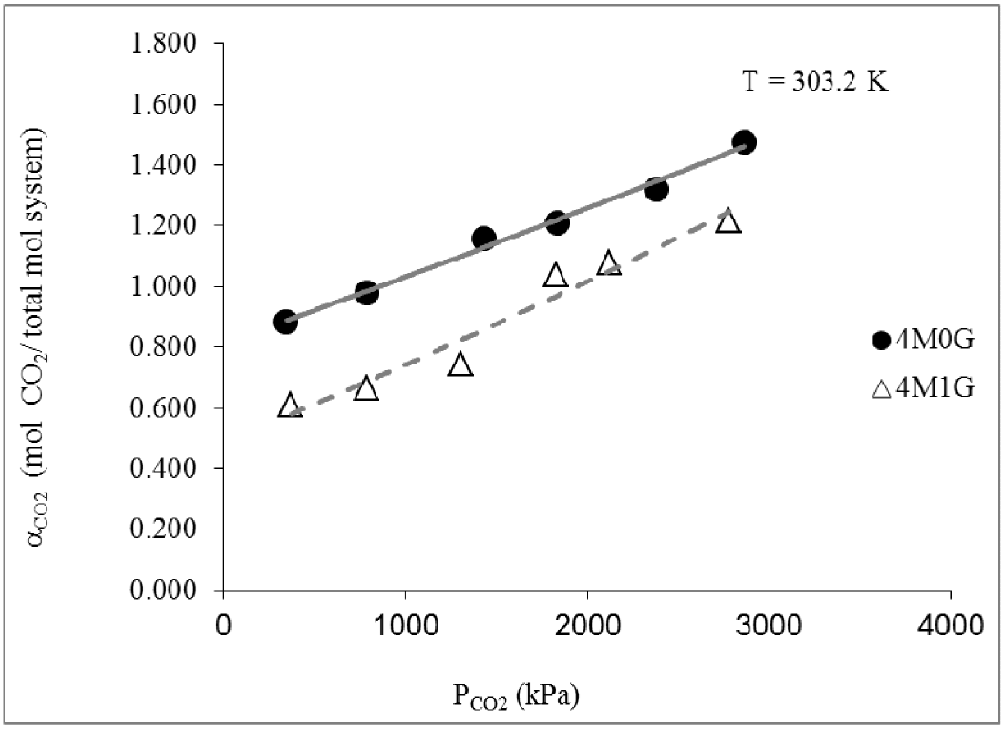

Figure 6.17. The effect of pressure on the solubility of $CO_2$ for 4M0G and 4M1G systems at T = 303.2 K.

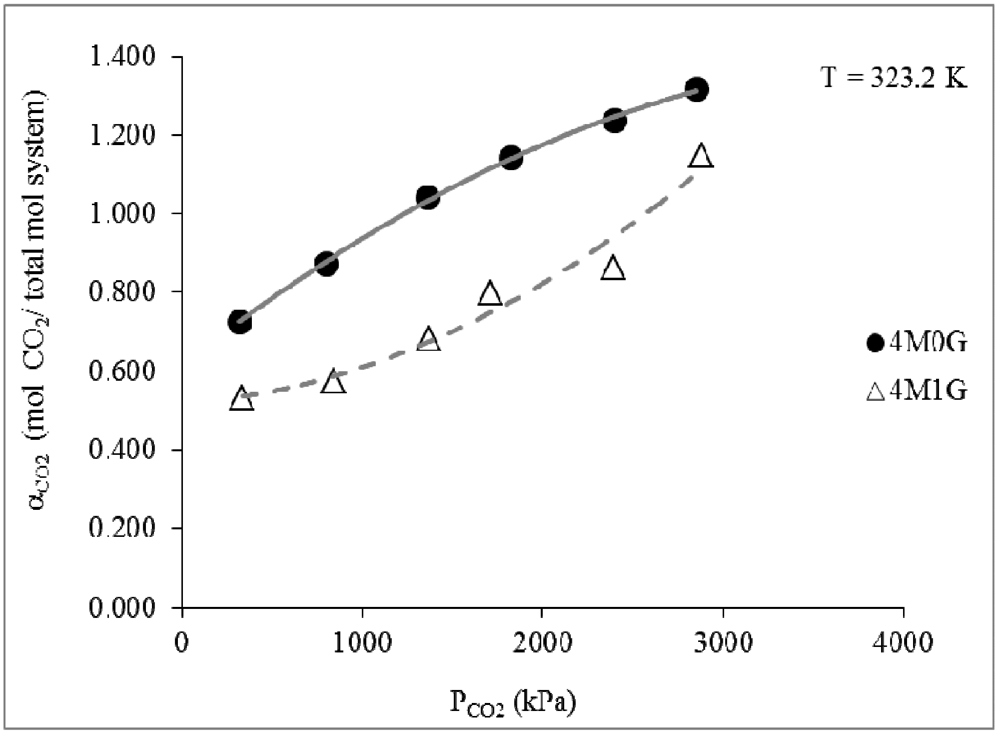

Figure 6.18. The effect of pressure on the solubility of $CO_2$ for 4M0G and 4M1G systems at T = 323.2 K.

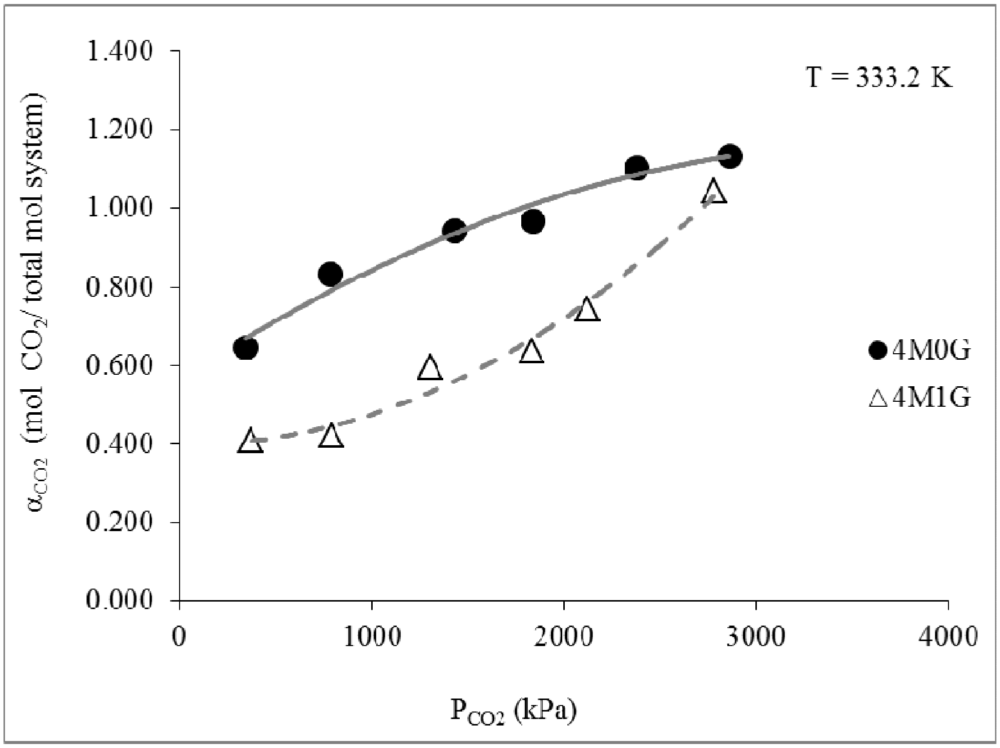

Figure 6.19. The effect of pressure on the solubility of $CO_2$ for 4M0G and 4M1G systems at T = 333.2 K.

As can be seen from Figure 6.14, the effect of $CO_2$ partial pressures at 303.2 K is the most pronounced for 0M1G. This was proved by the biggest slope formed for 0M1G system and 220.1 % deviation for $CO_2$ solubility from the lowest pressure studied *i.e.* 489 kPa to the highest pressure *i.e.* 2823 kPa. Meanwhile, 1M0G, 4M0G and 4M1G recorded 87.2 %, 67.0 % and 99 % for $CO_2$ solubility deviation in terms of effect of pressure at 303.2 K respectively.

This increasing manner of $CO_2$ solubility at high pressure can be explained by LeChatelier principle. According to this principal, as the $CO_2$ partial pressure or amount of $CO_2$ in the gas phase increases, the system will shift to a new equilibrium condition which will absorbed more $CO_2$ to diminish the effect of increasing $CO_2$ partial pressure.

## 6.5 Effect of addition ionic liquid

Table 6.3 and Figure 6.20 show the effect of the addition of 1 M [gua][OTf] to 4 M MDEA on the $CO_2$ equilibrium loading at a pressure range of 500 - 3000 kPa. The results indicate that the addition of [gua][OTf] reduces the solubility of $CO_2$ for all three investigated temperatures. This is due to the formation of triflic acid by reaction of [gua][OTf] and water, which lowers the basicity of the solvent. [Gua][OTf] was believed to hinder the tertiary amine of MDEA hence lesser free amine to absorb $CO_2$.

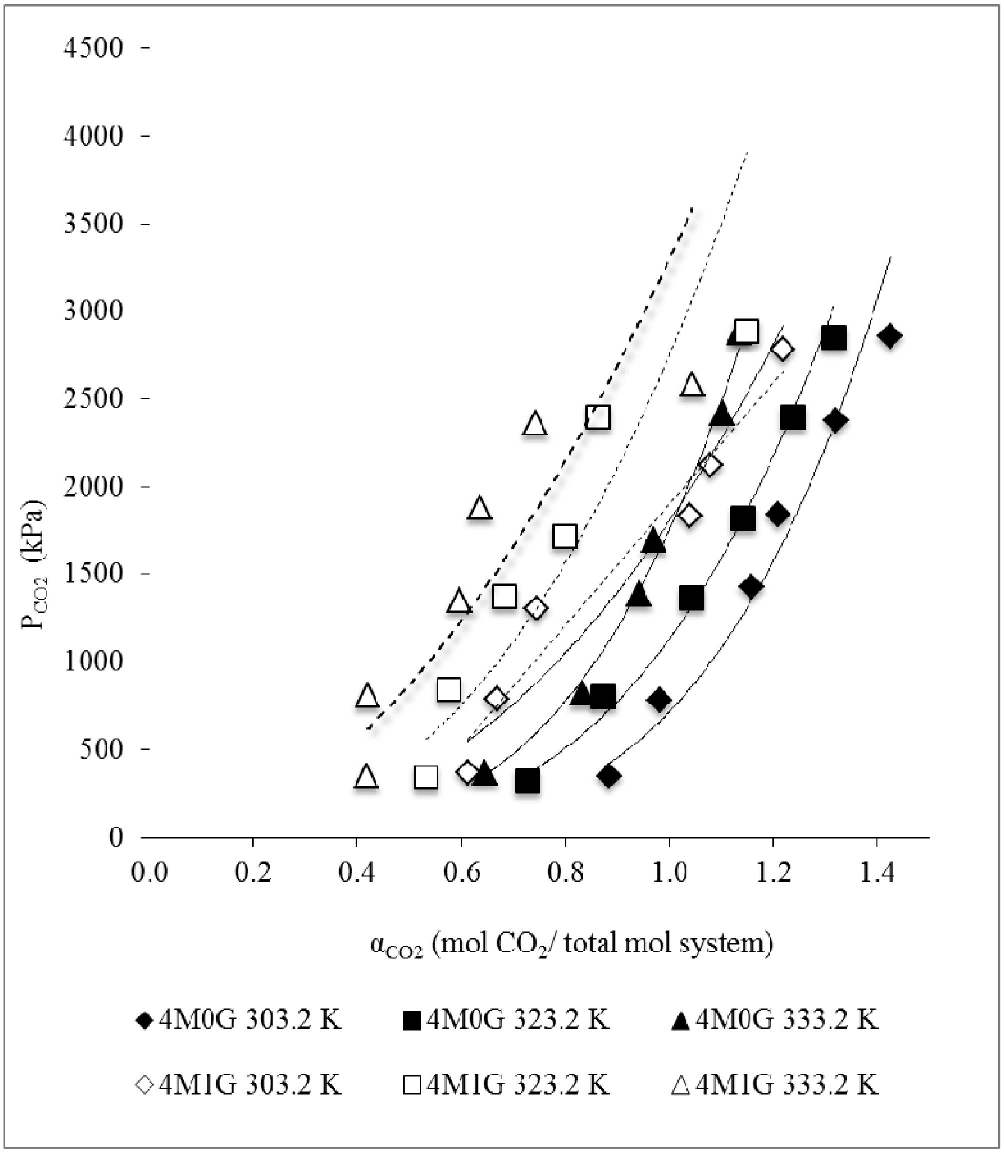

Figure 6.20. Effect addition of 1 M [gua][OTf] to 4 M MDEA and at temperatures 303.2, 323.2 and 333.2 K at pressure up to 3000 kPa.

Table 6.3. Effect of addition 1 M [gua][OTf] to 4 M MDEA at temperature 303.2, 323.2 and 333.2 K at pressure up to 3000 kPa.

| | 4M0G | | | 4M1G | | |
|---|---|---|---|---|---|---|
| T (K) | $P_{CO_2}$ (kPa) | $\alpha_{CO_2}$ (mol $CO_2$/ total mol system) | $x_{CO_2}$ | $P_{CO_2}$ (kPa) | $\alpha_{CO_2}$ (mol $CO_2$/ total mol system) | $x_{CO_2}$ |
| 303.2 | 345 | 0.884 | 0.054 ± 0.001 | 371 | 0.612 | 0.047 ± 0.001 |
| | 784 | 0.981 | 0.060 ± 0.001 | 789 | 0.667 | 0.050 ± 0.001 |
| | 1429 | 1.157 | 0.070 ± 0.001 | 1307 | 0.744 | 0.056 ± 0.001 |
| | 1837 | 1.209 | 0.073 ± 0.001 | 1830 | 1.039 | 0.077 ± 0.001 |
| | 2376 | 1.320 | 0.079 ± 0.002 | 2123 | 1.079 | 0.079 ± 0.002 |
| | 2861 | 1.476 | 0.085 ± 0.003 | 2780 | 1.218 | 0.089 ± 0.002 |
| 323.2 | 321 | 0.726 | 0.045 ± 0.001 | 338 | 0.532 | 0.041 ± 0.001 |
| | 800 | 0.873 | 0.054 ± 0.001 | 842 | 0.576 | 0.044 ± 0.001 |
| | 1366 | 1.041 | 0.063 ± 0.001 | 1372 | 0.681 | 0.052 ± 0.001 |
| | 1822 | 1.141 | 0.069 ± 0.001 | 1713 | 0.798 | 0.060 ± 0.001 |
| | 2399 | 1.236 | 0.074 ± 0.002 | 2395 | 0.864 | 0.064 ± 0.002 |
| | 2851 | 1.316 | 0.079 ± 0.003 | 2883 | 1.148 | 0.084 ± 0.003 |
| 333.2 | 367 | 0.645 | 0.010 ± 0.001 | 350 | 0.408 | 0.006 ± 0.001 |
| | 821 | 0.832 | 0.013 ± 0.001 | 810 | 0.420 | 0.007 ± 0.001 |
| | 1389 | 0.942 | 0.015 ± 0.001 | 1355 | 0.596 | 0.009 ± 0.001 |
| | 1697 | 0.969 | 0.016 ± 0.001 | 1880 | 0.636 | 0.010 ± 0.001 |
| | 2416 | 1.102 | 0.017 ± 0.002 | 2362 | 0.743 | 0.012 ± 0.001 |
| | 2879 | 1.134 | 0.018 ± 0.003 | 2582 | 1.043 | 0.016 ± 0.002 |

### 6.6 Comparison on the $CO_2$ absorption capacity between 1 M MDEA (1M0G) and 1 M [gua][OTf] (0M1G)

Table 6.4 shows the solubility data for both aqueous mixtures. These data are also plotted in Figure 6.21. The solubility of $CO_2$ in ionic liquid is dependent on the interaction between the ionic liquid and the molecules, and also the free space available to be occupied by the $CO_2$ molecules in the ionic liquid rich phase. As more clearly illustrated in Figure 6.22, the percentage of deviation in the solubility for both 1M0G and 0M1G is as high as 50 % at lower pressure but decreases as the pressure increases.

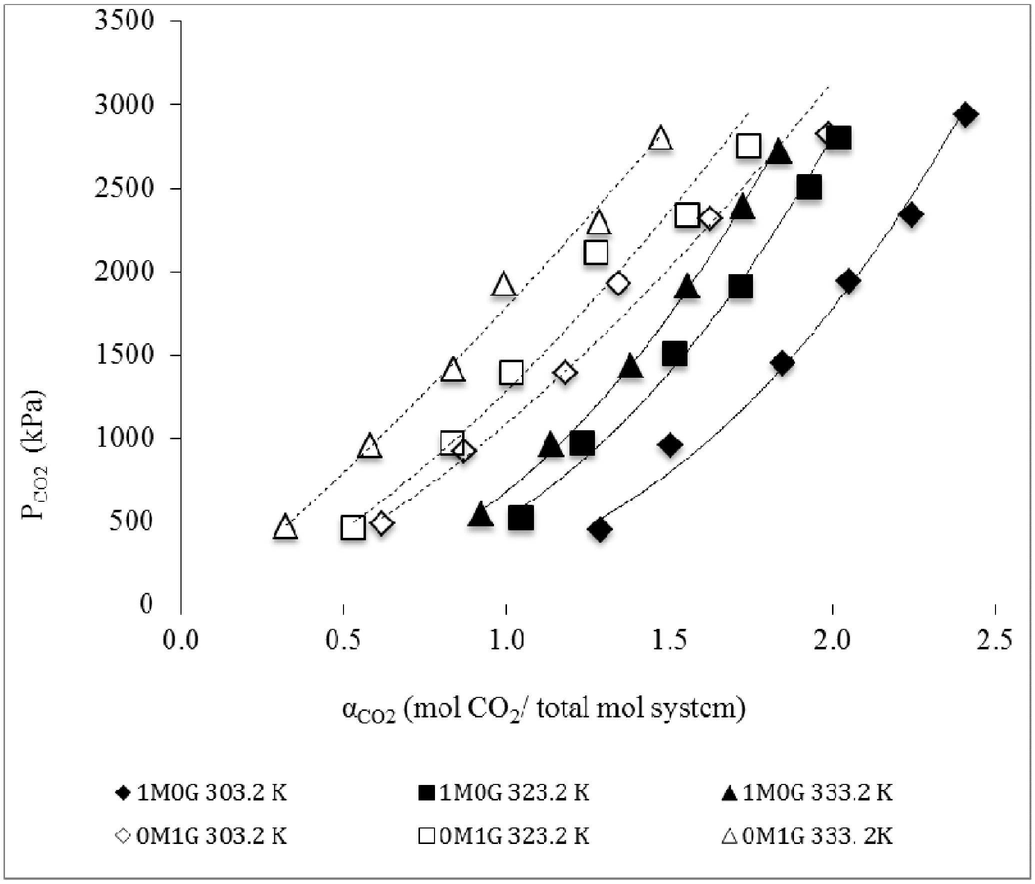

Figure 6.21. Comparison of absorption between 1 M MDEA (1M0G) and 1 M [gua][OTf] (0M1G) at temperatures 303.2, 323.2 and 333.2 K at pressure up to 3000 kPa.

Table 6.4. Comparison of absorption between 1 M MDEA (1M0G) and 1 M [gua][OTf] (0M1G) at temperatures 303.2, 323.2 and 333.2 K at pressure up to 3000 kPa.

| | 1M0G | | | 0M1G | | |
|---|---|---|---|---|---|---|
| T (K) | $P_{CO_2}$ (kPa) | $\alpha_{CO_2}$ (mol $CO_2$/ total mol system) | $x_{CO_2}$ | $P_{CO_2}$ (kPa) | $\alpha_{CO_2}$ (mol $CO_2$/ total mol system) | $x_{CO_2}$ |
| 303.2 | 450 | 1.288 | 0.021 ± 0.001 | 489 | 0.621 | 0.010 ± 0.001 |
| | 958 | 1.504 | 0.025 ± 0.001 | 921 | 0.870 | 0.015 ± 0.001 |
| | 1451 | 1.850 | 0.031 ± 0.001 | 1389 | 1.181 | 0.020 ± 0.001 |
| | 1939 | 2.052 | 0.034 ± 0.001 | 1923 | 1.346 | 0.022 ± 0.001 |
| | 2338 | 2.245 | 0.037 ± 0.002 | 2317 | 1.626 | 0.027 ± 0.002 |
| | 2937 | 2.411 | 0.039 ± 0.003 | 2823 | 1.988 | 0.033 ± 0.002 |
| 323.2 | 521 | 1.044 | 0.017 ± 0.001 | 468 | 0.529 | 0.009 ± 0.001 |
| | 971 | 1.233 | 0.021 ± 0.001 | 974 | 0.834 | 0.014 ± 0.001 |
| | 1504 | 1.514 | 0.025 ± 0.001 | 1394 | 1.016 | 0.017 ± 0.001 |
| | 1913 | 1.717 | 0.028 ± 0.001 | 2115 | 1.276 | 0.021 ± 0.001 |
| | 2504 | 1.928 | 0.032±0.002 | 2335 | 1.556 | 0.026 ± 0.002 |
| | 2802 | 2.020 | 0.033 ± 0.002 | 2754 | 1.743 | 0.029 ± 0.002 |
| 333.2 | 543 | 0.923 | 0.015 ± 0.001 | 470 | 0.324 | 0.006 ± 0.001 |
| | 964 | 1.138 | 0.019 ± 0.001 | 959 | 0.582 | 0.014 ± 0.001 |
| | 1437 | 1.380 | 0.026 ± 0.001 | 1411 | 0.837 | 0.014 ± 0.001 |
| | 1910 | 1.557 | 0.026 ± 0.001 | 1927 | 0.994 | 0.017 ± 0.001 |
| | 2386 | 1.725 | 0.029 ± 0.002 | 2295 | 1.286 | 0.021 ± 0.002 |
| | 2725 | 1.836 | 0.030 ± 0.002 | 2801 | 1.475 | 0.025 ± 0.003 |

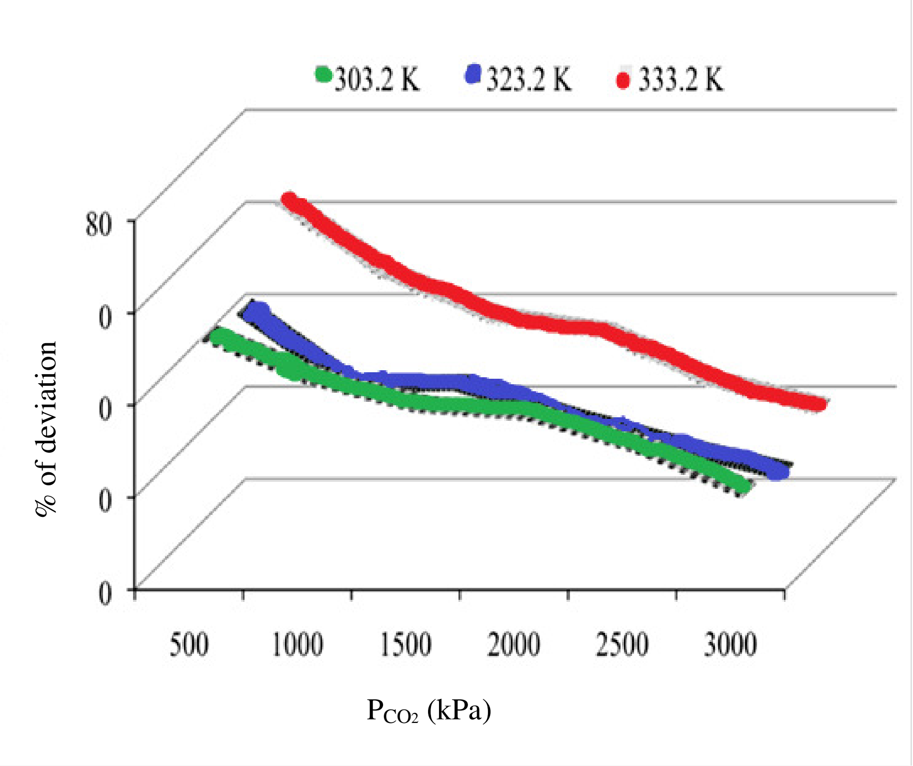

Figure 6.22. The deviation in $CO_2$ solubility between 1M0G and 0M1G at temperatures 303.2, 323.2 and 333.2 K and at pressure up to 3000 kPa.

## 6.7 Comparison with other ionic liquids

According to the structural features and fixation/ absorption mechanism, it is common to know that ionic liquid can be classified into two categories, conventional ionic liquid and task-specific ionic liquid. The conventional ionic liquids performed physical interaction between $CO_2$ and ionic liquids, which then led to less amount of $CO_2$ being absorbed. On the other hand, task-specific ionic liquids with alkaline groups could sequester larger amount of $CO_2$ than that of conventional ionic liquids.

This might be due to potential chemical interactions or reactivity between $CO_2$ and alkaline groups of ionic liquids. $CO_2$ is believed to react with amino group of the [gua][OTf]. Therefore, for instance, this might led to remarkable solubility of the amine-functionalized ionic liquid studied in this work. 1 M [gua][OTf] with other pure conventional ionic liquids [274] is illustrated in Figure 6.23.

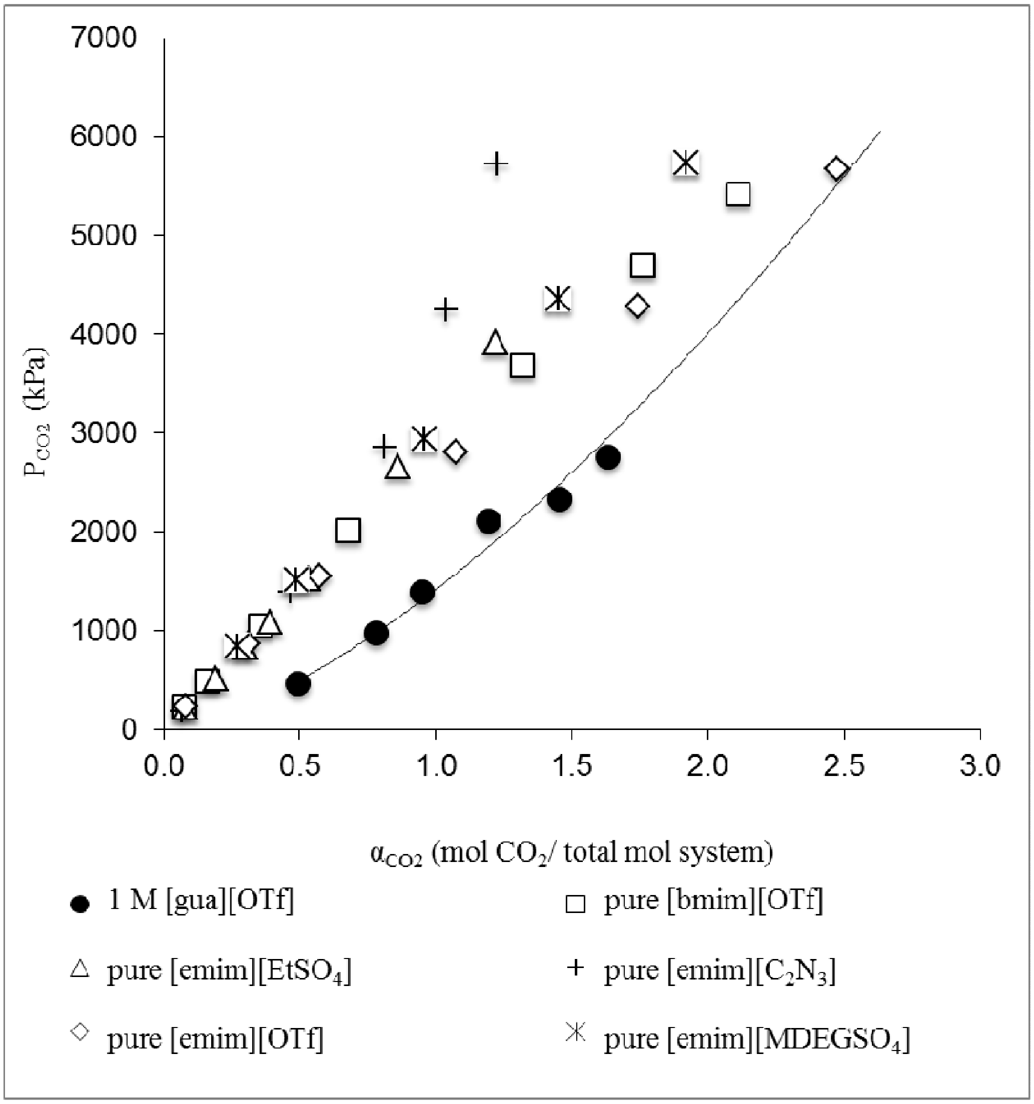

Figure 6.23. Comparison in solubility of $CO_2$ between 1 M [gua][OTf] (0M1G) and other conventional ionic liquids [274] at temperature 303.2 K and pressure up to 3000 kPa.

## 6.8 Correlation of solubility as function of pressure and temperature

The measured solubilities were linearly fitted as a function of partial pressure according to Equation 6.1 as suggested by Jou and Mather [57]. The coefficients of Equation 6.1 for the all studied systems are presented in Table 6.5.

$$\ln \rho = A \ln \alpha + B \qquad (6.1)$$

where;

$A_{4M0G} = -0.0243\ [T\ (K)] + 11.638$

$A_{4M1G} = -0.0138\ [T\ (K)] + 6.6903$

$A_{1M0G} = -0.0165\ [T\ (K)] + 7.7916$

$A_{0M1G} = -0.0104\ [T\ (K)] + 4.7207$

$B_{4M0G} = 0.029\ [T\ (K)] - 2.2444$

$B_{4M1G} = 0.0202\ [T\ (K)] + 1.3712$

$B_{1M0G} = 0.0331\ [T\ (K)] + 4.474$

$B_{0M1G} = 0.0154\ [T\ (K)] + 2.2903$

Table 6.5. The coefficients of Equation 6.1, the solubility as a function of pressure.

| Sample | T (K) | A | B | $R^2$ | Range $P_{CO}$ (kPa) |
|---|---|---|---|---|---|
| 4M0G | 303.2 | 4.3238 | 6.5761 | 0.98 | 500-3000 |
| 4M1G | 303.2 | 2.4265 | 7.5002 | 0.99 | 500-3000 |
| 1M0G | 303.2 | 2.8013 | 5.541 | 0.98 | 500-3000 |
| 0M1G | 303.2 | 1.5292 | 6.9913 | 0.98 | 500-3000 |
| 4M0G | 323.2 | 3.587 | 7.0325 | 0.97 | 500-3000 |
| 4M1G | 323.2 | 2.5284 | 7.9216 | 0.99 | 500-3000 |
| 1M0G | 323.2 | 2.4309 | 6.2548 | 0.99 | 500-3000 |
| 0M1G | 323.2 | 1.5009 | 7.1574 | 0.99 | 500-3000 |
| 4M0G | 333.2 | 3.6559 | 7.4773 | 0.99 | 500-3000 |
| 4M1G | 333.2 | 1.9194 | 8.1033 | 0.98 | 500-3000 |
| 1M0G | 333.2 | 2.3163 | 6.5209 | 0.98 | 500-3000 |
| 0M1G | 333.2 | 1.1728 | 7.4887 | 0.97 | 500-3000 |

A correlation of solubility as a function of temperature at different pressures was determined. Figure 6.24 to 6.27 display the comparison between calculated and experimental $CO_2$ loading for 1M0G, 0M1G, 4M0G and 4M1G at varying temperatures. The correlation of solubility, which was only valid for a pressure range from 500 to 3000 kPa, has the percentage difference of ± 0.957 %.

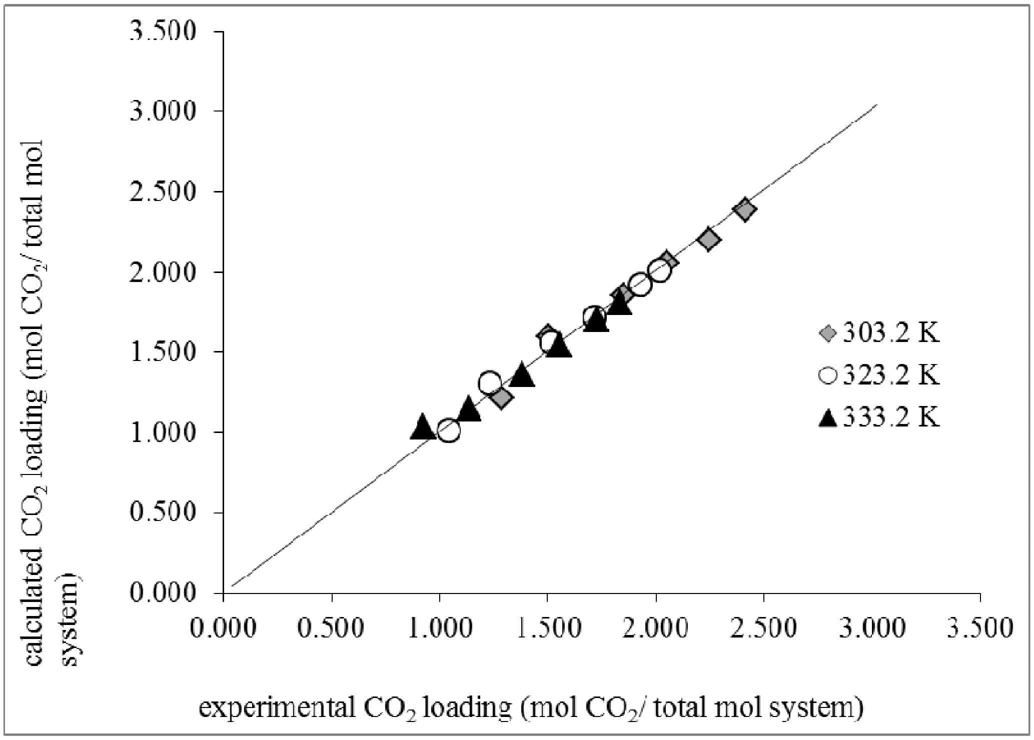

Figure 6.24. Comparison between the calculated and experimental $CO_2$ loading for 1M0G at various temperatures.

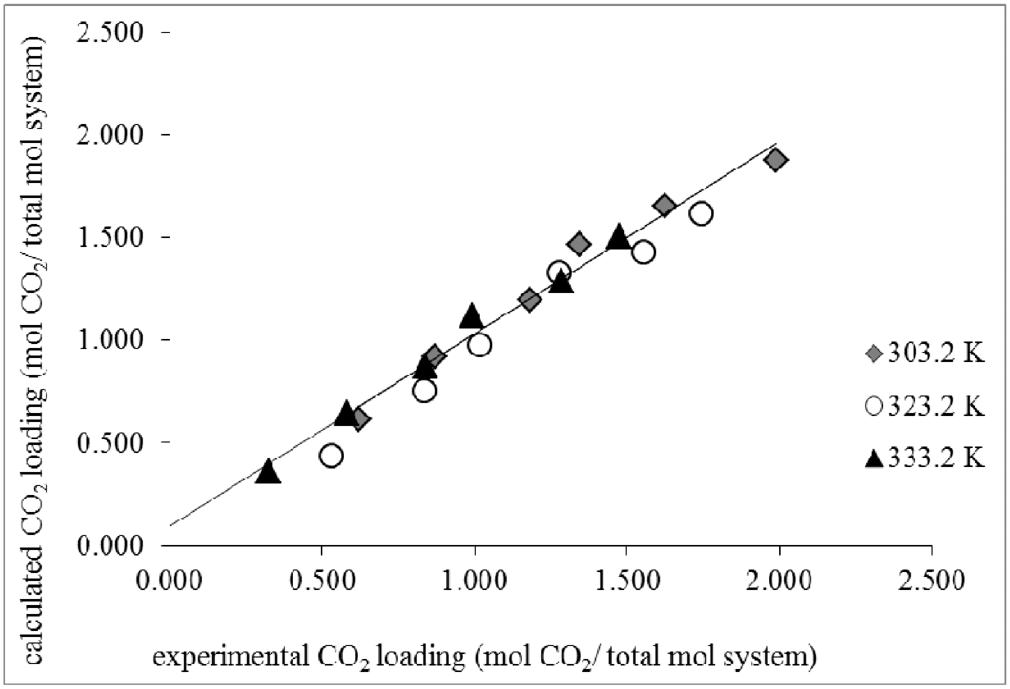

Figure 6.25. Comparison between the calculated and experimental $CO_2$ loading for 0M1G at various temperatures.

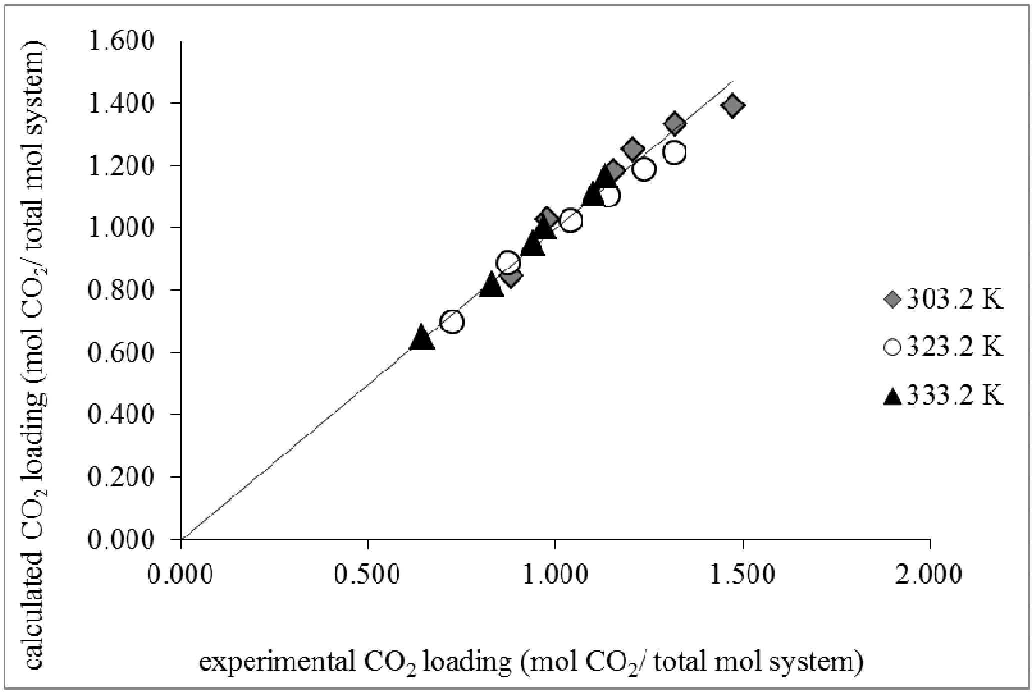

Figure 6.26. Comparison between the calculated and experimental $CO_2$ loading for 4M0G at various temperatures.

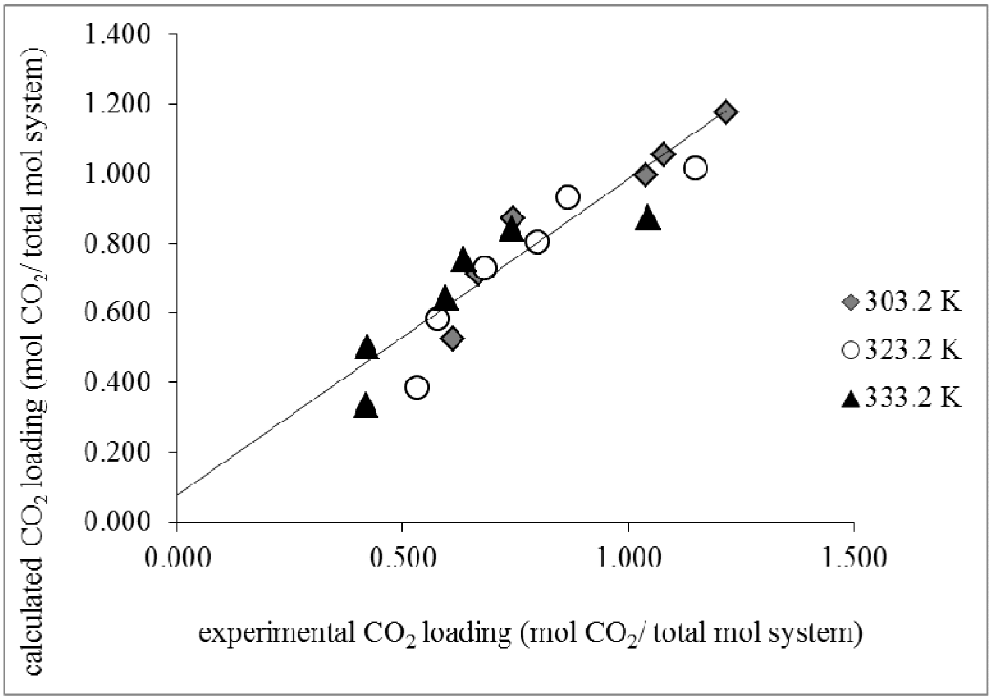

Figure 6.27. Comparison between the calculated and experimental $CO_2$ loading for 4M1G at various temperatures.

### 6.9 Conclusion

All systems show complete agreement to the expected trend in which the equilibrium loading decreases as the temperature increases and the pressure decreases. With having negative entropy in the systems, $CO_2$ in this exothermic process is predicted to become less soluble in binary and ternary systems with increasing temperature. This is due to the fact that when the temperature of a system at equilibrium is raised, the change will favour absorption of heat with respect to Van't Hoff's law of dynamic equilibrium. Meanwhile, according to Le Chatelier principal, as the $CO_2$ partial pressure or amount of $CO_2$ in the gas phase increases, the system will shift to a new equilibrium condition, which will absorb more $CO_2$ to diminish the effect of increasing $CO_2$ partial pressure. Therefore, the $CO_2$ absorption will increase as the pressure increases. The results also showed that the effect of $CO_2$ partial pressures at 303.2 K was the most pronounced for 0M1G, followed by 4M1G, 1M0G and 4M0G respectively with 220.2 %, 99.0 %, 87.2 % and 67.0 %, respectively.

On the other hand, the addition of [gua][OTf] however slightly reduced the solubility of $CO_2$ for all three investigated temperatures *i.e.* 303.2, 323.2 and 333.2 K. This is due to the formation of triflic acid by reaction of [gua][OTf] and water, which lowers the basicity of the solvent. The [gua][OTf] was believed to hinder the tertiary amine of MDEA hence lessen thews free amine to absorb $CO_2$. Furthermore, the solubility of $CO_2$ in ionic liquid is dependent on the interaction between the ionic liquid and the molecules, and also the free space available to be occupied by the $CO_2$ molecules in the ionic liquid rich phase. However, 1 M aqueous [gua][OTf] showed a competitive performance in capturing $CO_2$, which is up to 1.63 mol $CO_2$/ total mol system at 323.2 K and 3000 kPa, as compared to other pure ionic liquids such as [emim][$C_2N_3$], [emim][$MDEGSO_4$] and [emim][OTf] with 0.8132, 0.9587 and 1.0753 mol $CO_2$/ total mol system, respectively, all were recorded in the same environments. Correlations of solubility as a function of pressure and temperature have been determined with a difference of ± 0.957 %.

# Chapter 7: $CO_2$ ABSORPTION AND LOW PRESSURE

## 7.1 Introduction

The solubility of $CO_2$ in [gua][OTf] and/ or MDEA systems at low $CO_2$ partial pressure (10 – 100 kPa) was also carried out to investigate the ability of the systems (MDEA/ [gua][OTf]) as $CO_2$ capture solvent at low pressure and also to be compared with high pressure study. The study was not as extensive as that of high pressure and was only carried out at 303.2 K. A simple correlation was developed to predict the $CO_2$ loading in these systems. The correlation was successfully validated using the experimental data.

## 7.2 Validation of experimental procedure and comparison with literature

In order to establish the accuracy of the experimental procedures, validation experiments were carried out and the results were compared with $CO_2$ solubility data available in literature. The validation experiments were carried out on 4 M MDEA solution at 303.2 K with 100 % $CO_2$ at atmospheric pressure.

### 7.2.1 Comparison on the $CO_2$ loading with literature

The approach of this work was identical to Benamor [261] except that the liquid holdup volume in the reactor was maintained at 150 mL, instead of 50 mL as practiced in this work. The respective values obtained for 4 M MDEA on $CO_2$ loading are shown in the following Table 7.1. The deviation between Benamor's result and this work is less than 2 %. Therefore, it is verified that this experimental procedure is able to yield reproducible and accurate results.

Table 7.1. Comparison on $CO_2$ loading of 4 M MDEA solution at atmospheric pressure with 100 % $CO_2$ at 303 and 323 K.

| T (K) | $\alpha_{CO2}$ (mol $CO_2$/ total mol system) | | % of deviation |
|---|---|---|---|
| | This work | Benamor [261] | |
| 303 | 0.747 | 0.761 | -1.83 |
| 323 | 0.645 | 0.654 | -1.38 |

### 7.2.2 Validation of the titration method in determining the $CO_2$ loading

In order to establish the accuracy of the titration method used for the determination of $CO_2$ loading, a certain experiment was conducted on samples of mixed systems containing a known amount of sodium bicarbonate, $NaHCO_3$. Also, taking into account the presence of the new material, [gua][OTf], the confirmation test was performed.

Specifically, for this purpose, solutions with known amounts of $CO_2$ were prepared by dissolving 0.02 mol $NaHCO_3$ in MDEA and a mixture of MDEA and

[gua][OTf] and left to equilibrate for 24 hours. After equilibrium and dissolution of all bicarbonate, the samples were subjected to the procedure for the determination of $CO_2$ concentration. The respective results are shown in Table 7.2.

The results pointed out that the presence of ionic liquid did not interfere with $CO_2$ solubility measurement. Thus the chemical approach practiced in this research for the measurement of $CO_2$ solubility in low pressure (≤ 100 kPa) for alkanolamines was still relevant to the systems involving ionic liquids. According to the similar titration curves, the presence of ionic liquid did not interfere with the titration results.

Table 7.2. $CO_2$ loading of 4 M MDEA system containing a known amount of $NaHCO_3$.

| Solution | 4 M MDEA | 4 M MDEA + 1 M [gua][OTf] |
|---|---|---|
| $CO_2$ loading to be verified (mol $CO_2$/ total mol system) | 0.5 | 0.5 |
| Mol of $NaHCO_3$ in 5 mL sample | 0.02 | 0.02 |
| Actual $V_{HCl}$ (mL) | 20 | 20 |
| Calculated $V_{HCl}$ (mL) | 20.094 | 20.161 |
| % of deviation | 0.47 | 0.81 |

## 7.3 Amine concentration

It is crucial that the concentration of amine in solution during absorption process remains unchanged. This was confirmed by measuring the total amine concentration prior and later to each run. It was found that variation in amine concentration was within 3 % for most cases. However, at low $CO_2$ partial pressure, longer time was needed to reach equilibrium. Therefore evaporation of water was expected to occur. In this case, the variation of amine concentration was slightly higher reaching 5 %.

Table 7.3 compiled the MDEA concentrations prior and later to each run. Thus without introducing any significant error, it can be concluded that total amine concentration in the solution remained constant throughout each run. The other cause for the accuracy of the data depends on the measured quantities of $CO_2$ loading, vapour phase mol fraction of $CO_2$ and the total pressure of the system.

The $CO_2$ partial pressure at equilibrium was calculated by subtracting the water vapour pressure from the total pressure of the system. The $CO_2$ solubility results are the averages of three determinations of $CO_2$ solubility in aqueous MDEA, aqueous [gua][OTf] and mixtures MDEA and [gua][OTf] which are given later. The $CO_2$ solubility is expressed in terms of loading, mol of $CO_2$ absorbed per mol of total system which is mol of [MDEA + [gua][OTf] + $H_2O$].

### 7.4 pH profile of the systems

The variations of pH are continuously monitored throughout the absorption process. The high similarity of both 4 M MDEA and blended mixtures MDEA - [gua][OTf] is shown in Figure 7.1 and 7.2 respectively. Adversely, the aqueous [gua][OTf] gave a different trend, which indicated that a physical absorption was undergone. Apparently, such trend was because the pH for [gua][OTf] is about 5.85 similar to $CO_2$. This is shown in Figure 7.3.

Table 7.3. Amine concentrations before and after $CO_2$ absorption test at 303.2 K.

| Sample | MDEA concentration before test (M) | [gua][OTf] concentration before test (M) | $CO_2$ partial pressure (kPa) | MDEA concentration after test (M) | % of deviation |
|---|---|---|---|---|---|
| 4M1G | 4.105 ± 0.002 | 1.008 ± 0.001 | 10 | 4.184 ± 0.002 | 1.92 |
| | 4.133 ± 0.002 | 1.011 ± 0.001 | 50 | 4.094 ± 0.002 | 0.94 |
| | 4.095 ± 0.002 | 1.004 ± 0.001 | 100 | 4.066 ± 0.002 | 0.71 |
| 4M0G | 4.117 ± 0.002 | 0 | 10 | 4.211 ± 0.002 | 2.28 |
| | 4.012 ± 0.002 | 0 | 50 | 3.951 ± 0.002 | 1.52 |
| | 4.011 ± 0.002 | 0 | 100 | 4.006 ± 0.002 | 0.12 |
| 3M1G | 3.080 ± 0.002 | 1.005 ± 0.001 | 10 | 3.198 ± 0.002 | 3.83 |
| | 3.100 ± 0.002 | 1.002 ± 0.001 | 50 | 3.009 ± 0.002 | 2.94 |
| | 3.096 ± 0.002 | 1.003 ± 0.001 | 100 | 3.047 ± 0.002 | 1.58 |
| 2M2G | 1.986 ± 0.002 | 2.001 ± 0.001 | 10 | 1.043 ± 0.002 | 1.91 |
| | 2.006 ± 0.002 | 2.000 ± 0.001 | 50 | 1.985 ± 0.002 | 1.05 |
| | 2.013 ± 0.002 | 2.004 ± 0.001 | 100 | 2.000 ± 0.002 | 0.64 |
| 1M3G | 1.054 ± 0.002 | 3.003 ± 0.001 | 10 | 1.092 ± 0.002 | 3.61 |
| | 1.021 ± 0.002 | 3.002 ± 0.001 | 50 | 1.012 ± 0.002 | 0.88 |
| | 1.004 ± 0.002 | 3.005 ± 0.001 | 100 | 1.001 ± 0.002 | 0.30 |
| 1M0G | 1.009 ± 0.002 | 0 | 10 | 1.054 ± 0.002 | 4.46 |
| | 1.028 ± 0.002 | 0 | 50 | 1.014 ± 0.002 | 1.36 |
| | 1.044 ± 0.002 | 0 | 100 | 1.036 ± 0.002 | 0.77 |

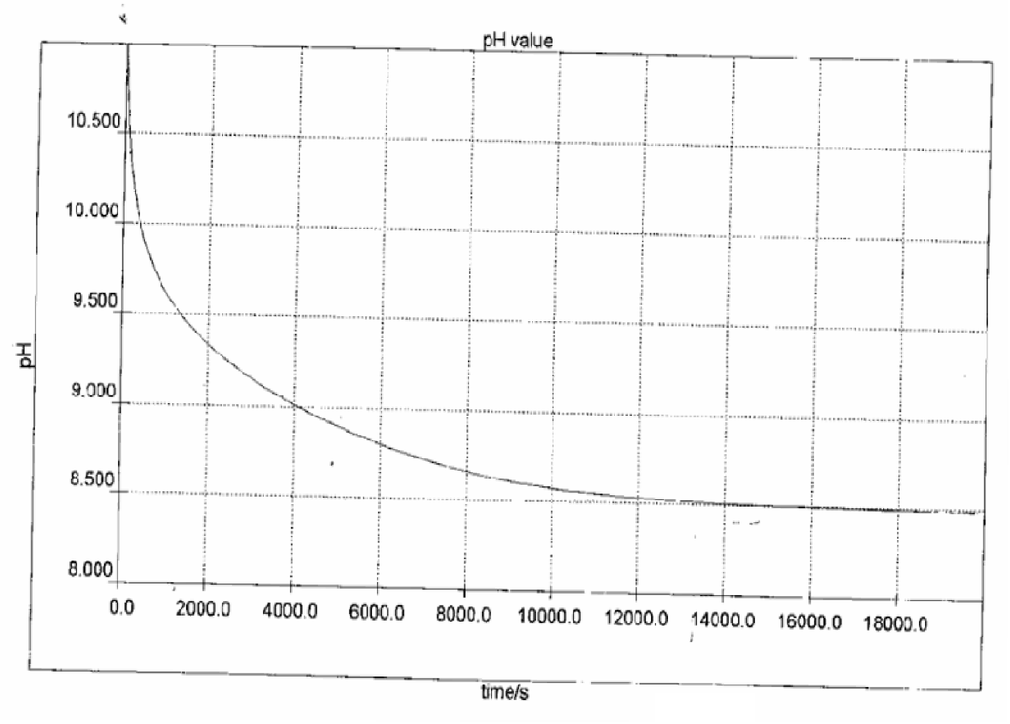

Figure 7.1. Equilibrium curve for reaction of 4 M MDEA with pure $CO_2$ at 303.2 K, 100 kPa.

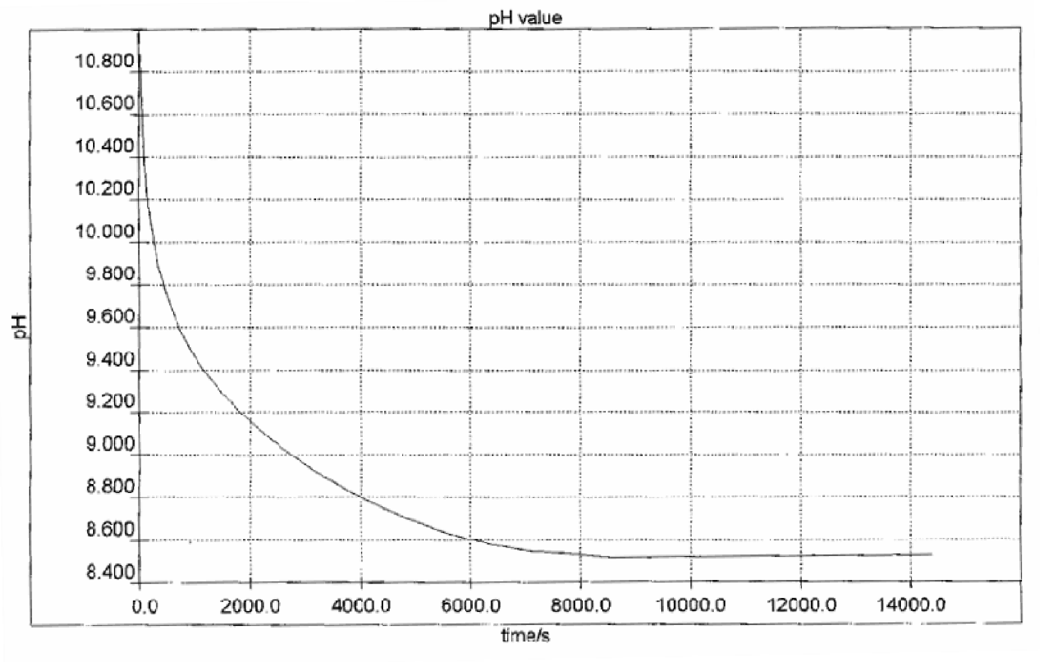

Figure 7.2. Equilibrium curve for reaction of 4 M MDEA + 1 M [gua][OTf] with pure $CO_2$ at 303.2 K, 100 kPa.

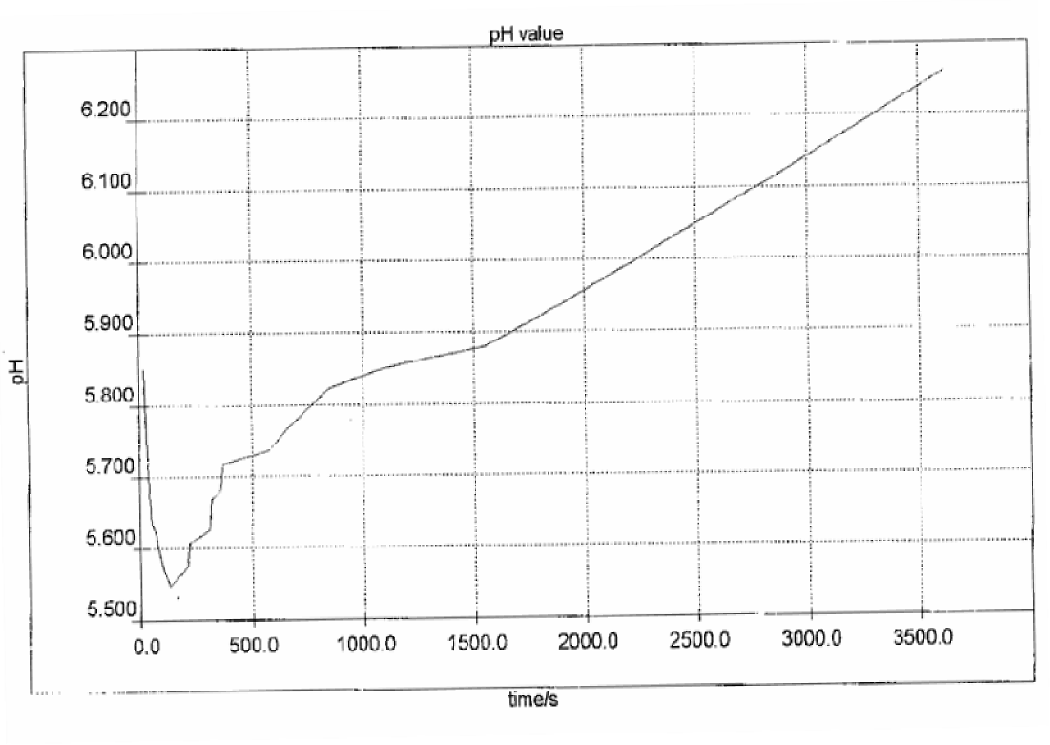

Figure 7.3. Equilibrium curve for 1 M [gua][OTf] with 100 % $CO_2$ at 303.2 K and 100 kPa.

Table 7.4 shows the difference of the systems at the equilibrium time. The duration for 4 M MDEA decreased from 5.6 to 3.9 hours after addition of 1 M [gua][OTf]. A significant decrement from 4.4 to 0.83 hours in total time reaching equilibrium has also been recorded by 1M3G, in which from 4.4 to 0.83 hours indicates that the presence of ionic liquid might increase the overall rate of $CO_2$ absorption.

This possible enhanced rate of absorption can be explained by the higher physically absorbed $CO_2$ in the presence of ionic liquid. Both 0M1G and 0M4G were generally noted as 0.5 hours respectively due to physical absorption (refer to Figure 7.3). More comprehensive kinetic studies should be carried out in order to explain this phenomenon.

Table 7.4. Equilibrium time for 4M0G, 4M1G, 3M1G, 2M2G, 1M3G, 1M0G 0M1G and 0M1G on pure $CO_2$ absorption at 303.2 K, 100 kPa.

| System | Time to reach equilibrium (minutes) |
|---|---|
| 4M0G | 333 |
| 4M1G | 233 |
| 3M1G | 113 |
| 2M2G | 100 |
| 1M3G | 50 |
| 1M0G | 266 |
| 0M4G | 30 |
| 0M1G | 30 |

### 7.5 Effect of $CO_2$ partial pressure on $CO_2$ loading

Figures 7.4, 7.5, 7.6 and 7.7 demonstrate the effects of $CO_2$ partial pressure on $CO_2$ solubility of the aqueous and blended mixture of MDEA and [gua][OTf] at 303.2 K. As expected, the $CO_2$ loading increases with the increase of $CO_2$ partial pressure. The $CO_2$ loading of blended system 4M1G (Figure 7.4) was found to be 0.3117 when the dry reaction gas only contains 10 mol% $CO_2$ (with the respective partial pressure calculated to be 9.842 kPa). It then experienced more than double increment when the partial pressure of $CO_2$ increased to 98.424 kPa equivalent to 100 mol% $CO_2$ in the dry reaction gas, with the respective $CO_2$ loading found to be 0.6498. Thus being a tertiary amine, MDEA showed a high loading approaching 1.

Also, it shows that the effect of $CO_2$ partial pressure is slightly pronounced for 4M0G, as indicated by the higher slope between 10 and 50 kPa as compared to 50 and 100 kPa. Also, the effect of partial pressure on $CO_2$ loading for 4M1G was about equivalent with 4M0G for all range of pressure.

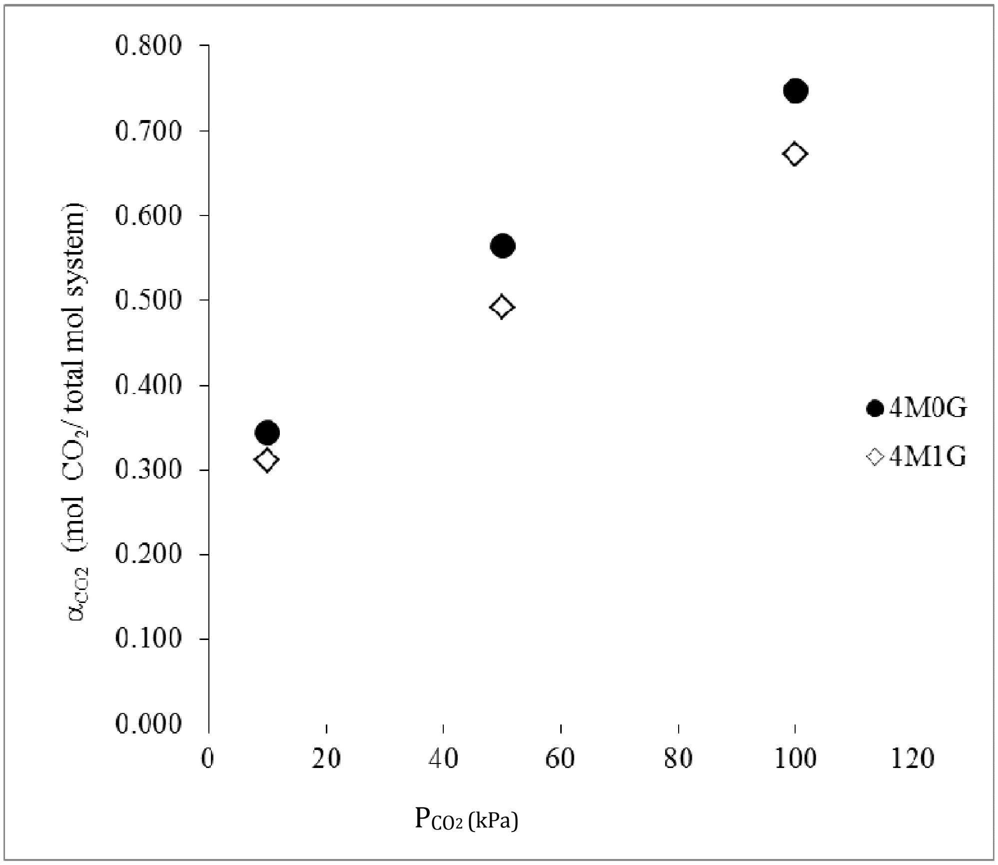

Figure 7.4. $CO_2$ loading for 4M0G and 4M1G at 303.2 K at different $CO_2$ partial pressure.

Figure 7.5 compares the solubility of $CO_2$ in 4M0G, 3M1G, 2M2G, and 1M3G. It suggested that $CO_2$ solubility decreases as the composition of [gua][OTf] in the systems increases. Furthermore, the decrement of $CO_2$ absorbed is led by decrement in concentration of MDEA. For binary systems, 1M0G and 0M1G (Figure 7.6), the solubility of 0M1G is lower compared to 1M0G at 303.2 K and 100 kPa of $CO_2$ partial pressure. Meanwhile, Figure 7.7 shows the difference of 37% of $\alpha_{CO_2}$ between 1 and 4 M [gua][OTf].

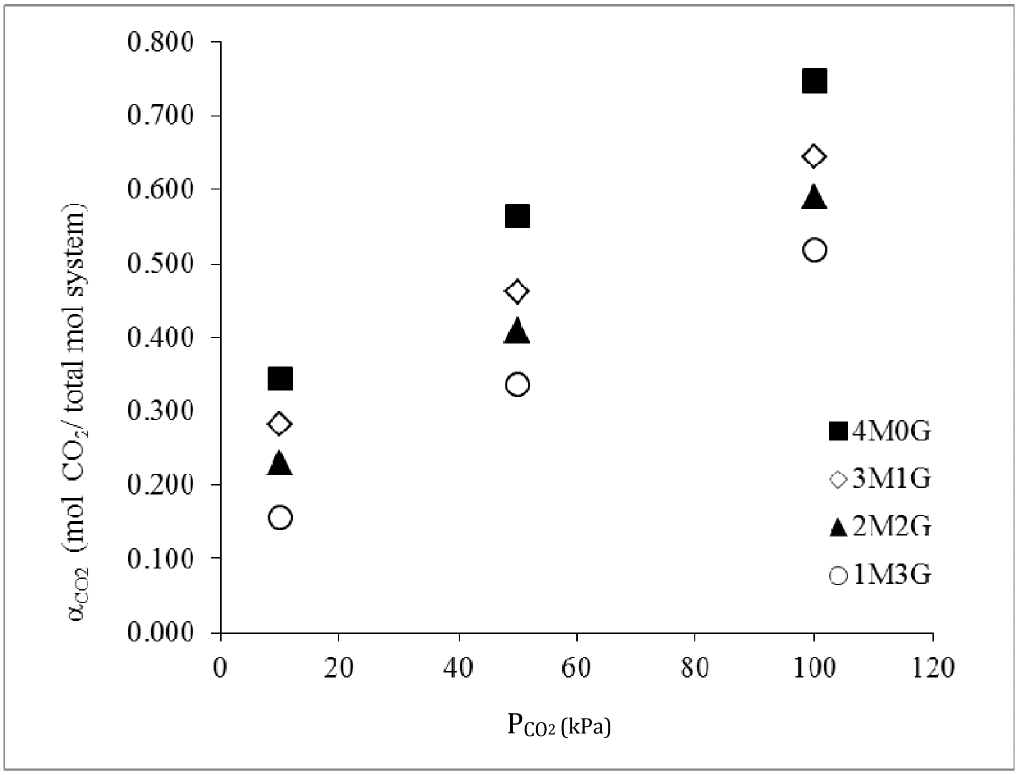

Figure 7.5. $CO_2$ loading for 4M0G, 3M1G, 2M2G and 1M3G at 303.2 K at different $CO_2$ partial pressure.

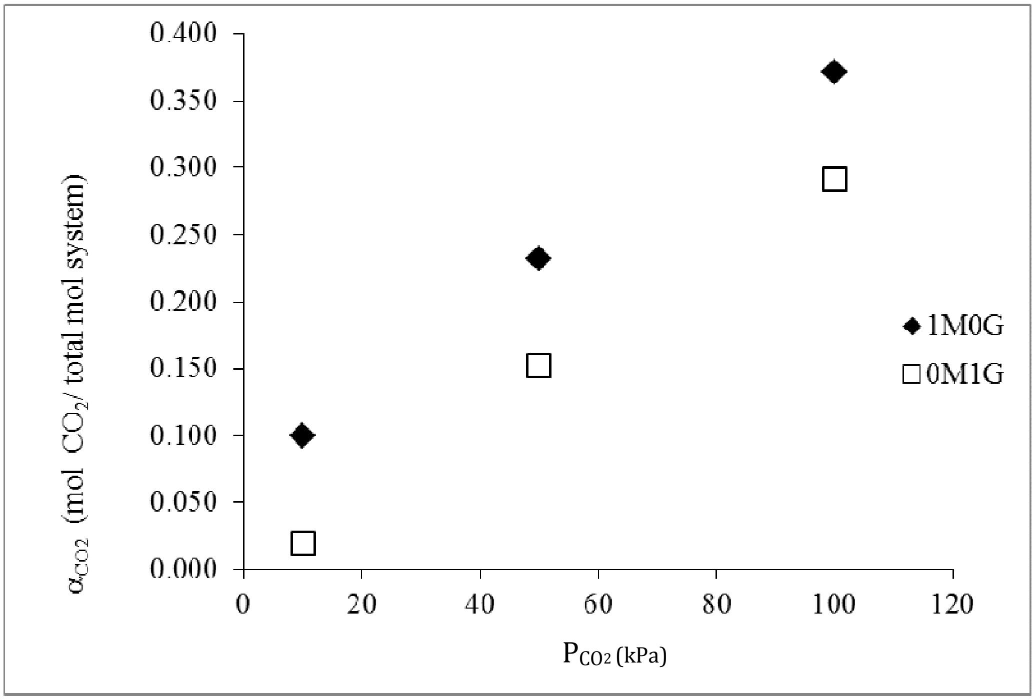

Figure 7.6. $CO_2$ loading for aqueous 1 M MDEA (1M0G) and 1 M [gua][OTf] (0M1G) at 303.2 K at different $CO_2$ partial pressure.

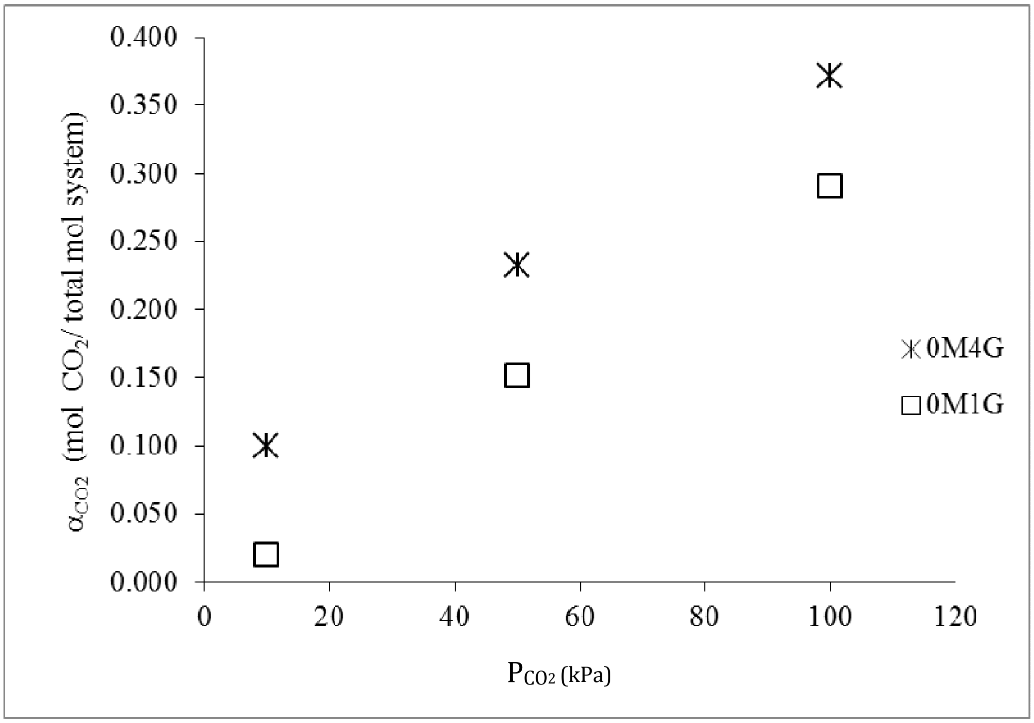

Figure 7.7. $CO_2$ loading for 0M4G and 0M1G at 303.2 K at different $CO_2$ partial pressure.

### 7.6 Effect of [gua][OTf] presence on the $CO_2$ loading

Table 7.5 presents the $CO_2$ loading for various composition of MDEA - [gua][OTf] at 303.2 K and 100 % $CO_2$. The results suggest that the presence of [gua][OTf] in MDEA gives similar decreasing effect as other ionic liquids as studied by Anthony *et al*. [107], Bates *et al*. [109] and Anthony *et al*. [159].

Since MDEA reacted with $CO_2$ through an acid base mechanism, this reduction of the $CO_2$ loading might be due to the decrease in its basic character. In fact, this result also supported the idea that anion plays a bigger role in ionic liquids. The acidity might be attributed to the triflate anion from ionic liquid. The fact was confirmed by the calculated overall equilibrium constants. The overall equilibrium constants ($K_{ov}$) were found to decrease in the presence of ionic liquid, which indicated a decrease in the MDEA basicity. Even though the cation of [gua][OTf] has amines attached to it, however, it is not sufficient enough to increase the basicity of the systems and therefore enhance the chemical absorption capacity.

Table 7.5. $CO_2$ loading for various composition of MDEA - [gua][OTf] at 303.2 K and 100 % $CO_2$.

| Sample | Concentration of MDEA (M) | Concentration of [gua][OTf] (M) | $\alpha_{CO_2}$ (mol $CO_2$/ total mol system) |
|---|---|---|---|
| 4M0G | 4 | 0 | 0.748 ± 0.001 |
| 4M1G | 4 | 1 | 0.673 ± 0.001 |
| 3M1G | 3 | 1 | 0.645 ± 0.001 |
| 2M2G | 2 | 2 | 0.631 ± 0.001 |
| 1M3G | 1 | 3 | 0.519 ± 0.001 |
| 1M0G | 1 | 0 | 0.713 ± 0.001 |
| 0M4G | 0 | 4 | 0.371 ± 0.001 |
| 0M1G | 0 | 1 | 0.291 ± 0.001 |

This phenomenon might also be explained by referring to the stoichiometric Equation 7.1, whereby sufficient amount of water is needed to be present in order to promote the dissociation of amine and absorb the $CO_2$ to form bicarbonate. With the addition of [gua][OTf], the amount of water in the mixed system is definitely reduced, and thus results in lower absorption capacity and lower $CO_2$ loading.

Reaction of $CO_2$ with tertiary amine:

$$CO_2 + R_3N + H_2O \rightleftharpoons R_3NH^+ + HCO_3^- \qquad (7.1)$$

As discussed in Section 7.4, [gua][OTf] is postulated to absorb $CO_2$ through physical mechanism instead of chemical reaction. According to Yu *et al.*, [275] the solubility of $CO_2$ in a variety of ionic liquids including [gua][OTf] is trivial at room temperature and atmospheric pressure, due to the physical nature of the absorption process. Physical absorption of $CO_2$ will only play a significant role at high operating pressure. Therefore, the presence of [gua][OTf] could not make up the loss of the $CO_2$ absorption capacity of MDEA due to the reducing amount of water with increasing amount of [gua][OTf].

However, it is important to point out that aqueous [gua][OTf] gave a much better capability to absorb $CO_2$ as compared to other pure studied ionic liquids such as [bmim][$BF_4$]. This could be seen in Figure 7.8. Yet, 4 M MDEA added with 1 M [gua][OTf] gave 27.5 % higher $CO_2$ loading compared to 1 M [bmim][$BF_4$] added with 4 M MDEA.

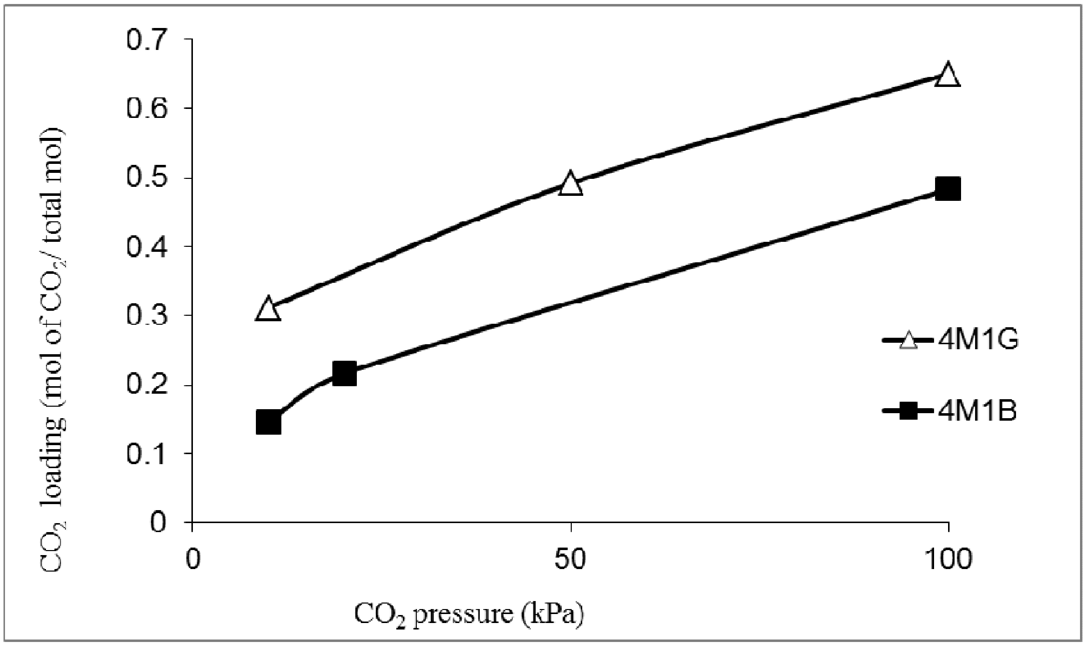

Figure 7.8. Comparison $CO_2$ loading in 4M1G (4 M MDEA + 1 M [gua][OTf]) and 4M1B (4 M MDEA + 1 M [bmim][$BF_4$]).

### 7.7 Correlation of solubility data at low pressure

The main reactions taking place were the protonation of MDEA and hydrolysis of $CO_2$.

$$MDEA + H^+ \rightleftharpoons MDEAH^+ \qquad \text{(protonation of MDEA)} \qquad (7.2)$$

$$CO_2 + H_2O \rightleftharpoons HCO_3^- + H^+ \qquad \text{(hydrolysis of } CO_2\text{)} \qquad (7.3)$$

As such the overall reaction between MDEA and $CO_2$ can be written as:

$$H_2O + MDEA + CO_2 \rightleftharpoons MDEAH^+ + HCO_3^- \qquad (7.4)$$

Assuming activities of $H_2O$ and activity coefficient of other species equal to 1, the overall equilibrium constant for reaction (7.4) can be written as:

$$K_{ov} = \frac{[MDEAH^+][HCO_3^-]}{[MDEA][CO_2]} \qquad (7.5)$$

The physically absorbed $CO_2$ is related to $CO_2$ partial pressure according to Henry's law:

$$P_{CO_2} = H_{CO_2}\,[CO_2] \qquad (7.6)$$

Where $H_{CO2}$ is the Henry's constant and $P_{CO2}$ are the partial pressures of

$CO_2$, in gas phase respectively. The Henry's constant is assumed to be equal to that in pure water.

Therefore,

$$K_{ov} = \frac{[MDEAH^+]\,[HCO_3^-]}{[MDEA]\,[P_{CO2} / H_{CO2}]} \tag{7.7}$$

The total mass balance on $CO_2$ is given by:

$$[CO_2]_t = [HCO_3^-] + [CO_2] + [CO_3^{2-}] \tag{7.8}$$

The $CO_2$ that is physically absorbed can be negligible as compared to the chemically absorbed $CO_2$ ($HCO_3^-$). The concentration of carbonate can be neglected since the pH of the carbonate solution is less than 8. This low pH indicates that the bicarbonate dissociation reaction is not significant.

Dissociation of bicarbonate:

$$HCO_3^- \rightleftharpoons H^+ + CO_3^{2-} \tag{7.9}$$

Therefore, it can be concluded that:

$$[CO_2]^- = [HCO_3^-] \tag{7.10}$$

$CO_2$ loading ($\alpha_{CO2}$) can be defined as mol of $CO_2$ per mol of total system.

$$\alpha_{CO_2} = \frac{[CO_2]_t}{[MDEA]_t} \tag{7.11}$$

Therefore, the total $CO_2$ can be written as:

$$[CO_2]_t = [HCO_3]^- = \alpha_{CO2}\ [MDEA]_t = [MDEA^+] \qquad (7.12)$$

The total mass balance on MDEA is given by:

$$[MDEA]_t = [MDEA] + [MDEAH^+] = [MDEA] + [HCO_3^-] \qquad (7.13)$$

Based on mentioned equation, the overall constant equilibrium can be written as:

$$K_{ov} = \frac{[MDEAH^+]\ [HCO_3^-]}{[MDEA]\ [CO_2]} \qquad (7.14)$$

Therefore, $P_{CO_2}$ can be written as;

$$\frac{K_{ov}\ P_{CO2}}{H_{CO2}} = \frac{[MDEA]_t \times \alpha_{CO_2}^2}{(1-\alpha_{CO_2})}$$

$$P_{CO_2} = \frac{H_{CO_2}\ [MDEA]_t}{(1-\alpha_{CO_2})\ K_{ov}} \times \frac{\alpha_{CO_2}^2}{(1-\alpha_{CO_2})} \qquad (7.15)$$

Equation (7.14) indicates that a plot of $P_{CO_2}$ versus ($\alpha_{CO_2}^2$/ 1 - $\alpha_{CO_2}$) should be linear with a slope equal to ($H_{CO_2}$ $[MDEA]_t$)/ $K_{ov}$.

This correlation was validated using the experimental $CO_2$ solubility data. Figures 7.9 to 7.12 show the plot of $P_{CO2}$ *versus* ($\alpha_{CO_2}^2$/ 1 - $\alpha_{CO_2}$). The $R^2$ values range from 0.94232 to 0.96272 for partial pressure between 0 - 100 kPa. These $R^2$ values were finely fitted.

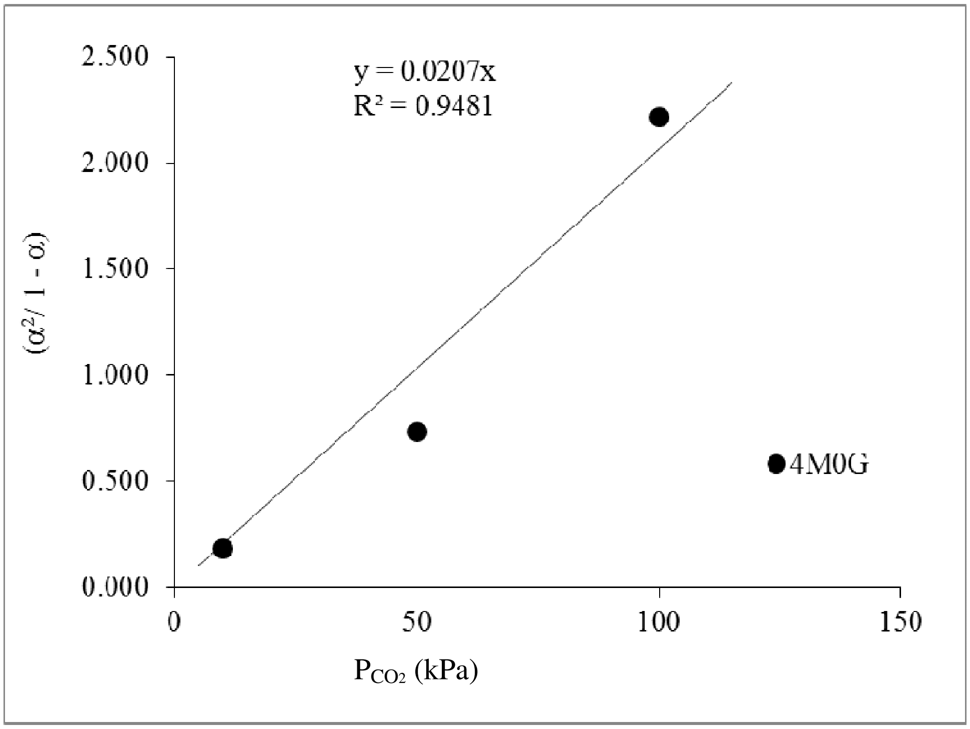

Figure 7.9. Correlation results of $CO_2$ absorption in a mixture of 4M0G at 303 K.

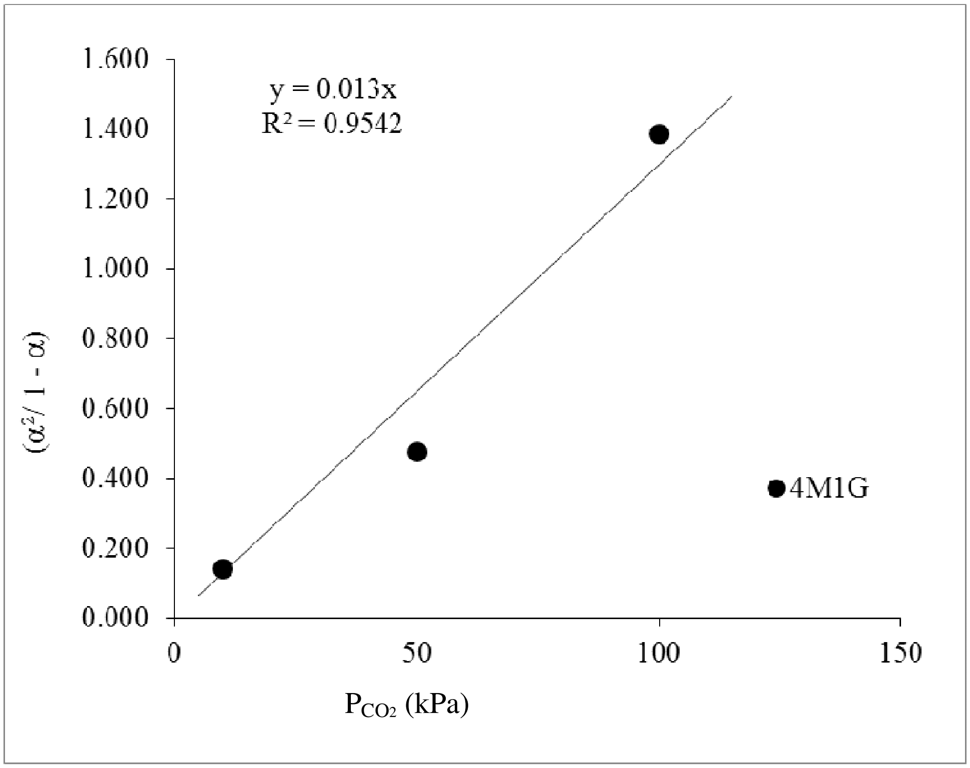

Figure 7.10. Correlation results of $CO_2$ absorption in a mixture of 4M1G at 303 K.

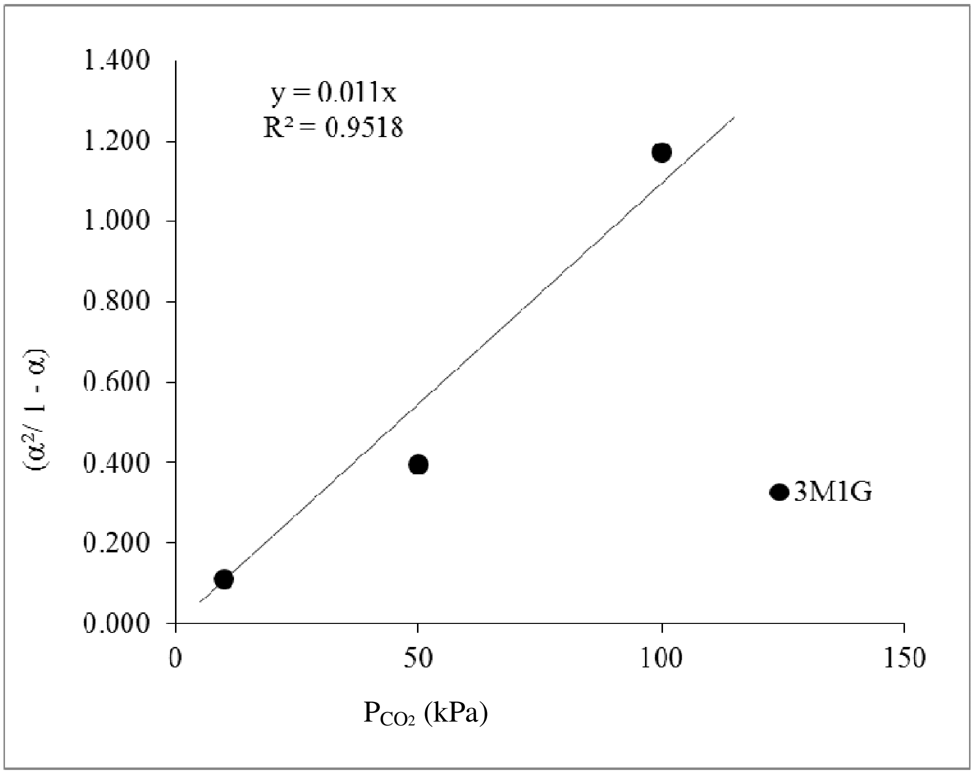

Figure 7.11. Correlation results of $CO_2$ absorption in a mixture of 3M1G at 303 K.

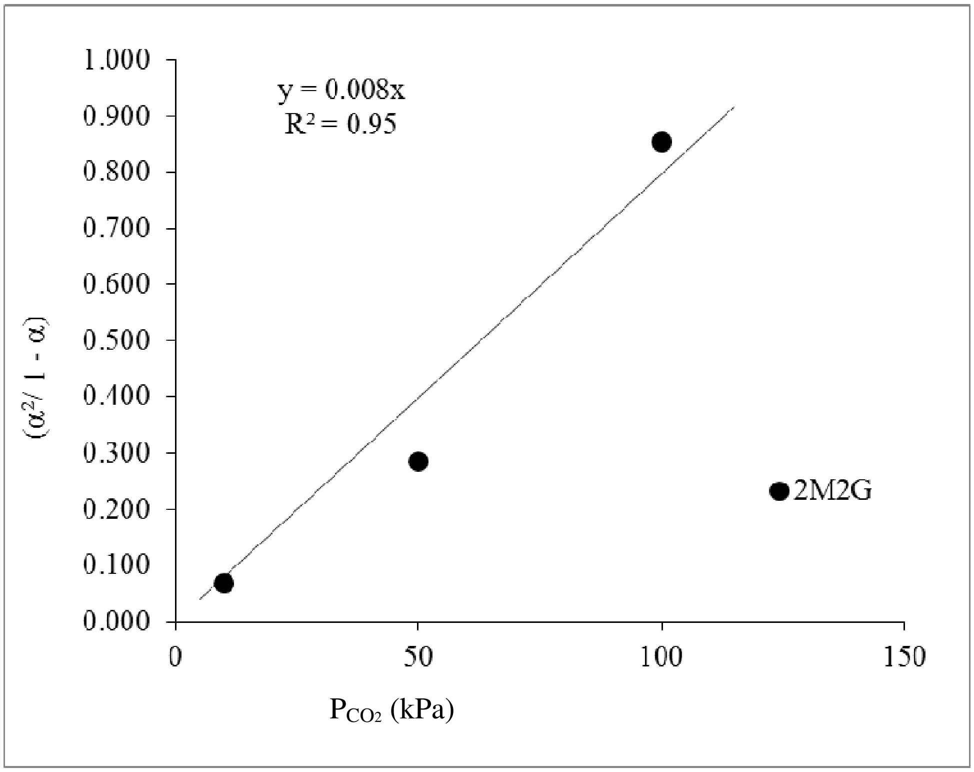

Figure 7.12. Correlation results of $CO_2$ absorption in a mixture of 2M2G at 303 K.

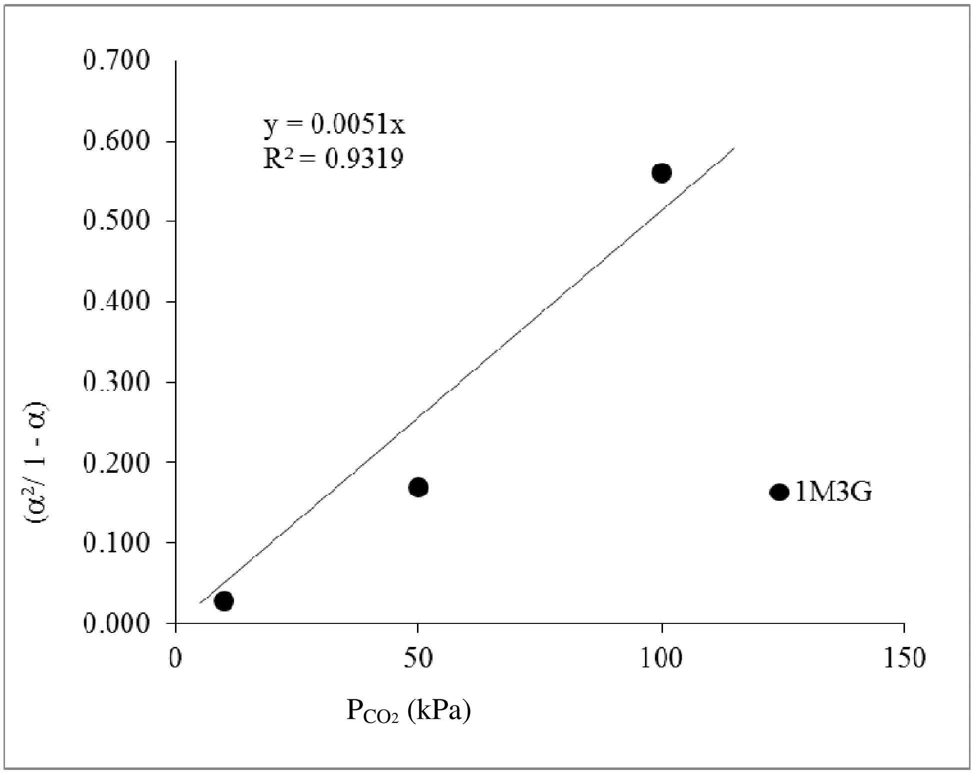

Figure 7.13. Correlation results of $CO_2$ absorption in a mixture of 1M3G at 303 K.

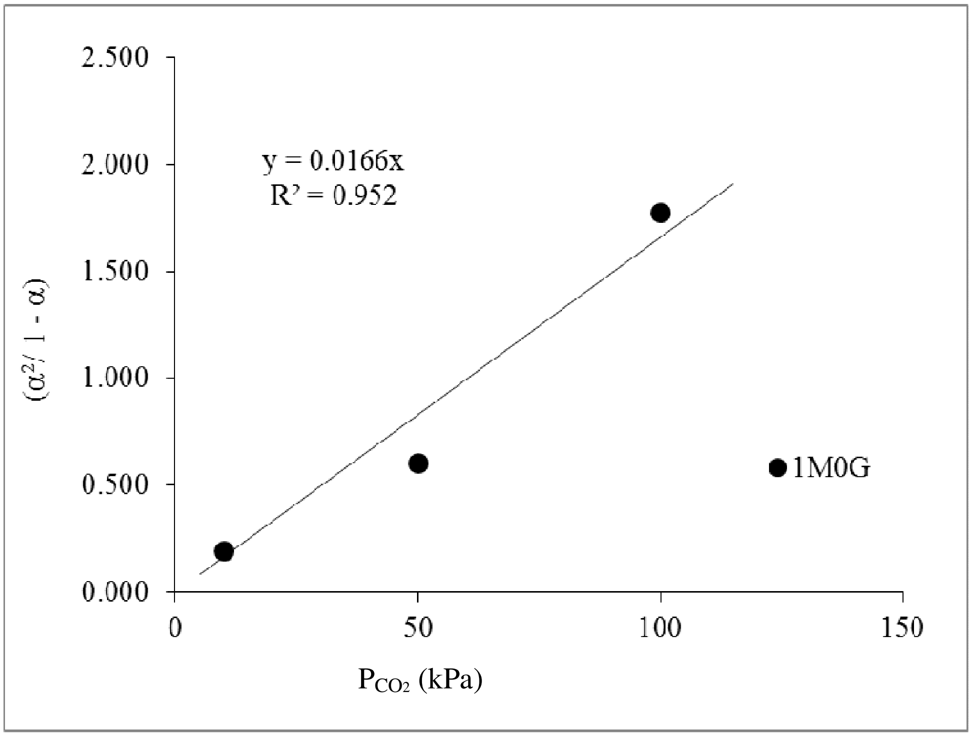

Figure 7.14. Correlation results of $CO_2$ absorption in a mixture of 1M0G at 303 K.

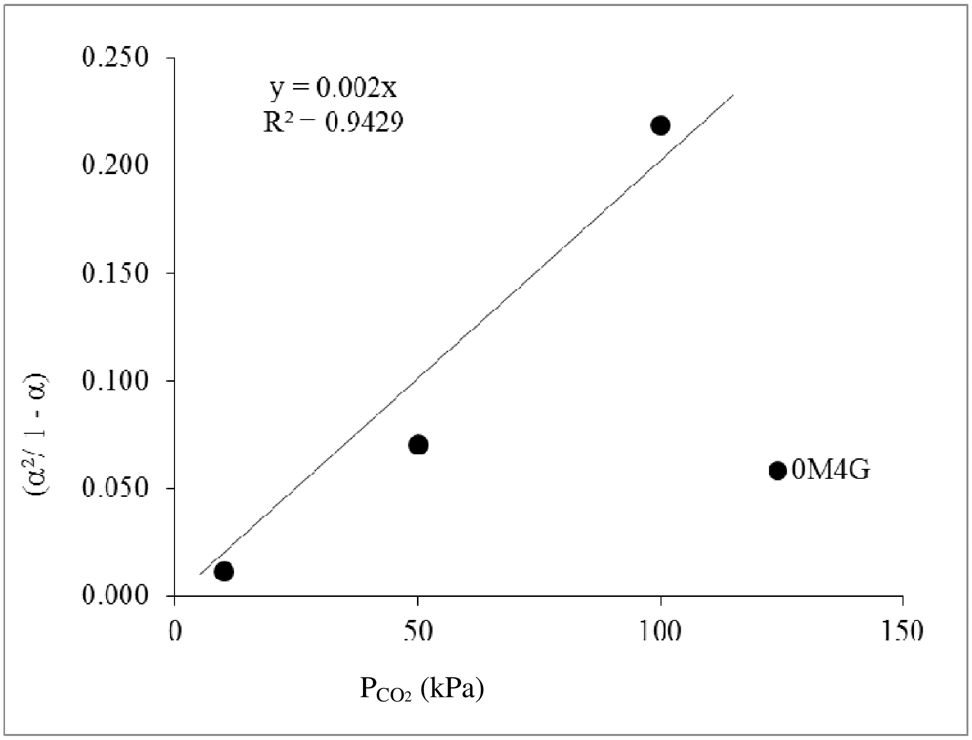

Figure 7.15. Correlation results of $CO_2$ absorption in a mixture of 0M4G at 303 K.

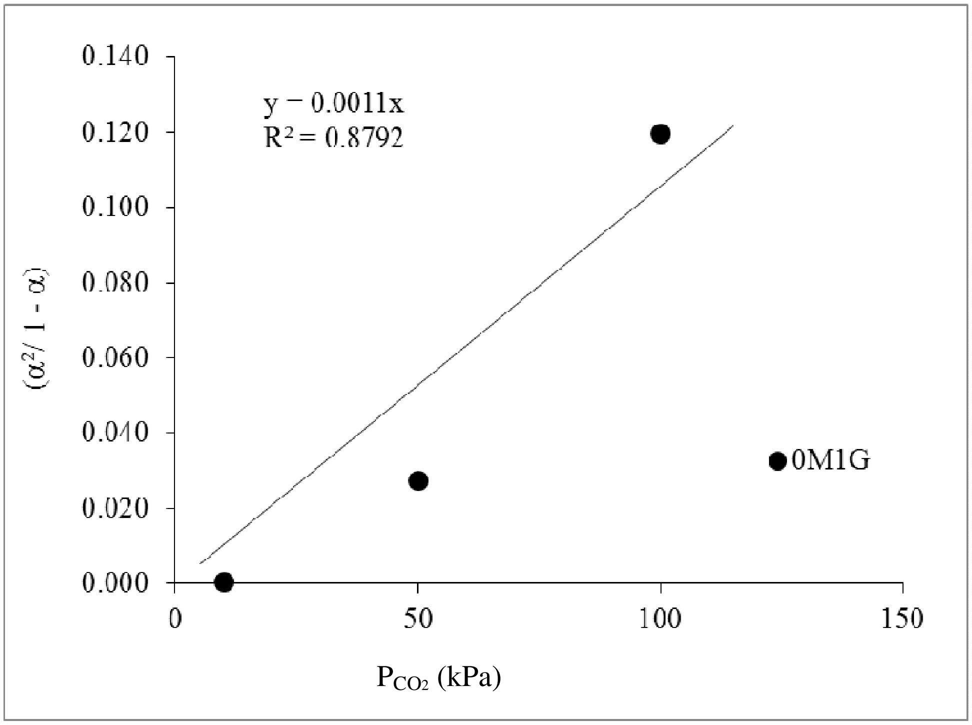

Figure 7.16. Correlation results of $CO_2$ absorption in a mixture of 0M1G at 303 K.

### 7.8 Conclusion

The chemical absorption took place essentially in lower pressure. The results suggest that the presence of [gua][OTf] in MDEA gives a similar decreasing effect as at higher pressure. It was found to be 0.6498 mol $CO_2$/ total mol system for 4M1G compared to 0.748 mol $CO_2$/ total mol system for 4M0G at 303 K, 100 kPa.

Since MDEA reacted with $CO_2$ through an acid base mechanism, this reduction of the $CO_2$ loading might be due to the decrease in its basic character. The acidity might also be contributed from the triflate anion in ionic liquid. Even though the cation of [gua][OTf] has amines attached to it, it is not sufficient enough to increase the basicity of the systems, so as to enhance the chemical absorption capacity.

Reducing the amount of water in the mixed system by adding [gua][OTf] might also led to reduction in $CO_2$ solubility. This is because sufficient amount of water is needed to be present in order to promote the dissociation of amine and absorb the $CO_2$ to form bicarbonate. However, it is important to point out that 4M1G gave a much better capability to absorb $CO_2$ as compared to other pure studied ionic liquids such as [bmim][$BF_4$]. 4M1G gave 27.5 % higher $CO_2$ loading (0.6498 mol $CO_2$/ total mol system) as compared to 4M1B with 0.4829 mol $CO_2$/ total mol system at 303 K, 100 kPa.

As expected, the $CO_2$ solubility increases as the pressure increases and temperature decreases. At 303 K, 4M1G recorded 0.3117 mol $CO_2$ per total mol system at 9.842 kPa and increased to 0.6498 mol $CO_2$/ total mol system at 98.424

kPa. For binary systems, the solubility of $CO_2$ in 0M1G is lower compared to 1M0G at 303.2 K and 100 kPa of $CO_2$ partial pressure. Meanwhile, the difference between 1 and 4 M [gua][OTf] was about 37 %. The $R^2$ values were finely fitted and ranged from 0.94232 to 0.96272 for partial pressure between 0 - 100 kPa.

# Chapter 8: GENERAL CONCLUSIONS AND FURTHER WORK

## 8.1 General conclusions

Ionic liquids posses an exclusive structural flexibility features that amine solvents do not have. It was possible to change the ionic liquid structure in order to improve its performance as a gas solvent. The absorption of $CO_2$ in ionic liquids increased almost threefold with primary amine groups incorporated to the ionic liquids structure. Yet, present study revealed it would be higher if it was presented in the form of aqueous solution such amine-functionalized ionic liquid, *i.e.* guanidinium trifluoromethanesulfonate ionic liquid, [gua][OTf]. 1 M aqueous [gua][OTf] showed almost doubled $CO_2$ solubility at 323.2 K and 3000 kPa which increased up to 1.63 mol $CO_2$/ total mol system as compared to other pure ionic liquids such as [emim][$C_2N_3$], [emim][$MDEGSO_4$] and [emim][OTf] with 0.8132, 0.9587 and 1.0753 mol $CO_2$/ total mol system, respectively at the same conditions.

Nevertheless, [gua][OTf] was believed to hinder the tertiary amine of MDEA hence lessen the free amine to absorb $CO_2$. Furthermore, the solubility of $CO_2$ in ionic liquid is dependent on the interaction between the ionic liquid and the molecules, and also the free space available to be occupied by the $CO_2$ molecules in the ionic liquid rich phase. The $CO_2$ solubility reduced from 0.981 to 0.667 mol $CO_2$/ total mol system at 303 K and 100 kPa. It has been found that the effect of partial pressures at 303.2 K was most pronounced for 0M1G. This was proven by 220.1 % deviation in $CO_2$ solubility from the lowest pressures studied, 489 kPa to highest, 2823 kPa. The high reliance of $CO_2$ solubility to its partial pressure also supported that 0M1G is involved mainly in physical absorption. Both 4M0G and 1M0G were recorded at 67.0 and 87.2 %, respectively. The correlation of solubility, which was only valid for a pressure range from 500 to 3000 kPa, had the percentage difference of ± 0.957 %.

$CO_2$ solubility in binary and ternary systems of [gua][OTf] - MDEA at lower pressure (< 100 kPa) resembles to at higher pressure (< 3000 kPa). The amount is increased as the pressure increases. At 303 K and 10 kPa, 0M1G, 1M0G and 4M0G recorded 0.0202, 0.1002 and 0.3438 mol $CO_2$ per total mol system, respectively, and increased to 0.291, 0.712 and 0.748 mol $CO_2$ per total mol system, respectively, at 100 kPa. Similarly, the ternary systems increase doubled as the pressure increased from 0.287 mol $CO_2$ per total mol system (3M1G), 0.245 mol $CO_2$ per total mol system (2M2G) and 0.164 mol $CO_2$ per total mol system (1M3G) to 0.645 mol $CO_2$ per total mol system (3M1G), 0.631 mol $CO_2$ per total mol system (2M2G) and 0.519 mol $CO_2$ per total mol system (1M3G) with descending trend as composition of [gua][OTf] increased. The results also suggested that the addition of [gua][OTf] in MDEA gave a similar decreasing effect. It was found to be 0.6498 mol $CO_2$ per total mol system for 4M1G compared to 0.748 mol $CO_2$ per total mol system for 4M0G at 303 K, 100 kPa.

However, the chemical absorption was more favourable in lower pressure. Since MDEA reacted with $CO_2$ through an acid base mechanism, this reduction of the $CO_2$ loading might be due to the decrease in its basic character. The acidity might also be contributed from the triflate anion of ionic liquid. Even though the cation of [gua][OTf] has amines attached to it, however, it is not sufficient enough to increase the basicity of the systems and enhance the chemical absorption capacity. Reduction on the amount of water in the mixed system by addition of [gua][OTf] might also led to reduction in $CO_2$ solubility. This is because sufficient amount of water is needed to be present in order to promote the dissociation of amine and to absorb the $CO_2$ to form bicarbonate.

However, even though 0M1G scored lower $CO_2$ solubility than 1M0G under the same condition, it is important to point out that 4M1G gave a much better capability to absorb $CO_2$ as compared to other pure studied ionic liquids such as [bmim][$BF_4$]. This is proved by 4M1G which gave 27.5 % higher $CO_2$ loading (0.6498 mol $CO_2$/ total mol system) compared to 4M1B with 0.4829 mol $CO_2$ per total mol system at 303 K, 100 kPa. The difference between 1 and 4 M [gua][OTf] at low pressure was approximately 37 %. The larger deviation was a result from [gua][OTf] absorbing less in low pressure but significantly high after reaching 100 kPa. The $R^2$ values were finely fitted and ranged from 0.94232 to 0.96272 for partial pressure between 0 - 100 kPa.

This work also presents the physicochemical properties of binary and ternary systems of [gua][OTf] – MDEA – $H_2O$. Ambient pressure, density and viscosity measurements at temperatures between 298.2 and 343.2 K reveal that the aqueous binary [gua][OTf] – $H_2O$ are lower in density and viscosity compared to the aqueous [bmim][$BF_4$], [hmim][Br] and [BuPy][$BF_4$], other pure ionic liquid and MDEA. The density of binary systems 4M0G, 1M0G, 0M4G, 0M1G at various temperature were approximately in the range of 0.96 - 1.10 g $cm^{-3}$. Meanwhile, the density of ternary systems 4M2G, 4M1G, 3M1G, 2M2G, 1M3G at various temperatures were in the range of 1.05 – 1.19 g $cm^{-3}$. Thermal expansion, $\alpha_p$, calculated from the density data, increased with the increase in temperatures and composition of [gua][OTf] with the values of $\alpha_p$ varying from 6.1795 x $10^{-6}$ to 7.9184 x $10^{-6}$ $K^{-1}$.

In the case of viscosity, the recorded data for 0M0.1G, 0M0.3G, 0M0.5G, 0M0.7G, 0M0.9G, 0M1G and 0M4G range from 0.7366 to 1.3611 mPas. On the other hand, viscosities for ternary systems *i.e.* 4M0.1G, 4M0.3G, 4M0.5G, 4M0.7G, 4M0.9G, 4M1G and 4M2G were between 7.1759 to 11.059 mPas. According to the Newtonian behaviour, both density and viscosity characters depended on the molar fraction and concentration of the mixtures. The presence of water strongly affects the density and viscosity. Also, temperature has a profound effect on the viscosities while densities are less affected by temperature. However, increasing the ionic liquid content of the mixture in the dilute region does not have much effect on increasing mixture viscosity. Both systems clearly exhibit less expansion than that of molecular organic solvents and the result of fitting for both ionic liquids system showed good agreement with the experimental values.

In a nutshell, the behavior of [gua][OTf] depicts that it possesses both chemical as well as physical tools for gas capture and amine moieties in the ionic liquid are found to be the most suitable substituted functional groups to enhance the absorption rate and capacity of amine-based absorbents. The results show that the correlated equations can represent the experimental $CO_2$ solubility of binary and ternary data with a reasonable accuracy. Most importantly, the ability of the systems to perform in continuous absorption-regeneration experiments indicate that both binaries and ternaries of [gua][OTf] – MDEA – $H_2O$ are good media for $CO_2$ capture in terms of absorption efficiency.

## 8.2 Suggestions for further work

Since the disadvantages of all ionic liquids, particularly functionalized ionic liquids are high viscosity and cost, more binary or ternary phase should be discovered. Adding [gua][OTf] greatly accelerated the absorption of $CO_2$ in MDEA aqueous solutions. Therefore, comprehensive kinetic study would be fruitful. These would provide a better description of the absorption in these kinds of solvents. Yet, untill the year 2010, only one paper on kinetic of amine functionalized ionic liquid has been published [270].

Besides that, $CO_2$ corrosion is one of the most serious forms of corrosion in oil and gas production and transport industries. Thus, a study on the effect of binary and ternary system [MDEA – [gua][OTf] – [$H_2O$] on corrosion rate behavior of carbon steel in carbonated solution of binary and ternary systems at different parameters such as temperature, $CO_2$ loading and exposure time using EIS, polarization curves, SEM and EDX could be beneficial.

Beyond doubt, the data of physical properties of binary and ternary systems are also very useful in process design but still is insufficient to support the applications. Thermophysical properties such surface tension, refractive index and heat capacity are among the essential keys.